SPATIAL AND TEMPORAL TRENDS OF SURFACE-BASED TEMPERATURE INVERSION IMPACT ON PERMAFROST DISTRIBUTION

NICHOLAS CRAIG NOAD
Bachelor of Science, **University of Lethbridge, 2019**

A thesis submitted
in partial fulfilment of the requirements for the degree of

MASTER OF SCIENCE

in

GEOGRAPHY

Department of Geography and Environment
University of Lethbridge
LETHBRIDGE, ALBERTA, CANADA

SPATIAL AND TEMPORAL TRENDS OF SURFACE-BASED TEMPERATURE INVERSION IMPACT ON PERMAFROST DISTRIBUTION

Nick Noad

Date of Defense: July 9, 2021

Dr. P. Bonnaventure	Associate Professor	Ph.D.
Thesis Supervisor		
Dr. H. Jiskoot	Professor	Ph.D.
Thesis Examination Committee Member		
Dr. L. Chasmer	Associate Professor	Ph.D.
Thesis Examination Committee Member		
Dr. S. Kienzle	Professor	Ph.D.
Chair, Thesis Examination Committee		

DEDICATION

To my family, friends, and colleagues who all supported me during the compiling of this research into a thesis. I could not have asked for more support than what I got from all those around me. In particular I thank my family for an upbringing that helped me learn the meaning of hard work and giving a best effort in all things. I also dedicate this thesis document the love of my life Elizabeth for her love and support as I wrote this document.

ABSTRACT

Preliminary findings from previous research in northwestern Canada suggest that surface-based temperature inversions (SBIs) have an influence on permafrost. The aim of this thesis was to quantify and discuss this impact of SBIs on a regional and local valley-to-valley scale. A new SBI characteristic called inversion impact (I_{imp}) was created to quantify and conceptualize the degree of impact SBIs had on surface air temperatures. I_{imp} was observed to be significant (≤5.8 °C) on annual average at each of the five sites within the region that had archived radiosonde data available. Significant influence of SBIs on permafrost distribution was observed in two near proximity dissimilar northcentral Yukon valleys using in-situ sensors. Overall, this study highlighted an interaction between SBIs and the state of permafrost that varied both spatially and temporally. This signifies a need to include the influence of SBIs when modelling current and future permafrost distribution in this region.

PREFACE

Literature was reviewed and organized by me into chapter one of this thesis. This section was designed to present the permafrost centered context that inspired research into the SBI phenomenon in the northwestern Canada region. Philip Bonnaventure and Hester Jiskoot provided direction and edits in the construction of this chapter. Nick Hassink also provided an edit to prepare this chapter for my final thesis.

Chapter two was written with extensive editing of my writing by Hester Jiskoot and Philip Bonnaventure. The idea for the manuscript was conceived by Philip Bonnaventure, Hester Jiskoot and Gaëlle Gilson. The computer program coding to extract SBIs from the radiosonde data archive was written by Gaëlle Gilson. Madeleine Garibaldi aided in creating maps and editing the final manuscript document in preparation to submit this manuscript to the Journal of Applied Meteorology and Climatology. I took the lead in analysis and write up of this work.

Chapter three was conceived by me, Philip Bonnaventure, and guided by discussions with my supervisory committee, and along the course of my Master of Science degree. I took the lead with the analysis and write up of this manuscript and Philip Bonnaventure did extensive edits of this work. Madeleine Garibaldi also went through the manuscript and implemented edits to improve it.

Chapter four was organized and written up by me with edits and proofreads completed by Phillip Bonnaventure, Tammy Noad, and Scott Vegter for preparation of inclusion in this thesis.

ACKNOWLEDGMENTS

I acknowledge all the great support provided by my lab, co-authors, supervisory committee, and supervisor who all spent countless hours reading through and editing this work. There was also great support from my lab mates in data collection for my thesis in the field as well as suggestions as how to proceed with aspects of my work. In particular I thank my supervisor Philip Bonnaventure who worked with me on this research every step of the way ensuring that I conducted quality research and remained on a good pace to finish this work and achieve the goals we set. I also thank Hester Jiskoot for her work and the many hours sacrificed serving on my supervisory committee and for extensive editing of my writing to make it clearer and more concise. I thank Laura Chasmer for all the guidance and assistance she provided in producing this thesis as she devoted many hours serving on my supervisory committee. I thank the University of Lethbridge for funding and for resources necessary to complete my work, particularly in the time of the COVID-19 pandemic. I thank the Northern Scientific Training Program that funded fieldwork necessary for completion of this work. Finally, I thank NSERC for the Discovery Grant awarded to my supervisor for purchase of equipment and ability to deploy it in the field. Furthermore, the NSERC CGS M program that funded me so that I could focus solely on my thesis work without worry of seeking financial support through work outside of my normal graduate teaching assistant responsibilities.

TABLE OF CONTENTS

LIST OF TABLES

LIST OF FIGURES

LIST OF ABBREVIATIONS

AMAT	Annual Mean Air Temperature
AO	Arctic Oscillation
CBL	Convective Boundary Layer
Depth MAGT	Mean Annual Ground Temperature
EFS	East Face Slope site
EFT	East Face Transect
ELR	Environmental Lapse Rate
ETA	Elevational Transect Analysis
I_{freq}	Inversion Frequency
I_{imp}	Inversion Impact
I_{mag}	Inversion Magnitude
I_{str}	Inversion Strength
MAAT	Mean Annual Air Temperature
MAGST	Mean Annual Ground Surface Temperature
NEST	Northern Ecosystem Soil Temperature
NFS	North Face Slope site
NFT	North Face Transect
NPI	North Pacific Index
NV	North Valley
PDO	Pacific Decadal Oscillation
REDCAPP	REanalysis Downscaling Cold Air Pooling Parameterization
RMSE	Root Mean Square Error
SAT	Surface Air Temperatures
SBI	Surface-Based Temperature Inversions
SFS	South Face Slope site
SFT	South Face Transect
SLP	Sea Level Pressure
SLR	Surface Lapse Rate
SST	Sea Surface Temperature

SSTA	Sea Surface Temperature Anomalies
SV	South Valley
TTOP	Temperature at the Top of Permafrost
WFS	West Face Slope site
WFT	West Face Transect

CHAPTER 1: BACKGROUND

1.0 PURPOSE

The purpose of this research is to review the interactions between SBIs and permafrost across northwestern Canada by building upon previous research on the subject in this region. Previous assumptions regarding variability of SBIs across a regional scale as well as across a local valley-to valley-scale will be tested. All of this work will aim to identify limitations in current modelling which either fails to account for SBI all together or for SBI variability across various scales. The overarching purpose is to provide understanding valuable to further improve the accuracy of permafrost modelling in northwestern Canada and in other regions with similar phenomenon of frequent and strong SBI.

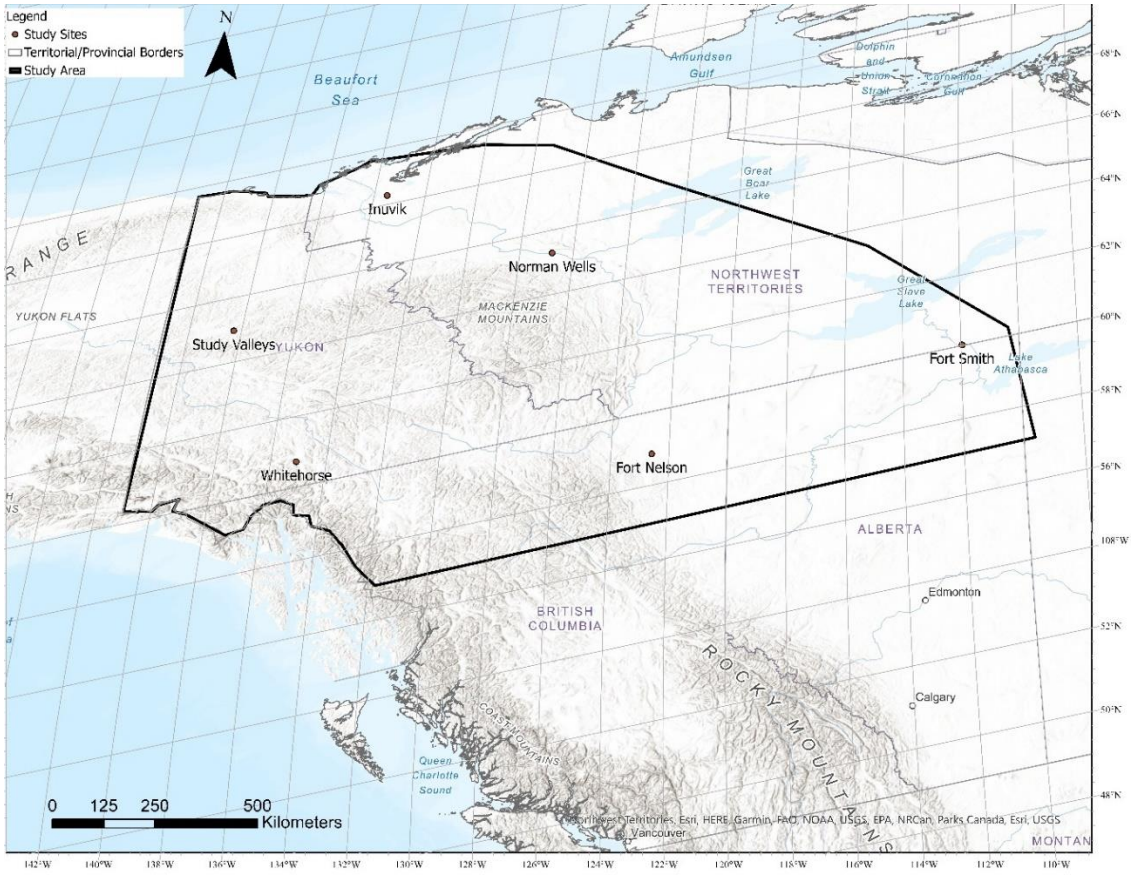

Figure 1.1: The Study Region for this thesis. Most of the focus is on mountainous areas of the high-latitude northwestern Canada region.

1.1 INTRODUCTION

Permafrost is defined as earth materials that remain at or below 0°C for two or more consecutive years (Harris et al., 1988; Riseborough et al., 2008). The layer overlaying permafrost subject to seasonal thaw is known as the active layer (Burn, 1998) and this active layer can vary greatly from a few centimeters to several meters thick (French & Williams, 2013). Permafrost distribution and active layer thickness are ultimatly a byproduct of past and current cold climatic conditions (French & Williams, 2013). Climate influences the distribution of permafrost directly through mean annual air temperature (MAAT) patterns (Smith & Riseborough, 2002), snow depth (Aalto & Luoto, 2014; Way & Lewkowicz, 2018; Garibaldi et al., 2021), and surface moisture (Qin et al.,

2017). Additionally, in areas with more variable climatic conditions, permafrost can be more indirectly influenced by dominant vegetation cover and ecological processes (Jorgenson et al., 2010). Permafrost distribution is organized into zones that are defined by the percent of the land surface that is underline with permafrost which includes continuous (90-100%), discontinues (50-90%), sporadic (10-50%), and isolated (<10%) (Heginbottom et al., 1995).

In the context of all these interconnected variables, permafrost distribution modelling proves to be a truly complex endeavor, especially in highly heterogeneous terrain such as mountainous regions (Etzelmüller, 2013). Accurate modelling of permafrost distribution is essential as permafrost thaw presents many significant challenges, including a release of previously sequestered carbon into the atmosphere (Olefeldt et al., 2016), harmful immobilized chemicals such as mercury (Rydberg et al., 2010), and of preserved prehistoric diseases such as anthrax (Revich & Podolnaya, 2011), as well as by compromising the structural integrity of terrain upslope of human-built infrastructure and homes in northern communities (Haeberli et al., 2010). Thus, it is of the utmost importance that we develop our understanding of the distribution of permafrost in these regions and the impact that climate change will have on the environmental variables that have the capacity to impact permafrost distribution across both spatial and temporal scales. One such variable that strongly impacts permafrost distribution in continental high-latitude mountains is persistent mountain valley surface-based temperature inversions (SBI). SBI change the typical, and often assumed, patterns of surface air temperature (SAT; defined as air temperature at 2 m above the Earth's surface) that exist as a result of elevational variability (Lewkowicz & Bonnaventure, 2011).

The central questions of this thesis include:

1) What are the spatiotemporal characteristics of SBI across northwestern Canada?

2) What is the potential impact of SBI on SAT across northwestern Canada?

3) What are the implications of variation in inversion impact on local and regional scales specifically with respect to permafrost distribution and susceptibility to degradation across northwestern Canada?

To answer these questions and fulfill the thesis objectives, four chapters are included: Chapter 1 consists of an introduction, highlighting relevant background through a literature review, as well as outlining the thesis objectives. Chapter 2 includes a submitted manuscript which aims to quantify and conceptualize the impact of SBI on SAT by introducing a new variable called “Inversion Impact”. Chapter 3 is comprised of a manuscript that compares the results of a field study which contrasts measured surface lapse rate (SLR) data in two northcentral Yukon valleys that have dissimilar geometric and vegetative characteristics despite their close proximity. Finally, Chapter 4 contains a summary of major findings and an extended discussion of the implications of thesis findings along with suggestions for future research.

1.2 CRYOSPHERIC ELEMENTS AND CLIMATE

Cryospheric elements, including sea ice, glaciers, and permafrost, are rapidly degrading across high-latitude areas of the Northern Hemisphere, (IPPC, 2019). The loss of these cryospheric elements is particularly concerning as they directly impact the local and global climate (Derksen et al., 2012). As these systems warm, they create positive feedback loops, such as the loss of reflective snow and ice causing a decrease in albedo, and the release of greenhouse gases, which in turn magnifies the initial impacts of warming (Derksen et al., 2012; Prestrud, 2007). Therefore, the strong connection between climate and cryospheric elements drives reciprocal changes that are the root causes of uncontrollable warming across northwestern Canada (Serreze & Barry, 2011).

While climate has generally been warming at accelerated rates across high latitudes in the northern hemisphere (IPCC, 2019), climate warming in northwestern Canada is occurring at a particularly accelerated rate. Zhang et al. (2019) found that from 1948-2016, much of northwestern Canada's mean annual air temperature increased (+2-3.5 °C) more rapidly than other parts of the country and the global trend. Warming of this magnitude even exceeded the Holocene maximum temperature by 1.7 °C (Porter et al., 2019). These findings suggest a need for understanding interactions between changing climate and cryospheric elements. Specifically, this thesis focuses on the cryospheric element permafrost, within the region of northwestern Canada.

1.3 WHY STUDY PERMAFROST?

Like all landscapes, areas underlain by permafrost today are a product of the past. As permafrost environments are a mixture of geomorphic and ecological mosaics, the development of these systems has been occurring for some time. As permafrost forms and persists, substantial quantities of organic matter can be trapped in the permafrost layer and water can accumulate and freeze into the permafrost layer resulting in permafrost with high ice content.

Permafrost provides key ecosystem services in regions where it is present and as permafrost deteriorates the integrity of these ecosystem services may be significantly reduced (Schuur & Mack, 2018). One ecosystem service provided by permafrost is the storage of this carbon-rich material that is no longer subject to decomposition due to its frozen state (McGuire et al., 2009). As permafrost thaws, however, stored carbon in these soil organics is subject to natural rates of decomposition (Loranty et al., 2018). As a result, this carbon (which in some cases has been stored for thousands of years) is now mobilized and can be released into the atmosphere through natural processes (Helbig et al.,2017). This process further exacerbates a positive feedback loop of increased atmospheric greenhouse gases causing accelerated climate change and subsequent amplified rates of permafrost thaw that (Schuur et al., 2008).

Another ecosystem service provided by permafrost is the storing of toxic elements such as mercury (Stern et al., 2012). Just like carbon, the frozen portions of our world have acted as one-way filters for material, as a result, permafrost currently holds substantial amounts of mercury in the range of 793 ± 461 Gigagrams of Mercury (Schuster et al., 2018). As permafrost thaws mercury is released into the active layer and

later distributed throughout the ecosystem (Smith-Downey et al., 2010), including the hydrological system that can transport these toxic elements downstream. This has a negative impact on both terrestrial and marine ecosystems across the Arctic (Leitch et al., 2007). Finally, diseases such a smallpox and anthrax can be preserved in permafrost soil (Revich & Podolnaya, 2011; Desyatkin, 2018). This puts both human and animal populations at risk, as ancient, unstudied, cultures of these deadly pathogens can be re-introduced into the environment (El-Sayed & Kamel, 2020).

Another attribute of permafrost is the presence of ground ice stored within. Ground ice is frozen water within a frozen substrate (O'Neill et al., 2019). The presence of ground ice has real consequence to permafrost thaw, generating a visual scar within the landscape as thermokarst features are developed. Additionally, the presence of ground ice can both influence the energy needed to thaw permafrost and the susceptibility of the ground and overlying ecosystem and infrastructure itself (Jorgenson et al., 2015). The distribution of ground ice is controlled by local and regional climate alongside geomorphological and hydrologic processes (Kokelj et al., 2017). One such example of the impacts of thawing permafrost in ice-rich permafrost soils is the process of thermokarst development (Kokelj & Jorgenson, 2013). Since permafrost is the only element of the cryosphere that humans live on year-round, the collapse of the landscapes associated with permafrost can have major implications on human infrastructure and safety (Hjort et al., 2018). One potentially major issue that stands out for northwestern Canada due to prevalent mountainous terrain is slope instability induced by permafrost degradation and thaw (Bartleman et al., 2001; Haeberli et al., 2010).

Changes in the landscape as a result of permafrost thaw impact regional hydrology (Quinton et al., 2011). Studies in northwestern Canada have documented changes in both the connectivity of hydrological systems and changes in the baseflows of prominent rivers located in discontinuous permafrost landscapes because of landscape alterations that stem from permafrost thaw (Jacques & Sauchyn, 2009; Cannon et al., 2012; Chasmer & Hopkinson, 2017). This could contribute to the increase in water moving through hydrological systems in northern Canada which has major implications for human populations and natural ecosystems across this region (Déry et al., 2009).

1.4 LIMITATIONS OF CURRENT RESEARCH IN MOUNTAIN PERMAFROST

Ground temperature conditions can vary by as much as 15 °C within 1 km of horizontal distance in mountainous areas (Riseborough et al., 2008). Thus, extreme variability can exist across small horizontal distances that are found in complex and heterogeneous mountain landscapes. Complex and heterogenous mountain landscapes are areas with highly contrasting elevation, valley geometry, vegetation, and rock types over small horizontal distances. Etzelmüller (2013) highlights that a major challenge in modelling mountain permafrost is high sub-grid cell variability in coarse resolution climate models. There is a gap between the spatial resolution of climate models and the spatial variability of mountain topography which significantly limits projections of how climate change will influence distribution of mountain permafrost (Riseborough et al., 2008). An additional complicating matter is a newly documented conceptualization known as Elevation Dependent Warming (EDW), whereby higher-elevation regions experience the effects of climate change at an accelerated rate compared to lower elevations (Pepin et al., 2015; Williamson et al., 2020). Some attributes contributing to

the heterogeneity of ground temperatures include atmospheric temperature, snow depth, albedo, aspect, soil or substrate type, vegetation, and topographic shading (Gubler et al., 2013).

Recent research in northwestern Canada has been completed regarding microscale variability of ground and permafrost temperatures caused by heterogeneity of snow depth (Garibaldi et al., 2021) and air temperatures along an elevational gradient (Lewkowicz & Bonnaventure, 2011; Lewkowicz et al., 2012). Recent modelling using MODIS land surface temperature data (Section 1.13.4) and the ERA-Interim climate reanalysis dataset (Section 1.13.3) had some success in counteracting underestimations of SBI driven cold valley bottom temperatures in Siberia. This modelling has not yet successfully accounted for SBI driven valley cold in northwestern Canada possibly due to narrower valleys (Obu et al., 2019). Even with recent breakthroughs in accounting for some of the heterogeneity in mountain permafrost distribution modelling (Bonnaventure et al., 2012) there is still considerable work to be done to improve accuracy of this modelling.

1.5 PERMAFROST DISTRIBUTION PATTERNS IN NORTHWESTERN CANADA

In northwestern Canada permafrost zones range from isolated patches to continuous zones (Heginbottom et al., 1995). Permafrost is the result of cold MAAT's which can be related to geographic position due to high latitude or high elevation (French & Williams, 2013). Thus, in most landscapes in the northern hemisphere, it can be assumed that permafrost has either a southern limit or a lower elevation limit.

The distribution of permafrost in northwestern Canada is complex because these two distinctive influences of climate coexist in an intricate way (Bonnaventure & Lewkowicz, 2013). This presents a complicating factor for traditional permafrost distribution modelling in northwestern Canada, which must rely on trends in elevation and latitude (Riseborough et al., 2008). Recently it has been discovered in northwestern Canada that the assumption of a lower elevation limit of permafrost in mountain environments breaks down, sometimes not being present in discontinuous permafrost environments (Lewkowicz & Bonnaventure, 2011). This is due to the dominance of SBIs across the region which are particularly common in mountain valleys. The remainder of this thesis will focus on the relationship between SBIs, SATs and subsequently permafrost distribution across northwestern Canada.

1.6 WHAT ARE SURFACE-BASED TEMPERATURE INVERSIONS?

The rate at which air temperature changes with height above the ground surface is described as a lapse rate (Oke, 1987; Whiteman & Richland, 2000). These lapse rates can be free-air lapse rates associated with changes in altitude (Feldl et al., 2020) or SLRs associated with changing elevation over topography (Lewkowicz & Bonnaventure, 2011). SLRs can vary considerably in mountainous areas. Many climate models often make assumptions of constant SLRs, which can introduce significant error (Minder et al., 2010).

Typically, the atmosphere cools at an environmental rate of 6.5 °C km^{-1} (Oke, 1987). This lapse rate occurs in response to reduction of air pressure as elevation increases, which results in expansion of the air parcel leading to adiabatic cooling. There is a dry adiabatic lapse rate (≈-9.8 °C km^{-1}) and a saturated adiabatic lapse rate (-6 °C km^{-}

^{1}) depending on if the temperature of the air parcel has reached the dewpoint temperature (Birkeland, 2016). The reason for these differences is that due to latent heat exchange a saturated air parcel cools more slowly that a dry air parcel. For these reasons, lapse rates were observed to cool at a rate greater than 9°C km^{-1} or can be gentler and closer to 0 °C km^{-1} (Blandford et al., 2008). In some cases, specifically during the night or winter months, the lapse rates can become inverted resulting in temperature increase with altitude or elevation (Gustavsson et al., 1998) (Figure 1.2). Patterns of inverse lapse rates are defined as temperature inversions (Kahl et al., 1992).

Three main types of temperature inversions occur, elevated temperature inversions, surface-based temperature inversions (SBI) (Whiteman, 2000), and near surface-based temperature inversions (Shahi et al., 2020). Elevated inversions form above the ground surface and normally have a convective boundary layer (CBL) underlying them in which normal lapse rates can be observed (Whiteman, 1982). Near surface-based temperature inversions are defined as inverted lapse rates that occur within 2 m of the ground surface (Shahi et al., 2020). SBI can be defined as temperature inversions that form at or just above the ground surface but extend higher than near surface-based temperature inversion (Bradley et al., 1992). SBI commonly occur in mountain valleys, in particular during times of negative net balance of surface radiation such as in the winter, or at night (Whiteman & Richland, 2000). As SBI form and persist they can have various impacts on surface conditions. SBIs are the type of inversion focused on for the remainder of this paper.

When measuring SBIs there are several inversion characteristics used to describe inversion. These include Inversion strength (I_{str}) which is the difference between the

temperature at the top and bottom of the SBI (Bourne et al., 2010; Wei et al., 2013) and is sometimes termed inversion intensity (e.g., Zhang et al., 2011; Joly & Richard, 2019). Inversion frequency (I_{freq}) is the proportion of soundings with an SBI recorded relative to the total number of radiosonde soundings. Inversion depth (I_z) is the difference between altitude/elevation of the SBI base and top of SBI layer (Shahi et al., 2020).

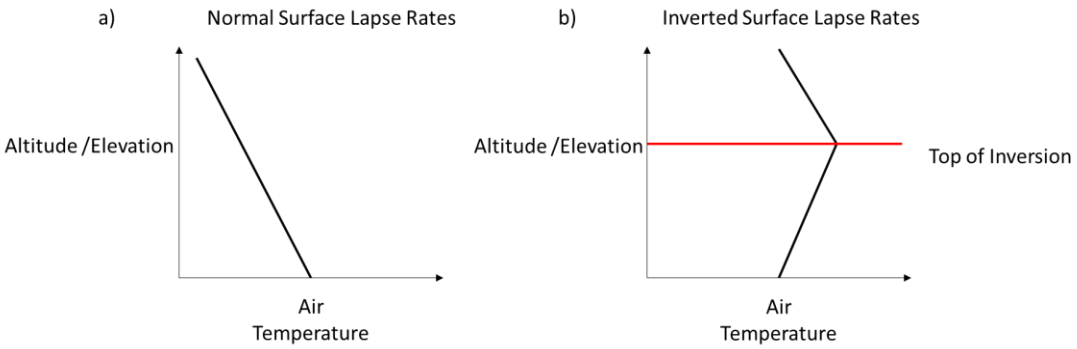

Figure 1.2: a) Normal SLRs occur when air temperature gets colder with increased elevation/altitude. b) Inverted SLRs occur when air temperature gets warmer with increased elevation/altitude. Notice the presence of a thermal line at the top of the SBI layer where temperature is the warmest along this vertical profile of air temperatures.

1.7 IMPACTS OF SURFACE-BASED TEMPERATURE INVERSIONS

SBIs have major implications on surface conditions, particularly in high-latitude regions where they are most frequent and strong. One implication is their impact on the prediction of SAT in areas with heterogeneity of surface elevations (Etzelmüller, 2013). For example, Dobrowski et al. (2009) observed significant errors (1.2-2 °C) in predicted annual nighttime temperatures in a series of valleys along the California and Nevada border. Errors were a result of assuming that lapse rates would be -6.5 °C km^{-1} while common nighttime SBI invalidated this assumption. Thus, higher elevations were predicted to be cooler while lower elevations were predicted to be warmer in areas of the region susceptible to cold-air pooling. In another example, Frei (2014) attempted to

improve SAT interpolation in the mountainous area of the Swiss Alps. They acknowledge that a major source of error (mean absolute error of ≥ 3°C) in some mountain valleys prone to frequent nighttime and wintertime SBIs.

Climate change has been well established to have major impacts on animals (Holt, 1990; Urban, 2015; Radchuk et al., 2019), insects (Volney & Fleming, 2000; Raza et al., 2015) and plants (Tape et al., 2006; Fraser et al., 2014). To predict the impact future climate warming will have on the tolerance ranges of organisms, existing and future SAT must be accurately interpolated in complex terrain (Roberts et al., 2019).

Agriculture is also influenced by the SBI phenomena as they play an important role in frost exposure and prevention (Simnitt et al., 2017; De Wekker et al., 2018). Radiation frost is most common in areas where frost susceptible fruit and vegetables are grown (Simnitt et al., 2017). At night the surface cools rapidly under clear skies and calm winds. Cooling air at the surface flows downslope and pools in low-lying areas making these zones the most susceptible to frost (Figure 1.3). De Wekker et al. (2018) suggests that part way up the slope a thermal belt can form. In this thermal belt, temperatures can stay warm enough to avoid frost allowing for lengthened growing seasons. As such, common practices with crops include confining fruit trees to slopes and avoiding valley bottoms (Kerr, 1970).

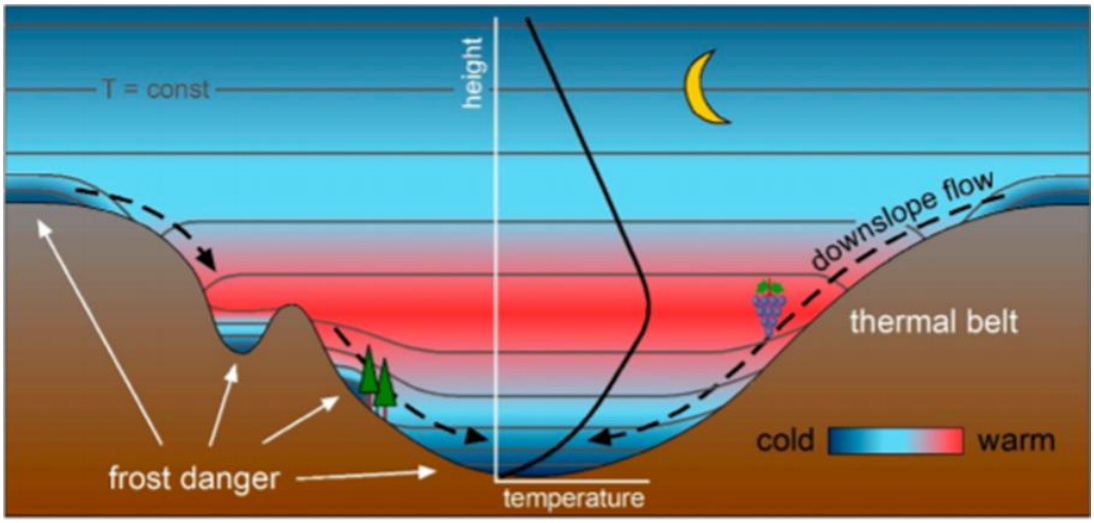

Figure 1.3: The effects of inversions on the formation of frost. The best location for crop preservation against frost in the thermal belt or the warmest location of the inversion. In this area the frost-free season can be extended considerably (De Wekker et al., 2018, p. 371).

There are three main impacts on surface meteorological conditions from SBI: freezing precipitation events, extreme cold conditions, and dense fog (Whiteman et al., 2001). When cold air is pooled near the Earth's surface while warm, moist air is advected aloft, this results in the potential for development of freezing precipitation (Whiteman & Richland, 2000). Freezing precipitation events can persist for long periods (>18 hours) depending on persistence of surface cold air advection and warm air advection aloft (McCray et al., 2019). Significant ice aggradation can occur during long duration freezing precipitation events that can result in substantial property damage which has required historically large sums of money to repair (Changnon, 2003). There is also a substantial threat to public safety from conditions imposed by ice aggregation on surfaces such as roads (Barszcz et al., 2018). During intense cold-air drainage, extreme cold temperatures that can be record breaking have been recorded (Harris, 1982; Whiteman et al., 2004). Finally, dense fog can develop in association with the presence of SBIs (Gilson et al.,

2018b) which can substantially reduce visibility producing dangerous condition particularly for all aspects of transportation (LaDochy, 2005).

High concentrations of atmospheric pollutants near the Earth's surface are most often coupled with calm and stable conditions associated with high pressure systems (Whiteman & Richland, 2000). Largeron and Staquet (2016) describe the sinking motion of upper air as well as warm air advection in the upper levels of the atmosphere as the result of a strong midlevel inversion. This midlevel inversion decouples the lower atmosphere from the free-atmosphere above. Decoupling of the lower atmosphere in valleys allows for deep SBIs to form during nightly cold drainage, persisting during the day due to the CBL at the surface not getting thick enough to allow mixing out. Thus, this does not allow for the inversion reconnection between the lower atmosphere with the free upper atmosphere (Largeron & Staquet, 2016). Air pollution can cause health issues including the development or worsening of chronic respiratory illnesses such as asthma and can increase mortality rates (Dockery, 1994; Klot et al., 2002; Kappos et al., 2004).

1.8 SURFACE-BASED TEMPERATURE INVERSIONS IN HIGH-LATITUDE LOCATIONS

With broad impacts of SBIs now reviewed the attention of this literature review will be turned more specifically towards SBIs and their impacts in high latitude areas. Bradley et al. (1992) conducted a comprehensive review of inversions at nine coastal Arctic locations in North America. Their main findings consist of inversions during the winter months setting up and persisting for more than 70 % of the days. Additionally, inversions would often be strong, sometimes registering a rate of temperature increase of 30 °C km^{-1} during times of strong warm air advection above the surface inversion.

Inversions tend to be 400 to 850 m deep at these locations. Similarly, Zhang et al. (2011) reviewed characteristics of SBI including I_{str}, I_z, and I_{freq} for 39 Arctic locations and 9 Antarctic locations. These authors correlate stronger, deeper and more persistent SBI with increasing latitude. Furthermore, clearer, calmer, and more stable persistent areas of high-pressure subsidence such as the Siberian anticyclone are associated with deeper and stronger SBI. Other studies using radiosonde data highlight similar patterns of noticeably stronger, deeper, and persistent inversions in high-latitude regions (>60°N) when compared to other regions, particularly in the winter months (Kahl, 1990; Kahl et al., 1992; Serreze et al., 1992; Bourne et al., 2010; Mayfield & Fochesatto, 2013; Gilson et al., 2018a).

Additionally, not only are there studies using radiosonde data to highlight the high impact of SBIs in high-latitude areas; there is research using elevational transects of loggers. For example, Smith and Bonnaventure (2017) found that there were extended periods of time where a station 100 m higher than the valley bottom station at Alert Canada (82.50° N, 62.35° W) in the High Arctic was 8 °C warmer. This led to MAAT anomalies of warmer conditions at locations with higher elevations which resulted in the top of permafrost being 0.8 °C cooler in the valley bottom than 100 m up the slope. Other studies are conducted using similar transects to account for the high impact of SBI variation with elevation change (Taylor et al., 1998; Lewkowicz & Bonnaventure, 2011; Pike et al., 2013).

Overall, inversions in high-latitude locations play a significant role in the weather and climate of this region (Klock et al., 2002; Lovatt, 2009; Mayfield & Fochesatto, 2013; C. Burn et al., 2015). Understanding these impacts and how they vary spatially and

temporally is an essential aspect of research that is missing in this region. Furthermore, due to the high I_{freq}, SAT patterns along an elevational gradient are influenced greatly on an annual basis across a large portion of high-latitude mountainous areas (Lewkowicz & Bonnaventure, 2011; Bonnaventure & Lewkowicz, 2013). Thus, the need for further research into all aspects of SBI is greater in no place other than the Arctic, Subarctic, and Antarctic. Most needed is an understanding of how these SBI characteristics of strength, depth, development, frequency, persistence, and breakup vary both spatially and temporally across the region and on smaller valley-to-valley scales. The potential for impact of SBIs on MAATs in these high latitude areas must be quantified as this has not been directly reviewed in previous SBI research.

1.9 SURFACE-BASED INVERSION IMPACT ON PERMAFROST DISTRIBUTION

MAAT is a major factor in driving permafrost distribution (French & Williams, 2013). Since there is a link between SAT/MAAT patterns and SBIs, it can also be concluded that there is also a link between SBI and permafrost distribution. For example, interpolation of ground temperatures in areas susceptible to cold-air pooling led to a misrepresentation of upwards to 1.5 °C when modelling permafrost distribution in Scandinavia (Gisnås et al., 2017). Several studies theorized or discussed this potential link between these two phenomena (Taylor et al., 1998; Cote, 2002; Lewkowicz & Ednie, 2004; Bonnaventure & Lewkowicz, 2008; Lovatt, 2009).

It has not been until more recently that the effect of SBIs on permafrost distribution in mountainous areas was quantified and included in permafrost distribution modelling (Lewkowicz & Bonnaventure, 2011; Bonnaventure et al., 2012; Lewkowicz et

al., 2012; Smith & Bonnaventure, 2017). Recently a model was created using MODIS land surface data and the Interim ERA climate reanalysis dataset to account for variable SBI influence across the landscape. This resulted in some success for mountain valleys of Siberia but underpredicted the probability of permafrost occurring in cold valley bottoms for areas of northwestern Canada (Obu et al., 2019).

To understand the relationship between SBI and permafrost one must first recognize temperature offsets associated with interactions between permafrost, active layer, and the atmosphere. French and Williams (2013) define the two temperature offsets as a thermal offset and surface offset (Figure 1.4). The thermal offset is the temperature difference between the ground surface and the top of permafrost. This ratio is reliant on both the air thaw index and thermal conductivity ratio (r_k) of the soil or bedrock (French & Williams, 2013). Riseborough et al. (2008) defines that the temperature at the ground surface is dependent on the surface offset, which is explained by n-factors for thawing (n_t) and freezing (n_f). These n-factors are associated with snow cover in the winter and vegetation in the summer, illustrating the decoupling between atmospheric temperatures and SATs. Surface offset defines the difference between MAAT and Mean Annual Ground Surface Temperature (MAGST) and can be 0 °C or up to ~ 5.8 °C warmer on annual average at ground surface than in the air (Smith & Riseborough, 2002). Air temperature is defined by atmospheric conditions which include the atmospheric lapse rate, especially in mountainous areas where there is considerable variation in elevation across small horizontal distances. Thus, further study of SLRs and SBI characteristics becomes vital to modelling air, ground, and permafrost temperatures in mountainous terrain.

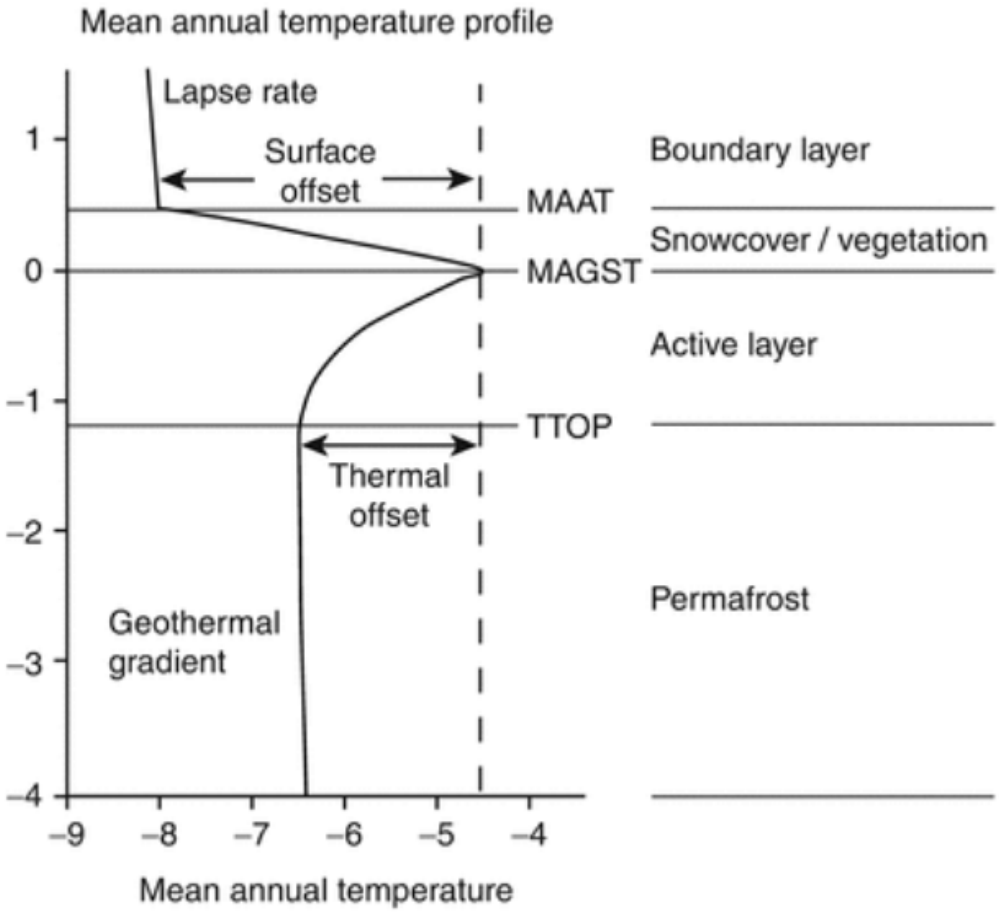

Figure 1.4: Conceptualization of the Temperature at the Top of Permafrost model. This framework highlights the interaction between air, ground surface, and top of permafrost temperatures (Riseborough et al., 2008, p. 141).

Although known for some time, it has recently been conceptualized that permafrost distribution is impacted by SBIs in high-latitude areas of complex topography (Bonnaventure and Lewkowicz (2013) (Figure 1.5). This conceptual framework is based on annual average SLRs. Annual average SLRs have been observed to be closer to normal (-6.5 °C km^{-1}) in maritime areas including the southwestern Yukon, which are influenced more by airmasses moving in from the Pacific Ocean (Lewkowicz et al., 2012). Further from the ocean to the Northeast, however, SLRs on an annual scale were shown to typically be gentle to inverted due to the influence of the more dominant, stable, polar continental airmass (Lewkowicz & Bonnaventure, 2011). Additionally, at a local

level this framework highlights that locations near treeline are most likely to experience permafrost thaw as they are the warmest along the elevational transect (Bonnaventure & Lewkowicz, 2013). Bellow treeline the presence of trees can reduce turbulence of the airmass which is theorized to allow for cold air pooling and subsequent SBIs to be stronger and present more often. This results in a permafrost spatial loss pattern termed bidirectional spatial loss. Here, thaw is highest from treeline and decreases downward towards the valley bottom, and upwards towards the ridgetop or mountain peak (Bonnaventure & Lewkowicz, 2013). Effectively, permafrost models created for areas which have annual average inverted SLR show permafrost distributions where terrain have no lower limit of permafrost such as those typically found in mountain locations like the Southern Rockies or the European Alps (Bonnaventure et al., 2012). Although this is well understood conceptually, continued research and monitoring is needed to better assess the variability and extent of SBI impact on patterns of SAT. This will allow for proper inclusion of climate processes present in mountain and valley landscapes, an essential aspect to understanding permafrost distribution and patterns of potential thaw. One such approach to this is to understand the magnitude and variability of SBI characteristics in the region of northwest Canada to determine how they vary spatially and temporally.

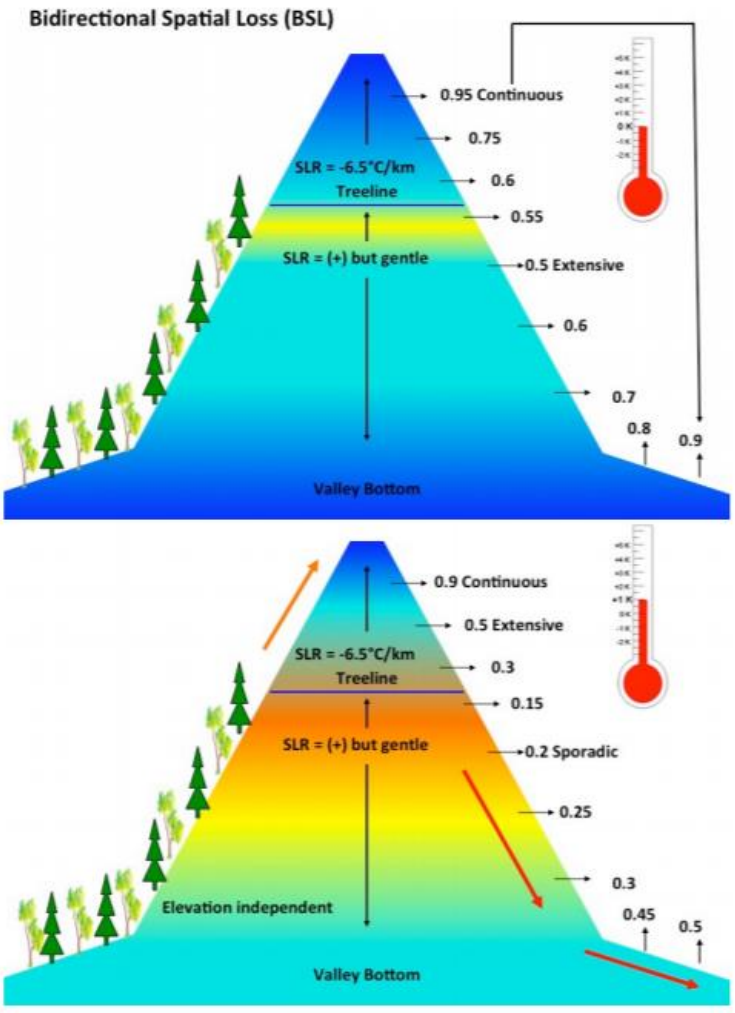

Figure 1.5: Conceptual model of the bidirectional spatial loss of permafrost (Bonnaventure & Lewkowicz, 2013, p. 943).

1.10 INVERSION DEVELOPMENT, PERSISTENCE AND BREAKUP

To understand how inversion characteristics vary spatially and temporally a description of how SBIs develop, persist, and breakup must be made. There are five main mechanisms of SBI formation: the first mechanism is net negative energy balance at the surface that results in rapid radiative cooling. As the surface rapidly cools, cold air begins to run downslope (Whiteman & Richland, 2000). These downslope winds are known as katabatic winds (Vergeiner & Dreiseitl, 1987). Katabatic winds drive cold-air pooling in

low lying areas including in valley bottoms or small depressions in the landscape (Clements et al., 2003; Vosper & Brown, 2008; Smith et al., 2010a). The second mechanism is warm-air advection overtop of a cold airmass entrenched near the surface (Bradley et al., 1992). The third mechanism, a cold front and associated cold-air advection drive a cold airmass underneath the warmer airmass aloft (Whiteman & Richland, 2000). The fourth mechanism is through subsidence of air parcels aloft that warm as they are compressed while surrounding pressure increases. This compression warms the air parcel to be warmer than cold dense air underlying it (Whiteman & Richland, 2000). In continental high-latitude areas high pressure systems and resulting subsidence of air aloft are a frequent occurrence, particularly in winter months (Przybylak, 2016). If this subsidence pattern persists long enough, elevated inversions can develop into strong and stable SBI events (Palarz et al., 2018). The fifth mechanism is the development of an inversion at the surface through the melt of snow or ice due to latent heat transfer in the process of melting limiting sensible heat increase in the atmosphere near the surface (Chutko & Lamoureux, 2009). This type of inversion is most often observed over sea ice (Palo et al., 2017) or glaciers (Mernild & Liston, 2010). There are also some indications these types of inversions could occur over land during melt of snowpack (Maykut & Church, 1973). These aforementioned mechanisms can work in unison to develop SBI (Serreze et al., 1992; Gustavsson et al., 1998).

Whiteman et al. (2001) defined two types of cold-air pooling events, diurnal, and persistent (> 18 hours in length). These authors selected several distinct persistent cold pool events in the Columbia Basin of Washington state to review and discuss. Most of these SBIs were strengthened by the advection of warmer air over an SBI already in

place. Similarly, other studies conclude that the SBI can strengthen due to warm air either being advected above or warming of air through subsidence above the SBI layer (Bradley et al., 1992; Wei et al., 2013; Lu & Zhong, 2014). A stratus cloud deck that overtop of a persistent SBI layer can block solar radiation from warming the surface and stopping the initiation of a CBL development necessary to mix the SBI out (Whiteman, 1982). Another factor that may inhibit formation of a CBL thick enough to mix out the SBI is the presence of snow cover or wet soil at the surface that prohibit surface warming (Whiteman, 1982). Furthermore, studies have linked the persistence of cold dry Arctic synoptic weather patterns to more persistent cold pooling air events and longer inversion persistence (Blandford et al., 2008). As these airmasses anchor into a region and persist, cold-air pooling can both drive development and then maintain SBI by keeping SATs several degrees colder than the airmass aloft (Lareau et al., 2013). Overall, persistent SBIs are generally linked to prolonged periods of solar radiation deficit at the surface, allowing for the persistence of cold-air pooling and subsequent increased I_{freq} (Whiteman et al., 2001; Mayfield & Fochesatto, 2013). Higher I_{freq} has been directly correlated with increased I_{str} (Zhang et al., 2011).

Inversion breakup processes and associated mechanisms are important in defining both spatial and temporal variability in SBI characteristics. Whiteman (1982) described inversion breakup in a conceptual framework that is still widely referenced today and has been measured in many studies to be a physical pattern (e.g. Kossmann et al., 1998; Chemel & Chollet, 2006; Dawn Reeves et al., 2011). In this physical framework, there are three distinct processes of inversion breakup in mountain valleys (Figure 1.6). The first pattern is the breakup of SBIs from the bottom up as the valley surface is warmed by

incoming solar radiation. This results in a CBL forming from the surface upwards until vertical mixing is achieved in the entire stable inversion layer. The second process is through the descent of the top of the inversion into the valley, resulting in warming valley temperatures until the inversion erodes away. The air aloft begins sinking down towards the surface where air pressure is lower due to up-valley wind development. These parcels of air that are compressed and warmed as they sink and erode away the cold core of the SBI layer from top to bottom (Müller & Whiteman, 1988). This process has been observed to occur at times as the airmass aloft becomes increasingly unstable which can erode away the stable cold core of the SBI through mixing from aloft due to wind (C. D. Whiteman et al., 2001). Whiteman (1982) observed the second pattern of inversion dissipation occurred when there was substantial snow cover in the valley that resulted in little to no surface warming. The third pattern is a combination of the first two processes, where there is both sinking of the stable core and warming of the surface leading to a thickening CBL. This third process was observed in the vast majority of occurrences in the valleys of Colorado where the observation of the Whiteman (1982) SBI case study.

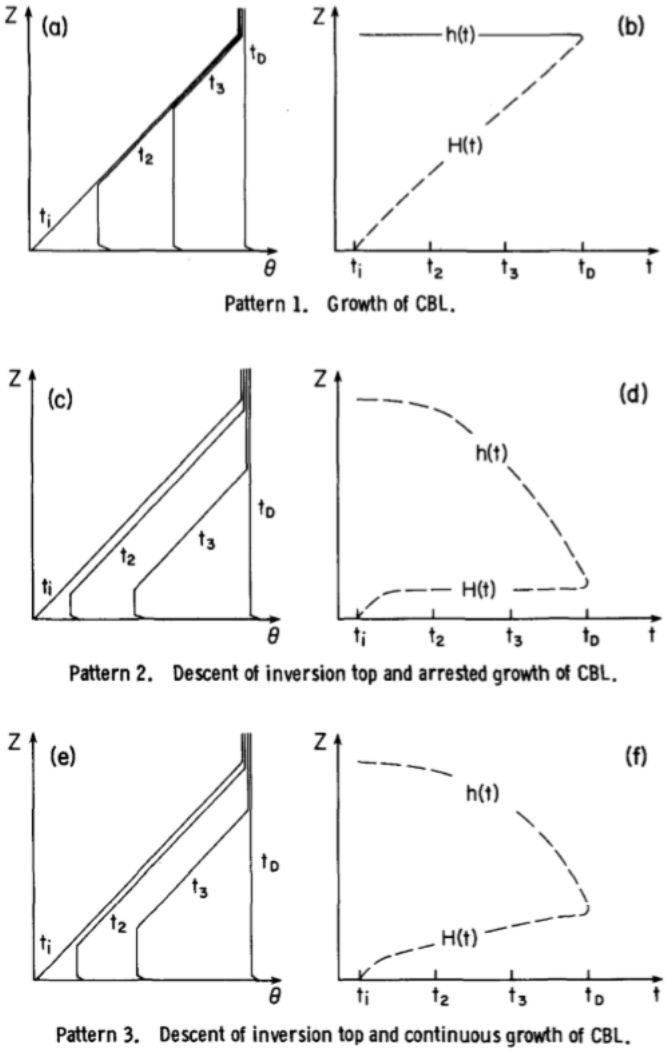

Figure 1.6: Conceptual model of the three processes of inversion breakup. Panels a, c and e represent vertical potential temperature profiles and b, d, and f have the bottom and top of the inversion layer marked with the broken lines (Whiteman, 1982, p. 273, © American Meteorological Society. Used with permission).

A fourth pattern of SBI breakup is less common but at times important in high-latitude regions, particularly over the Arctic Ocean. This process involves longwave radiation being trapped by cloud cover or surface water vapor and emitted back to the surface increasing the incoming radiation and bringing the surface radiation balance closer to zero (Maykut & Church, 1973). Serreze and Barry (2011) report that cloud cover and water vapor have been increasing in parts of the Arctic due to climatic change,

resulting in increased capture and emittance of longwave radiation, potentially influencing SBI breakup. This mechanism is particularly impactful in the winter months at high latitudes as there is little to no incoming solar radiation (Cohen et al., 2014). Thus, in the future this process may become an important mechanism to understand possible changes in SBI breakup due to climate change.

Each of these mechanisms have interconnecting elements. For example, Whiteman et al. (2001) found that inversions persisted until warmer more unstable air advected above the inversions and started mixing out the persistent layer of stratus cloud. This allowed for solar radiation to warm layers, resulting in the development and thickening of a CBL that broke up the persistent SBL layer. Interconnectedness of inversion breakup mechanisms produces the need to understand how macro and microclimate characteristics contribute to the breakup process in valleys.

1.11 MICROCLIMATIC AND MACROCLIMATIC INFLUENCES ON INVERSION CHARACTERISTICS

Differing valley characteristics and regional synoptic conditions result in local and regional spatial variability in how inversions develop, persist, and break up. Thus, macroclimatic and microclimatic factors need to be a focus of research when considering spatial variability of SBIs. Microclimatic and macroclimatic factors on SBI have been discussed throughout the literature, most commonly for mid-latitude mountainous areas.

Microclimate in this study refers to local scales across a landscape such as valley-to-valley conditions in mountainous locations. In the context of microclimate influences, Bader and McKee (1985) found in their modelling that there is a significant impact that

topography and vegetation have on inversion breakup in valleys. Colette et al. (2003) found a connection between inversion breakup patterns and shading of different parts of the valley on a sunny day. Furthermore, Anquetin et al. (1998) discussed that the time it takes for an SBI to breakup was impacted significantly by how effectively the valley wind patterns developed due to variable surface warming across the landscape. Sakiyama (1990) studied inversions in two Alberta valleys with differing attributes of orientation and geometry. One valley was wide and orientated East-West while the other was narrow and orientated North-South. They made significant conclusions regarding more extreme swings in temperature in the narrow valley compared to the wider valley due to rapid cold-air pooling at night and effective inversion breakup during the day. Joly and Richard (2019) found that SBIs were most frequent and intense at locations with high amplitudes between maximum and minimum temperatures.

Katabatic winds drive cold-air drainage and can be influenced by vegetation and angle of the slope (Garrett, 1983). Chen and Yi (2012) found that katabatic wind was slowed by forest canopy considerably. Oldroyd et al. (2014) developed a model for katabatic winds on slopes with short vegetation and slopes with forest canopy. They also found that the strength of canopy winds was reduced substantially on slopes with forest canopy. Katabatic wind strength and depth are stronger over gentle slopes (Haiden & Whiteman, 2005; Smith & Skyllingstad, 2005). For example, Grisogono and Axelsen (2012) found in their modelling that katabatic winds on gentle 3° slopes were as much as 3 m/s faster than 6 ° slopes. Longer fetch lengths are also conducive to a stronger katabatic wind layer (Wagner et al., 2015). Thus, katabatic winds are an example of

microclimate factors playing a substantial role in defining mechanisms of cold-air pooling and subsequent SBI development.

Macroclimate, or weather and climate on a global and regional scale, also influences SBI development, persistence, and breakup. Several studies highlight a strong variation from year to year in SBI characteristics (Kahl et al., 1996; Bourne et al., 2010; Zhang et al., 2011). On an interannual scale Bourne et al. (2010) found oscillations of inversion characteristics in Alaska that they attributed in part to large scale climate oscillation associated with the Pacific Decadal Oscillation (PDO). They found that there was a significant correlation of decreased I_z with increased PDO Index between 1957-1989 while this pattern was absent from 1990-2007. In another regional study regarding SBI in Greenland, Shahi et al. (2020) discussed that that the strengthening Greenland anticyclone is reducing cloud cover allowing for efficient radiative cooling during the night hours increasing I_z and I_{str}. SBIs have been observed to be associated with high pressure synoptic weather systems (Pepin et al., 1999; Blandford et al., 2008; Lu & Zhong, 2014). These conditions commonly occur in many high-latitudinal areas and are linked to frequent SBIs in Eurasia (Serreze et al., 1992) and Alaska (Mayfield & Fochesatto, 2013). Overall, macroclimatic influences in high-latitude areas have some connection, particularly through synoptic weather conditions. Limited work has been done to specifically quantify these interactions between macroclimate and SBIs in northwestern Canada. Thus, there is a need to research and discuss how SBI development, characteristics, persistence, and breakup are influenced by macroclimate regionally in northwestern Canada.

1.12 SPATIAL AND TEMPORAL VARIABILITY OF SURFACE-BASED TEMPERATURE INVERSIONS

The variability of microclimatic and macroclimatic factors across space and time result in temporally and spatially variable SBI characteristics at both local and larger regional to planetary scales. Several previous studies have reviewed this variability on different scales.

SBI are temporally variable on diurnal, interseasonal, interannual, and longer periods of time associated with changes in climate. Frequently studied is the pattern of SBI development following sunset at night with a gradual breakup after sunrise in the morning (Whiteman, 1982; Pepin, 2001; Colette et al., 2003; Mayfield & Fochesatto, 2013; Palarz et al., 2018). Peak I_{freq} transpires during times of day when the radiation balance at the surface is negative, and the subsequent breakup of inversions occurs when the radiation balance is positive (Whiteman & Richland, 2000) (Figure 1.7).

Beyond short-term temporal variability of SBI presence or absence is interseasonal variation. In high-latitude regions SBI are most frequent, stronger, and deeper during the winter season while they are the opposite during the summer season (Kahl et al., 1992; Serreze et al., 1992; Seidel et al., 2010; Mayfield & Fochesatto, 2013) (Figure 1.7). There is some disagreement to which season has the second greatest inversion attributes. Some have found SBIs to be most frequent and stronger during autumn compared to the spring (Zhang et al., 2011; Shahi et al., 2020) while other findings suggest the reverse of this pattern (Bourne et al., 2010).

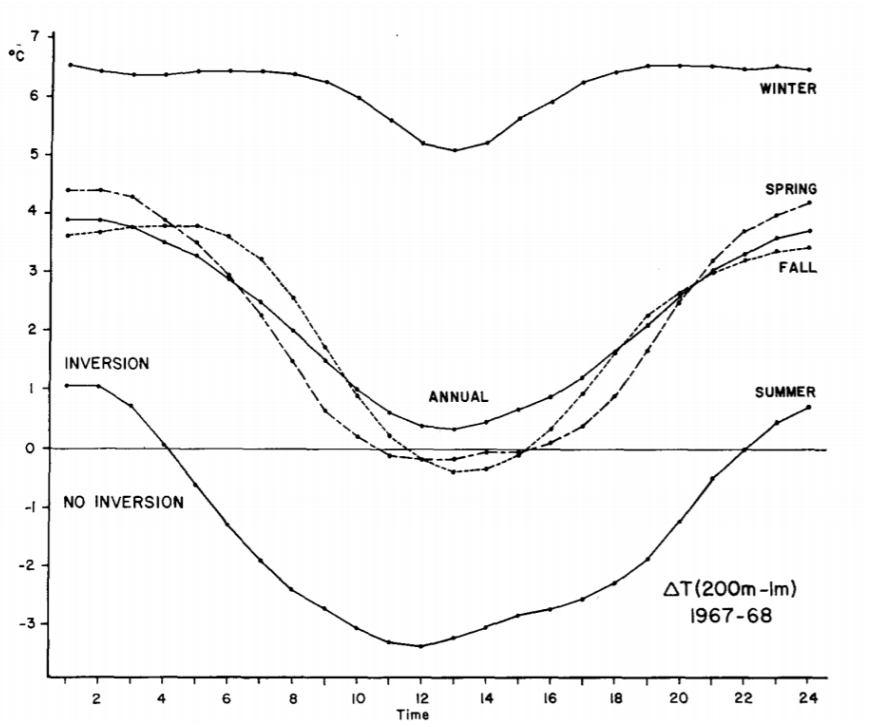

Figure 1.7: In this graph SLR from an elevational transect of 200 m in the high-latitude location Fairbanks Alaska (64.84° N, 147.72° W). Average SLR is determined for different times of the day depending on the season. Notice the seasonal and diurnal pattern of SLR. When SLR is positive there is an inversion present. On an annual basis SLR was gently inverted. The strongest inversions occurred in the winter while inversions were weak to non-existent during the summer (Wendler & Nicpon, 1975, p. 38).

An important aspect of temporal variability with SBI is the prospect of interaction between climate change over longer interdecadal or greater periods of time and SBI characteristics. With the impact SBIs impose on elevationally controlled SAT patterns in areas where they persistent frequently, adjustments to this SBI impact could prove significant. For example, if these SBIs are significantly altered by climate change there could be feedback loops of warming that further Arctic amplification (Chapman & Walsh, 1993). Therefore, understanding the interaction between SBI and changing climate is an essential aspect of research moving forward, particularly in regions such as northwestern Canada where SBI traditionally dominate.

Several physical reasons exist as to why climate change may drive alterations to SBI development, persistence, and break up. One reason is that atmospheric blocking may be leading to stagnant synoptic weather patterns at the surface (Röthlisberger et al., 2019). Changes can occur to the suitability for SBI development, persistence, and breakup depending on the type of synoptic patterns that may stagnate in a region (Blandford et al., 2008). For example, a high-pressure system promotes development of subsidence inversions as well as radiative cooling ground inversions due to clear skies and calm winds (Serreze et al., 1992). Another example was observed over southern Greenland where I_z, I_{str} and I_{freq} all increased temporally due to a stronger and more persistent high-pressure system (Shahi et al., 2020). Furthermore, changes in the frequency of synoptic weather conditions have been observed in Canada, including high-latitude regions where synoptic weather patterns are transitioning away from cold and dry synoptic patterns to more wet and warm synoptic patterns (Vanos & Cakmak, 2014). Finally, the rate of loss of sea ice has accelerated in the Arctic Ocean in recent decades (Derksen et al., 2012) which is consistent with the profound changes in atmospheric circulation is undergoing due to sea ice loss and climate in both high-latitudes (Serreze & Barry, 2011) and midlatitudes (Cohen et al., 2014).

There are multiple examples of research that have attempted to quantify the impact of climate change on SBI characteristics. Some studies used remote sensing techniques over the Arctic Ocean to review trends in inversion characteristics over time. For example, Liu et al. (2006) determined that SBIs and elevated inversions were decreasing in strength significantly in the Beaufort Sea from 1980-1996, but that some parts of the Arctic Ocean saw a significant increase in I_{str} during the same period. More

frequently, radiosonde data are used, which have records over several decades to provide the data necessary to review climate trends (Lovatt, 2009; Bourne et al., 2010; Zhang et al., 2011; Ji et al., 2019). Several radiosonde studies indicate that there is a trend towards decreasing I_z over time (Bradley et al., 1992, 1993; Walden et al., 1996; Bourne et al., 2010). Zhang and Seidel (2011) studied temporal trends in SBI characteristic across the Arctic and Antarctic and found that most trends from 1990 to 2009 in homogenous datasets of radiosonde date were not significant. The only trends that were significant at most of the stations was a positive correlation between trends in I_z and I_{str}. Shahi et al. (2020) suggest that differential warming across the surface related to snow cover and ice compared to exposed land surfaces drove strong variability of trends of I_{str} in this region. Some areas over exposed ground had decreasing I_{str} over time while areas over snow had increasing I_{str}. Lovatt (2009) reviewed trends from 1956 to 2003 in Whitehorse for I_z and I_{freq} using radiosonde data. They found that across that time period inversions generally were getting less deep but more frequent in Whitehorse. Overall, SBI trends discussed in the literature vary from region to region and across smaller areas within regions. There are no widespread trends of SBIs globally and in most cases even regionally. Trends discussed in this section temporally may be connected to changes to climate or, at least in part, inhomogeneities in radiosonde datasets (section, 1.13.1) (Lanzante, 1996; Zhang et al., 2011).

For spatial variability of SBIs we look at the regional or large scales which are defined in this research as SBI patterns from region to region and globally across the high latitudes such as from Siberia to Scandinavia, to Greenland, and to northwestern Canada. Regional scale, spatial patterns of SBI characteristics are better understood. The main

observed spatial pattern of SBI is increased I_{freq} has more broadly been observed with higher latitudes (>60 ° North or South) in both the Northern and Southern Hemispheres (Kahl et al., 1992; Seidel et al., 2010). One observed spatial pattern is that areas with higher I_{freq} were strongly correlated to being areas with both stronger and deeper SBI (Zhang et al., 2011).

Second, we review variation of SBIs across local or microscales which ranges from SBI pattern changes over small tens of km areas between mountain valleys to variable patterns of SBI occurring over hundreds of m distance within valleys. Microclimatic factors in valleys play a significant role in defining how SBI can develop, persist, and breakup which is manifested through inversion characteristics. Due to microclimatic factors significant differences in SBI characteristics have been observed in near proximity dissimilar valleys (Sakiyama, 1990). Studies comparing near proximity dissimilar valleys in high-latitude valleys are lacking. In doing so a better understanding of how SBI vary on the local scale will be made. Furthermore, quantification of how much SBI characteristics can change from one valley to the next is important in understanding and correcting for what limitations are in these small-scale variations. This will allow for an advance in understanding of how SBI influence on SAT differs from valley-to-valley, and what it means for the spatial variability of SBI impact on phenomena at and below Earth's surface, including permafrost.

1.13 METHODS OF MEASURING INVERSIONS

It has been established that research of SBIs in high-latitude areas is needed, particularly to improve understanding of interactions of SBI with permafrost. An important question is how SBI are quantified for the purpose of research. There are multiple methods to measure SBIs, each having advantages and disadvantages. An examination of these methods will be the focus of this section.

1.13.1 RADIOSONDE OBSERVATIONS OF INVERSIONS

Radiosondes are instruments carried up high into the atmosphere using large helium balloons that collect information on the vertical profile of Earth's atmosphere. Normally, at each participating location around the world ($n \approx 1300$) the sensors are released twice a day at 000 UTC and 1200 UTC (Lovatt, 2009). The benefit of these sensors is that they give an accurate vertical profile of the atmosphere that includes temperature, wind speed, wind direction, humidity, and atmospheric pressure over select locations twice a day using in-situ measurements (Gilson et al., 2018a).

The use of radiosonde data has been the most common form of measuring and studying free-atmosphere inversion characteristics (Liu & Key, 2003). Many studies have used radiosonde data to study SBI and elevated inversions in high-latitude locations (Bradley et al., 1992, 1993; Connolley, 1996; Lovatt, 2009; Bourne et al., 2010; Zhang et al., 2011; Gilson et al., 2018a). Zhang et al. (2011) used radiosonde data to review I_z, I_{str}, and I_{freq} across Arctic and Antarctic areas and determined that these SBIs were weaker, less deep, and less frequent in northwestern Canada compared to Alaska and Siberia. Gilson et al. (2018a) connected fog presence to deeper inversion occurrence in Greenland

using a radiosonde dataset. I_{freq} dropped rapidly, and elevated inversions occurred much more commonly during the summer months at radiosonde locations in the Canadian Arctic (Kahl et al., 1992). While inversion characteristics across the high-latitudes have been quantified using radiosonde data, the actual impact of SBI on SATs across high-latitude areas has yet to be completed for most locations. This work was started in an M.Sc. thesis for one location (Whitehorse) (Lovatt, 2009) but was never published. Thus, there is an opportunity to expand on this type of research and quantify the impact of SBI on SATs at select locations with radiosonde data. There are three limiting factors of using radiosonde data to measure SBIs. First, they are only collected twice a day which makes the temporal resolution of the dataset low (Bourne et al., 2010). Second, there are few locations where radiosonde data are collected (mostly World Meteorological Organization weather stations), particularly in high-latitude locations (Zhang et al., 2011). For example, in the immense area of Northwestern Canada (roughly 1.7 million km^2) there are only five locations at which radiosonde data is collected. Third, temporal trends in radiosonde data may be connected to, at least in part, inhomogeneities in radiosonde datasets rather than actual physical processes of climate change. Inhomogeneities in radiosonde datasets most often originate from changes in radiosonde equipment through time to improve vertical resolution of the climate condition measurements (Walden et al., 1996). Increased vertical resolution tends to result in artificially produced decreasing trends of I_z while I_{str} can also be significantly altered. Thus, finding trends of SBIs, if any, using radiosonde data can be challenging particularly across long periods of data where large inhomogeneities exist (Zhang & Seidel, 2011). There have been some methods created and applied to clean up data inhomogeneities in radiosonde datasets to improve accuracy and predict trends that are solely linked to natural phenomena rather than

instrumentation change (Lanzante, 1996; Lanzante et al., 2003; Zhang & Seidel, 2011; Zhou et al., 2021).

1.13.2 ELEVATIONAL TRANSECTS USING TEMPERATURE LOGGERS

The lack of radiosonde data across large remote areas has begun to be addressed by the set-up of a multitude of elevational transects of temperature loggers. These have also been used to quantify I_{str} and I_{freq} (Taylor et al., 1998; Antoni G. Lewkowicz & Bonnaventure, 2011; Pike et al., 2013; Williams & Thorp, 2015; S. L. Smith & Bonnaventure, 2017). This method requires only one visit a year to the site to download data collected by the sensors which makes it possible to deploy these sensors in areas that are difficult to access in seasons other than summer. One limitation to this method is that it is labour intensive and requires considerable time and effort in the field to deploy and maintain every 1-2 years. However, this method is useful for the acquisition of accurate in-situ measurements of SLRs in areas that can be compared directly with other methods of lapse rate quantification.

1.13.3 CLIMATE REANALYSIS DATASETS

Another method of addressing large spatial gaps in SBI data is by utilizing climate reanalysis products (e.g. Shahi et al., 2020). Climate reanalysis datasets are interpolated estimates of atmospheric parameters such as air temperature, precipitation, or air pressure across a continuous surface-based on observations combined with climate modelling (Compo et al., 2011). Limits of using climate reanalysis data is that they are based on coarse resolution climate models which can cause significant error in areas of complex terrain (Riseborough et al., 2008). Recent efforts have been made to incorporate elevation

algorithms in complex terrain and downscale the climate surface data to adequately account for temperatures and precipitation across these areas (Cannon et al., 2012). A few examples of such downscaled climate data specific to a point location rather than a continuous surface include the program ClimateNA (Wang et al., 2016) and GlobSim (Cao et al., 2019). These programs attempt to account for local variation in climate conditions but there are still significant limitations in predicting variability of lapse rates over small distances as is observed from in-situ measures (Minder et al., 2010). Direct comparisons between in-situ measures and those predicted by downscaled climate reanalysis data will lead to identification of any limitations of these models in predicting accurate SLRs. Comparison of SLR data collected in-situ to SLR predicted by downscaled climate reanalysis products in northwestern Canada where SBIs dominate has not yet been completed.

1.13.4 REGIONAL CLIMATE MODELS

Regional Climate Models (RCMs) are an alternative to Coupled Global Climate Models that have a high computational cost and too course of a grid to resolve many climatological processes in a meaningful and accurate way (Laprise, 2008). RCMs simulate processes in the atmosphere and include interactions of these with surface conditions on a regional and local scale (Rummukainen, 2016). Some processes that are missed by Global Climate models due to their coarse resolution, include mesoscale convective systems, sea-breeze and valley wind type circulations, and surface wind variability (Christensen et al., 2007). RCMs developed for high-latitude regions produce relatively widely differing results depending on the climate model selected and physical parameterizations of the models (Rinke et al., 2006). RCMs were used in the Arctic to

review interactions between inversions and warming SATs. A significant positive relationship was found for the winter months in continental areas indicating a potential breakdown of Arctic atmospheric stability that may contribute to accelerated surface warming (Akperov et al., 2019). The Weather Research and Forecasting regional model reviewed moisture levels and temperatures over snow covered surfaces of high-latitude areas in the Arctic and Antarctic. The authors noted an underestimation of temperature inversions using the regional climate modelling (Sterk et al., 2015). RCMs are continuing to be improved and can operate upwards to 1 km resolution (Rummukainen, 2016). That said, these spatial resolutions remain too coarse to capture the variability in complex topography (Etzelmüller, 2013). Best practices to predict SATs with RCMs in complex terrain are to incorporate temperature lapse rate corrections based on topography to locate areas prone to cold-air pooling and subsequent SBI prevalence (Praskievicz & Bartlein, 2014).

1.13.5 REMOTE SENSING METHODS

Remote sensing provides an opportunity to measure continuous spatial data (grid data) for inversion characteristics (Palarz et al., 2018). First, Liu and Key (2003) used MODIS satellite data (7.2-μm water vapor and 11-μm infrared window bands) with some success to measure and quantify SBI over the Arctic Ocean from 2000 to 2002. In this study the mean square error of I_{str} was able to be kept below 3 °C for times during clear sky conditions. Similar methods were used on High Resolution Infrared Radiation Sounder data from the TIROS-N OperationalVertical Sounder satellite (Liu et al., 2006). The authors did this to quantify I_{str} over the Arctic Ocean and coastal land areas for the period of 1980 to 1996. In their research the authors identified spatial patterns of SBI

including the strongest SBI being situated in deep river valleys of Canada and Russia. The most obvious limits of quantifying I_{str} using this method on MODIS (High Resolution Infrared Radiation Sounder) satellite data is spatial resolution of only 1 km (17 km) and that cloudy conditions derailed any ability to quantify I_{str} (Liu & Key, 2003; Liu et al., 2006). Devasthale et al. (2010) further highlights that the limit of this work is that there is no quantification of I_{freq} due to lack of measurements during cloudy conditions. In 2002 an Atmospheric Infrared Sounder (AIS) was launched onboard the Terra and Aqua satellites (Devasthale et al., 2010). This AIS provides data regarding the vertical profile of the atmosphere that has a sharp vertical resolution (Chang et al., 2018). Devasthale et al. (2010) applied the new AIS to analyze I_{str} and I_{freq} over the Arctic during winter and summer from 2003 to 2008. The limits of their data still included issues of coarse spatial resolution and cloud cover impeding the ability to analyze the inversions. Chang et al. (2018) attempted to address the issue of cloud cover by applying cloud fraction to their analysis. They successfully developed a process of determining I_z and I_{str} with root mean squared error of <86 m and <1.7 °C respectively. Another promising method of remote sensing that provides an improved understanding of SBI in the Arctic is radio occultation sensors that work in all weather conditions (Chang et al., 2017). Furthermore, MODIS land surface temperature data were used in permafrost modelling coupled with a climate reanalysis dataset (ERA-Interim). This method had some success that was limited to the Siberian region in predicting influence of SBI on SAT (Obu et al., 2019). There is an increasing number of options when using remote sensing methods to monitor inversions, particularly over more homogeneous areas of land or sea, including over the Arctic Ocean. The major issue of remote sensing methods in mountainous areas remains coarse spatial resolution of data collected (Sun et al., 2010). Thus, local

heterogeneity of areas with complex terrain is left unaccounted for by coarse resolution methods such as these remote sensing methods (Etzelmüller, 2013).

1.14 KNOWLEDGE GAPS

This chapter introduced the two primary phenomena, SBIs and mountain permafrost, that that are the focus of this thesis. Connections between these phenomena in the atmosphere and the state of permafrost are extensively discussed. The most pertinent knowledge gaps are summarized in the following points:

- The lack of a regional study of how SBI characteristics vary spatially and temporally across the region of northwestern Canada.
- Conceptualization and quantification of the impact of SBI on SAT and how this varies with elevation.
- Understanding how regional macroclimatic patterns and Earth surface patterns (incl. ocean oscillations and sea ice coverage) impact SBI characteristics across northwestern Canada.
- Application of elevational transects positioned in near proximity high-latitude dissimilar valleys where SBI dominate to compare local scale variation of SBI characteristics.
- An assessment of the ability of climate reanalysis downscaling products and their ability to accurately predict SLRs in SBI-dominated high-latitude valleys using in-situ SLR data.
- The overarching knowledge gap driving this work is how elevation SAT patterns that are being driven by variability of SBI characteristics across space and time

are contributing to permafrost distribution patterns and future thaw patterns of permafrost.

1.15 HYPOTHESES

The objectives of this thesis are shaped around several hypotheses that were developed from current understanding of how SBIs, SATs, and permafrost interact. The overlying hypothesis driving the objectives of this thesis research is that SBI inversions have a significant impact on SATs and subsequent permafrost distribution in northwestern Canada. The hypotheses reviewed in this thesis include:

- SBI impact varies spatially between the five sites sampled in the northwestern Canada region
- SBI impact on SAT varies temporally due to climatic factors including climate change and macro scale climate oscillations
- Mountain valley locations have the largest inversion impact in northwestern Canada due to cold air pooling.
- Significant impact of inversions on SATs and permafrost distribution occurs on a local valley scale in northcentral Yukon
- SBI characteristics vary significantly between the two valleys due to valley dissimilarities including orientation, geometry, and vegetation cover.
- Variation in microclimate conditions such as air temperature, wind speed, wind direction, incoming solar radiation, and snow cover between the valleys significantly influences patterns of SLRs.
- Downscaled climate reanalysis data needs to have SBI impact below treeline in northcentral Yukon valleys considered when utilized for local scale applications.

1.16 OBJECTIVES

The overarching objective of this thesis project is to quantify and describe the impact SBIs have on SATs and subsequent permafrost distribution in northwestern Canada. If there is indeed a significant impact of SBI, spatial and temporal variability will be reviewed on regional and local scales. The main objective can be broken down into two broad objectives that are the central objectives for each of the two manuscripts included in chapters 2 and 3 of this thesis. These two chapters each contain objectives and sub-objectives that include:

1. To test whether there is a significant impact of SBI on SAT and how this impact varies geographically and temporally by using radiosonde data from five sites in northwestern Canada and explain the resulting patterns that are observed.
    1.1. To define and quantify a new variable, Inversion Impact (I_{imp}), which combines various SBI properties and can be used to express the impact of SBI on SAT.
    1.2. To compare the new inversion characteristic to the traditional characteristics to assess whether this new metric highlights spatial and temporal variability not observed in any single traditional SBI characteristic
    1.3. To quantify the spatiotemporal patterns and trends of SBI across northwestern Canada.
    1.4. To discuss these temporal and geographical patterns and how they relate to macroclimatic phenomena such as coupled ocean-atmospheric climate variability and sea ice coverage.

2. To test the regionally assumed SLRs in two dissimilar valleys in the Ogilvie Mountains in Yukon, northwestern Canada and assess whether there is significant variance of SBI characteristics between the valleys.

2.1. To quantify and compare inversion characteristics of I_{freq} and I_{str} and resulting SLRs in each valley.

2.2. To compare observed SLRs with previously assumed SLRs for this region

2.3. To investigate possible correlations between microclimatic conditions and SLRs in the two valleys.

2.4. To assess the limitations of using downscaled climate reanalysis data in valleys with strong and frequent SBIs.

2.5. To conceptualize and discuss how the local scale variability of inversion characteristics between the two valleys effects the distribution of permafrost on a local scale.

Chapter 2

Surface-based temperature inversion characteristics in northwestern Canada from radiosonde data between 1990 and 2016

Manuscript planned for submission to: Journal of Applied Meteorology and Climatology

Authorship: *Nick C. Noad[1], Philip P. Bonnaventure[1], Gaëlle F. Gilson[2], Hester Jiskoot[1] & Madeleine C. Garibaldi[1]

[1]Department of Geography and Environment, University of Lethbridge, Lethbridge, AB, T1K 3M4, Canada

[2]Earth and Life Institute, Université catholique de Louvain, Louvain-la-Neuve, Belgium

*Corresponding Author email: nick.noad@uleth.ca

Key words: Radiosonde, Surface-based temperature inversions, Arctic Canada, Climate change, Cryosphere

2.0 ABSTRACT

Assumptions regarding lapse rates in regions prone to frequent and persistent surface-based inversions (SBIs) can generate significant biases in the prediction of surface air temperatures (SATs). Although studies of SBI in Arctic regions are common, few regional studies of SBI characteristics exist in high-latitude regions with significant topography, and in particular those investigating the impact of SBI on SAT. To address this regional gap, vertical atmospheric temperature profiles for five sites in northwestern Canada were analysed using archived radiosonde data from 1990-2016. A novel SBI metric, Inversion Impact (I_{imp}), was developed by combining the traditional SBI characteristics of depth, strength, and frequency, and was used to quantify the impact of SBI on cooling SAT on annual and seasonal scales. Annual I_{imp} > 5°C and winter I_{imp} of ~ 10°C occur locally, while regional and macroclimatic elements influence the magnitude of I_{imp} uniquely at each site. A weak relationship between sea ice extent in the Beaufort Sea and I_{imp} manifests across both coastal and some inland parts of the study area. Additionally, topographic analysis of areas surrounding each radiosonde location reveal highly variable I_{imp} in complex mountain areas and more consistent I_{imp} across areas of low relief. I_{imp} significantly declined over the period 1990-2016 at most sites though the magnitude of these trends varied spatially, and some sites suffer from radiosonde data inhomogeneities. The results from our study are important for regions where SBI contribute to climatic conditions maintaining cryospheric elements such as permafrost.

2.1 INTRODUCTION

The free-atmosphere within the troposphere has an average environmental lapse rate (ELR) of 6.5°C km^{-1}, but there can be significant deviations from this gradient of temperature decrease with increasing altitude or elevation (Oke, 1987). In some cases, typically during nighttime or in winter months, lapse rates can become inverted in which temperature increase with altitude or elevation (Gustavsson et al., 1998). This phenomenon is known as a temperature inversion (Kahl et al., 1992). Temperature inversions that begin at or near Earth's surface are known as surface-based inversions (SBIs) and can vary in thickness and intensity. SBIs are primarily measured at weather station locations where weather balloons with radiosonde sensors are released manually, typically at diurnal frequencies. In regions with complex mountainous terrain or in remote high-latitude areas, such as in northern Canada, weather stations are sparse and unevenly distributed (Urban et al., 2013; Pepin et al., 2015). As a result, the occurrence and strength of lapse rates is often inferred, which can generate significant errors associated with the prediction of surface air temperature (SAT) roughly 2 meters from the ground surface, particularly over complex topography (Etzelmüller, 2013). Frei (2014) modeled air temperatures in the European Alps and found that during the winter months systematic mean absolute errors in SAT of >3°C were expected in valley bottoms that experienced consistent local cold-air drainage. Furthermore, cold-air pooling and consequent atmospheric decoupling in mountain valleys indicate that local climates in mountainous regions may not respond in the same way to changes in synoptic circulation patterns and regional atmospheric warming (Daly et al., 2009). Therefore, a lack of understanding or consideration of cold-air pooling can have a significant impact on the accuracy of

modelled SAT distribution. Thus, the development of persistent or frequent SBIs repetitively in the same locations can have an impact on elevational patterns of SAT across elevation in mountain valleys (Bonnaventure & Lewkowicz, 2013).

The presence and characteristics of inversions at high latitudes have been researched quite extensively (Bintanja et al., 2011; Lesins et al., 2012; Serreze and Barry, 2014; Gilson et al., 2018a; Shahi et al., 2020). However, few studies have examined inversion interactions with medium-scale geomorphic features and elements of the terrestrial cryosphere such as glaciers (Mernild and Liston, 2010), sea ice (Liu et al., 2006), or its influence on the distribution of permafrost (Bonnaventure and Lewkowicz, 2013). Permafrost is perennially frozen earth materials which remain at or below 0°C for two or more consecutive years. As permafrost thaws, previously frozen organic matter is able to decompose which contributes to the increase of greenhouse gas concentrations in the atmosphere (Helbig et al.,2017). A major driving factor of permafrost distribution and thaw is mean annual air temperature (MAAT) (Smith & Riseborough, 2002; Riseborough et al., 2008). Permafrost distribution and thermal state at high latitudes is theorized to be influenced by SBI because cold stable air collects and persists in valley bottoms due to minimal turbulent fluxes and low sun angle limiting mixing potential. Several studies have addressed the potential link between permafrost distribution and SBIs in mountainous environments (Taylor et al., 1998; Cote, 2002; Lewkowicz & Ednie, 2004; Bonnaventure & Lewkowicz, 2008; Lovatt, 2009). Recently, the effects of inversions on permafrost distribution in complex topography has been better quantified and incorporated into permafrost distribution modelling (Lewkowicz & Bonnaventure, 2011; Bonnaventure et al., 2012; Smith & Bonnaventure, 2017). This inclusion allowed for the

creation of a conceptual framework by Bonnaventure and Lewkowicz (2013) which was developed based on in-situ air, ground, and TTOP sensor measurements. The framework predicted that permafrost distribution in high-latitude, continental mountain regions is at least in part a product of persistent SBIs. Hence, permafrost is present in valley bottoms and on mountain tops, while often absent around treeline (Bonnaventure and Lewkowicz, 2013). These hypothesis and assumptions need to be tested on a regional scale in northwestern Canada and this is the main aim of this research.

As climate change has been and is predicted to be amplified in high-latitude areas (Serreze & Barry, 2011) understanding how SBIs evolve becomes critical. One approach to study changing inversion characteristics is to use radiosonde data to review climate trends (Lovatt, 2009; Bourne et al., 2010; Zhang et al., 2011). Long-term trends in inversion characteristics have been examined using radiosonde data in the coastal Arctic Ocean of North America (Kahl, 1990; Bradley et al., 1992; Bradley et al., 1993), the Canadian Arctic (Kahl et al., 1992; Lesins et al., 2012) and more broadly across the entire Arctic and Antarctic (>60°N & °S) (Zhang et al., 2011). However, more detailed analyses of SBIs in relatively smaller regions, like those found in Alaska (Bourne et al., 2010) or Greenland (Shahi et al., 2020), are still lacking. Thus, few studies have examined SBIs in high latitude, continental areas that are experienceing rapid changes in climate. The objective of this research is to test whether there is a significant impact of SBI on SAT and how this impact varies geographically and temporally by using radiosonde data from five sites in northwestern Canada. To achieve this objective, we expand on the traditional SBI characteristics of strength, depth, and frequency by creating a new term called inversion impact (I_{imp}). Partly inspired by an unpublished study (Lovatt, 2009), I_{imp} allows

for the quantification of theoretical SBI contribution to SAT. We aim to then compare I_{imp} to the traditional SBI characteristics and assess whether it can highlight spatial and temporal variability absent in the individual traditional characteristics. The assumption that SBIs are correlated with colder SATs will be tested by comparing annual average SAT anomalies and annual average inversion impact. Macroclimate telecommunications influence on inversion impact such as climate oscillations or sea ice area will be examined. Finally, we will discuss the variation of I_{imp} across the topography surrounding each site and test the assumption that I_{imp} is strongest in mountain valley locations due to cold air pooling. Findings from these analyses will provide opportunity to better understand the evolution of SBIs in a changing climate and how SBIs and elements of the cryosphere are linked.

2.2 STUDY REGION

Five stations in northwestern Canada were selected as they represent the only stations with continuous archived radiosonde data within the (sub-) Arctic climate zone in northwestern Canada (Table 2.1; Figure 2.1). Specific sites range from mountain valleys (Whitehorse, Fort Nelson, and Norman Wells) to flat forested areas (Fort Smith), and a coastal delta (Inuvik). Inuvik is maritime Arctic and located 80 km from the Arctic Ocean (Beaufort Sea) which typically remains ice-covered between October to late May each year (Johnson and Eicken, 2016) while the other four sites are continental. SBI have been frequently observed during the winter months at both Fort Nelson and Norman Wells (Klock et al., 2002; Klock & Mullock, 2002) and year-round across the maritime Arctic (Serreze and Barry, 2014; Przybylak, 2016). Permafrost at Whitehorse, Fort Nelson, and Fort Smith is classified as sporadic discontinuous meaning 10-50% of the landscape is

underlain by permafrost. Norman Wells is classified as extensive discontinuous (50-90% coverage) while Inuvik is classified on the boundary between extensive discontinuous and continuous (90-100% coverage) (Heginbottom et al., 1995). All sites, with exception of Inuvik, are surrounded by forest.

Table 2.1: Summary of study site attributes for each radiosonde location. These attributes include latitude, longitude, elevation, Köppen Classification (Atlas of Canada, 1957), mean annual air temperature MAAT (1981-2010) (Environment Canada, 2020), Increase of mean annual temperatures from 1948-2016 (Zhang et al., 2019), temperature amplitude (the absolute value of the difference between the warmest and coldest month average temperature) annual precipitation (Environment Canada, 2020), percent range of land surface underline with permafrost (Heginbottom et al., 1995), and time zone where PST stands for Pacific Time zone and MST stands for Mountain Standard Time zone.

	Whitehorse	Fort Nelson	Fort Smith	Norman Wells	Inuvik
Latitude (°N)	60.71	58.84	60.02	65.28	68.31
Longitude (°W)	135.08	122.59	111.92	126.79	133.49
Elevation (m a.s.l.)	706	382	205	73	68
Köppen Classification	Dsc	Dfc	Dfc	Dfc	Dfc
MAAT (°C)	-0.1	-0.4	-1.8	-5.1	-8.2
MAAT Increase 1948-2016 (°C)	2.3	2.0	2.5	3.0	3.3
Temperature Amplitude (°C)	29.5	37.4	39.6	43.0	40.1
Annual Precipitation (mm yr^{-1})	262.3	452.1	353.6	294.4	240.6
Permafrost Coverage (%)	10-50%	10-50%	10-50%	50-90%	90-100%
Time Zone	PST	MST	MST	MST	MST

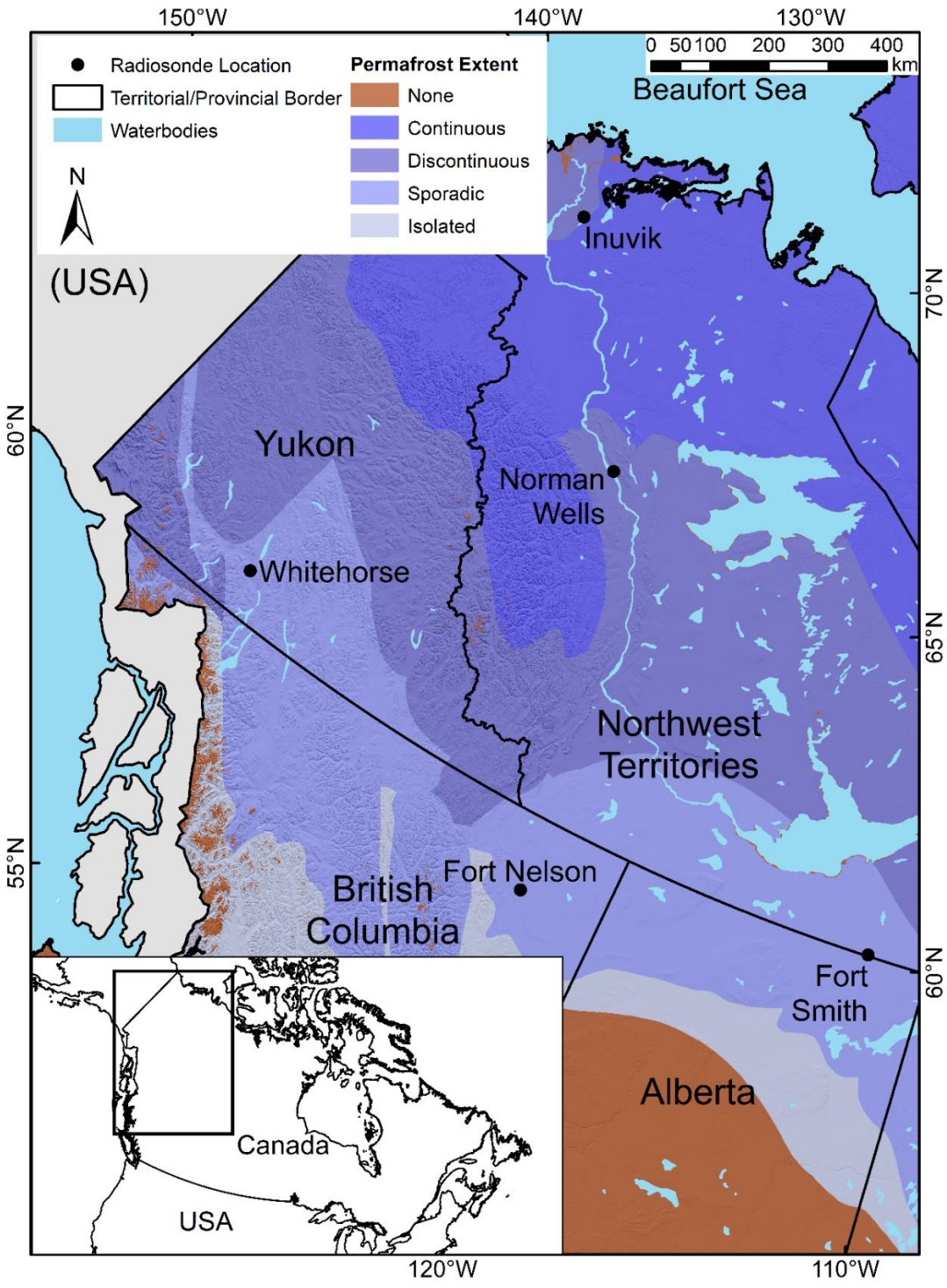

Figure 2.1: Study area with the location of five weather stations for which radiosonde data were obtained through the Integrated Global Radiosonde Archive. Permafrost distribution zones are also included on the map (Brown et al., 2002).

2.3 METHODOLOGY

2.3.1 EXTRACTION OF SOUNDINGS

Upper-air soundings were obtained from the quality-controlled Integrated Global Radiosonde Archive (IGRA) (Durre et al., 2006) for the five locations in Northwestern Canada (Figure 2.1). The period selected for this study was 1990-2016 in order to avoid inhomogeneities caused by sonde switches, station relocations and radiation corrections. Since the early 90s, all stations have been using Vaisala sonde models RS80, RS90 and RS92. IGRA usually contains twice-daily soundings for each station, typically at 0000 UTC and 1200 UTC. Each sounding contains information at mandatory pressure levels (e.g., 1000, 925, 850, 700 hPa, etc.), as well as additional pressure levels where slope breaks in temperature or humidity occur. Dry-bulb temperature (T) (resolution 0.5 °C) and geopotential height (resolution 25 m) were extracted. In addition, we used the atmospheric pressure to select the 700 hPa pressure level (~3000 m a.s.l.), below which the sounding must contain at least five levels in order to be retained for inversion analyses (Kahl, 1990; Gilson et al., 2018a, b). Over the 27-year study period, the total number of soundings at each station varied slightly between the sites (Table 2.2). Missing soundings were often found clustered together in groups of months, with the most notable data gaps at most sites occurring in winter and spring of the mid-1990s (Figure 2.2).

Table 2.2: The number of actual radiosonde soundings, possible radiosonde soundings, and percent completeness of the dataset during the study period (1990-2016).

	Actual Soundings	Possible Soundings	Completeness of Data (%)
Whitehorse	17278	19724	88
Fort Nelson	16995	19724	86
Fort Smith	17998	19724	91
Norman Wells	17656	19724	90
Inuvik	18143	19724	92

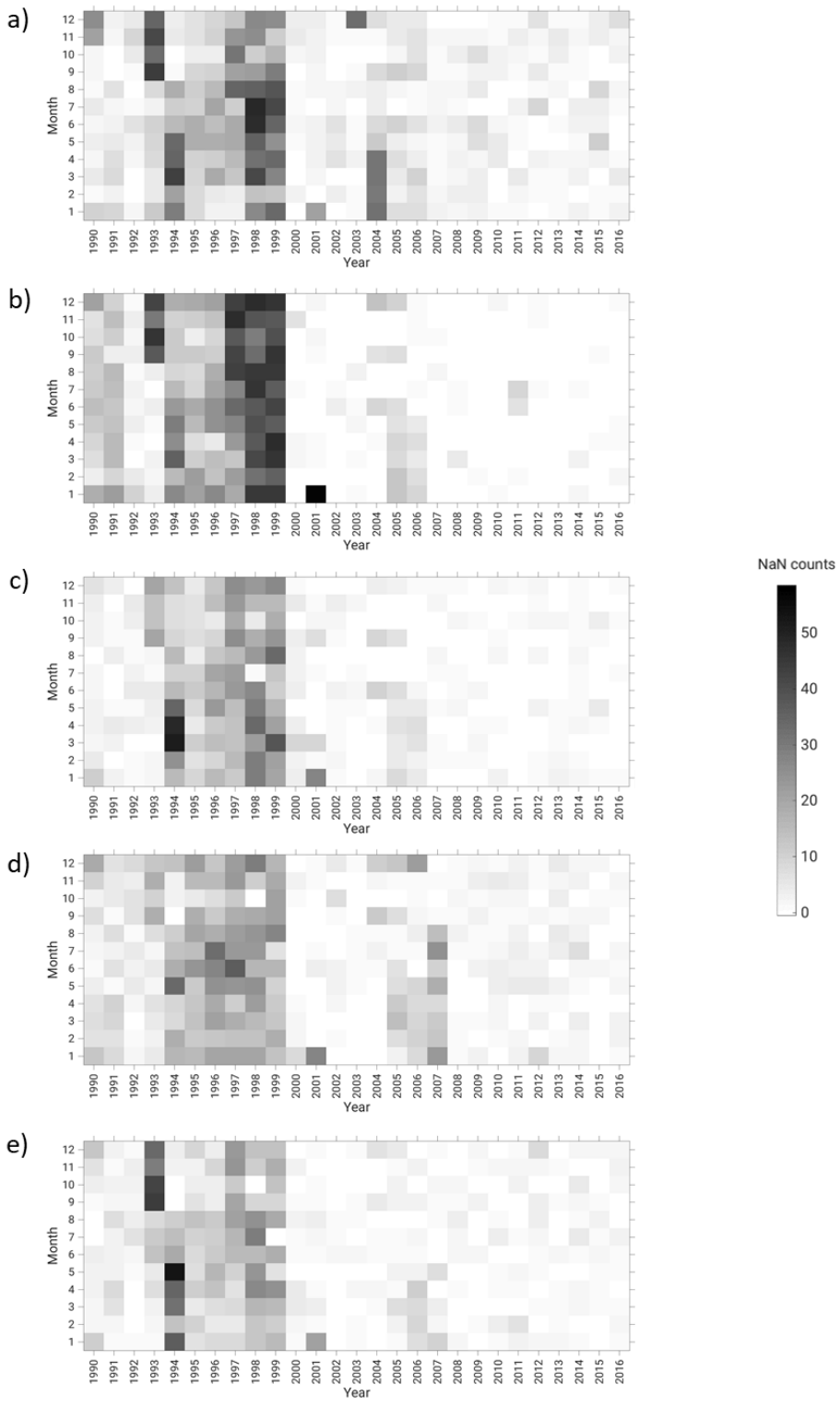

Figure 2.2: Monthly sum of missing sounding observations (NaN counts) based on twice-daily radiosonde launches for the period 1990-2016 at a) Whitehorse, b) Fort Nelson, c) Fort Smith, d) Norman Wells, and e) Inuvik.

2.3.2 IDENTIFICATION OF SURFACE-BASED INVERSIONS AND METRICS

We used the method developed by Kahl (1990) to identify SBIs in IGRA soundings. Archived radiosonde data were parsed using an R coded computer program specifically developed for this work which identified soundings where T started to increase with elevation within 100 m of the surface. The top of an SBI is the altitude where T starts to decrease with height above an inversion layer. Thin layers (< 100 m) of positive T lapse rates embedded within an inversion or located below a low-level inversion (shallow mixed layers), were considered part of that inversion.

2.3.3 INVERSION CHARACTERISTIC METRICS

Once the SBI events were identified at each site, traditional descriptive characteristics of inversion depth, strength and frequency were calculated to describe important aspects of how an inversion develops and persists. These inversion characteristics were calculated on monthly, seasonal (based on four meteorological seasons e.g., December, January and February comprise winter months), and annual basis. Inversion strength (I_{str}) is the difference between the temperature at the top and bottom of the SBI (Bourne et al., 2010; Wei et al., 2013) and is sometimes termed inversion intensity (e.g. Zhang et al., 2011; Joly & Richard, 2019). Inversion frequency (I_{freq}) is the proportion of soundings with an SBI recorded relative to the total number of radiosonde soundings. To account for missing soundings, monthly I_{freq} was calculated by dividing the sum of the number of soundings with an SBI present by the total number of radiosonde soundings recorded each month. Inversion depth (I_z) is the difference between altitude of the SBI base and top of SBI layer.

First the projected surface air temperature (PSAT) was computed by taking the product of the I_z and the average ELR of -0.0065 °C m^{-1} (Equation 2.1). PSAT quantifies how much warmer the surface would be if the lapse rate remained at the normal ELR from the top of the SBI layer to the surface. Inversion magnitude (I_{mag}) is the sum of I_{str} and the PSAT (Figure 2.3; Equation 2.2).

$$PSAT = (I_z \times ELR) \quad (2.1)$$

$$I_{mag} = PSAT + I_{str} \quad (2.2)$$

The product of I_{mag} and I_{freq} is taken to determine an overall theoretical inversion impact (I_{imp}) on surface MAAT (Equation 2.3).

$$I_{imp} = \frac{I_{mag\ (000\ UTC)} \times I_{freq\ (000\ UTC)} + I_{mag\ (1200\ UTC)} \times I_{Freq\ (1200\ UTC)}}{2} \quad (2.3)$$

Here, $I_{mag\ (000\ UTC)}$ ($I_{mag\ (1200\ UTC)}$) represents the inversion magnitude in °C and I_{freq}. 1200 UTC soundings for all sites (except for Whitehorse) are taken at 500 local time (400 local time) and 000 UTC soundings at 1700 local time (1600 local time).

In addition, SBIs were classified according to duration: either as transient or persistent, based on a classification system developed by Whiteman et al. (2001). Transient SBI events occur when a SBI is recorded in two or less consecutive radiosonde readings (SBI length <24 hours). Persistent SBI events have three or more consecutive radiosonde readings with an SBI present (SBI length ≥24 hours).

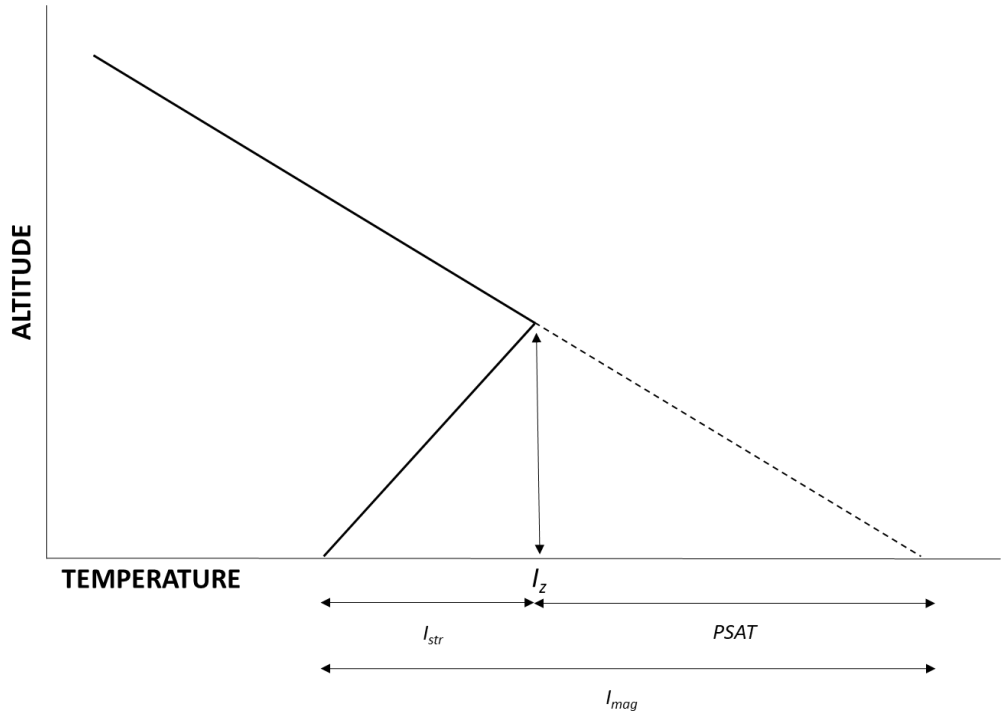

Figure 2.3: Conceptualization of surface-based inversion metrics used in this study: inversion depth (I_z), inversion strength (I_{str}), inversion magnitude (I_{mag}), and projected surface air temperature (PSAT). The dashed line highlights how much warmer the temperature would be if the SBI was absent and lapse rates averaged the ELR. The I_{str} added to the projected surface warming gives the magnitude of the inversion.

2.3.4 DATA ANALYSIS

For each of the five sites, the descriptive monthly, seasonal, and annual SBI characteristic statistics were produced for the 27-year study period (1990-2016), allowing for a geographical, interannual, and long-term trend analysis of SBIs. Statistical differences between sites and seasons were tested using an analysis of variance (One-way ANOVA) ($p<0.05$) as the data were normally distributed. Data normality was determined through Kolmogorov–Smirnov goodness of fit test.

2.3.5 TRENDS OF INVERSION CHARACTERISTICS

A trend analysis for each inversion characteristic across the 27-year study period was completed using linear regression with a significance of $p<0.05$. To account for possibility of skewed data due to outlying data points, Theil-Sen regression with a Mann-Kendall test was also completed for the 27-year each inversion characteristic at each study location.

Inhomogeneities are common in radiosonde data and can skew existing or create artificial trends when using linear regression for long-term change analysis on these datasets (Gaffin, 1994; Lanzante, 1996). Points of change or step changes in radiosonde data occur commonly due to instrumentation change, which can very from country to country (Walden et al., 1996; Zhang and Seidel, 2011). Zhang et al. (2011) found that large step-changes in SBI characteristics occurred because of radiosonde data inhomogeneities. Step-changes are linked to vertical resolution improvements for radiosonde readings which can significantly alter I_z and strength (Zhang et al. 2011).

The number of soundings below the 500 hPa pressure level were plotted for each site (Figure 2.4) and a series of step changes were found (with exception of Norman Wells). The periods inbetween these step-changes were considered homogeneous periods. These were identified by using linear regression to find periods of time where the number of soundings were significantly unchanging or consitstant. In some cases, there were outlying years within the homogenous period with significantly more or less radiosonde soundings below the 500 hPa layer (Figure 2.4). As such, the years 1993, 1994, 1998, and 1999 at Whitehorse and 1993 and 1994 at Inuvik were excluded from the homogeneous period. When these years were excluded from the linear regression consistency in the

number of soundings below 500 hPa was found. Trends across the homogeneous periods were then compared to trends during the entire study period.

While this method does not remove all potential data inhomogeneities, the bulk of the inhomogeneities that drive artificial temporal change of SBI characteristics are removed (Zhang and Seidel, 2011). The main contributor of data inhomogeneity in the radiosonde datasets, increasing number of soundings, are accounted for through the selected homogenous periods within the datasets.

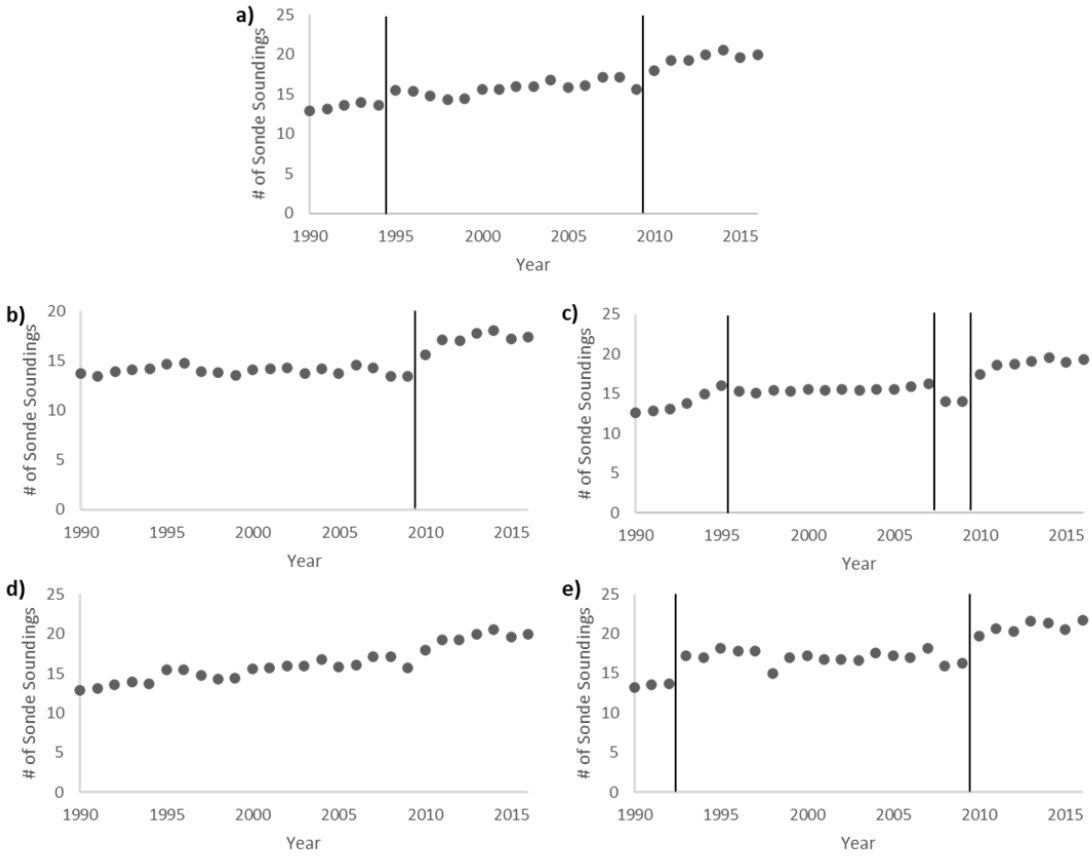

Figure 2.4: Changes in the number of radiosonde soundings collected below 500 hPa during the study period (1990-2016). The step changes in the mean number of soundings below 500 hPa for each radiosonde release is denoted by the vertical solid black lines on the graph. The five locations are as a) Whitehorse, b) Fort Nelson, c) Fort Smith, d) Norman Wells, and e) Inuvik.

2.3.6 CLIMATE NORMALS AND ANOMALIES

For the purposes of this research climate data for 1981-2010 was collected from environment Canada climate stations in each community the radiosonde sensors were released from. This gave us annual and seasonal WMO station climate normals. The climate stations were typically at the same airport within 700 m of the release point for the radiosonde sensors with Norman Wells having the radiosonde sensor released at the same point as the climate station, Whitehorse within 500 m, Fort Nelson within 600 m, and Inuvik within 700 m. Fort Smith was the outlier with the climate station located in the community about two km away from the point at the airport where the radiosonde sensor was released. This climate normal data was used to calculate the climate anomalies for each year at the five sites. These anomalies are defined as difference between the expected annual or seasonal average temperature and what was observed each year. These anomalies were then plotted against annual average I_{imp} at each location to determine any relationship between these two variables.

2.3.7 MACROCLIMATE OSCILLATION INDICES

Datasets containing annual average macroclimate indices of Pacific Decadal Oscillation (PDO) (NOAA, 2020a), North Pacific Index (NPI) (Trenberth & Hurrell, 1994), and Artic Oscillation Index (AO) (NOAA, 2020b) were collected. These were then plotted with annual inversion impact during the study period (1990-2016). Linear regression trend analysis was completed to test for any significant (p-value < 0.05) correlations between these phenomena and I_{imp}.

2.3.8 SEA ICE

To examine correlations between sea ice area (i.e., area with at least 15% of sea ice concentration) in the Beaufort Sea region (124° - 157° W and 70° - 80° N; 1.1 million km^2 area) monthly sea ice coverage data was collected from the Fetterer et al. (2020) dataset. Over the period 1990-2016 monthly sea ice extent in the Beaufort Sea region ranged from $59 \times 10^3 – 936 \times 10^3$ km^2.

2.3.9 TOPOGRAPHIC ANALYSIS

Analysis of topography surrounding each site was reviewed through the construction of hypsometric curves (Figure 2.8) for a 25 km radius surrounding each radiosonde site. This was completed by using 30 X 30 m resolution DEMs in ArcGIS Pro version 2.6 to construct 10 elevation bins for each site. The area within and below each elevation bin was divided by the total area of the 25 km radius. This proportion was then multiplied by 100 to give a percent area that falls at or below each elevation bin. The percent area was plotted against elevation. The hypsometric curves represents the topography and relative elevation within the terrain surrounding each site. By reviewing the hypsometric curves surrounding each site the hypothesis that mountain valley SATs will be impacted the most by inversions was tested. Furthermore, possible limits to I_{imp} over higher surrounding elevations in complex mountainous terrain is reviewed.

2.3.10 ADJUSTED INVERSION IMPACT

The ELR represents the average lapse rate to occur throughout the troposphere around the Earth. Lapse rates can vary considerably based on temperature and the moisture level in the atmosphere at any particular time (Whiteman and Richland, 2000).

In complex terrain lapse rates can vary considerably across a region (Minder et al., 2010). Thus, using ELR in calculating the lapse rate can result in significant error if lapse rates are different than the assumed ELR when SBIs are absent. To address the potential for overestimating inversion impact due to using the ELR, average I_{imp} were calculated for the entire study period (1990-2016) at each site based on a reduced assumed lapse rate in the lower free atmosphere of -3.0 °C km^{-1}.

2.4 RESULTS

2.4.1 REGIONAL DISTRIBUTION OF INVERSION CHARACTERISTICS

On annual basis, Whitehorse ranked lowest for all inversion characteristics, while for the other four sites the relative ranking of each characteristic was variable (Table 2.3). Fort Nelson was the location with the highest I_{str}, I_{mag} and subsequently, I_{imp}. Inuvik showed the deepest and most frequent inversions within the region but I_{str} was substantially lower than at Fort Nelson and thus I_{imp} was lower. The annual and seasonal means of inversion characteristics between the five sites were significantly different (Table 2.3 and 2.4). Each SBI characteristic had groups of locations with no statistically significant differences between the means. These groups of locations were not the same for each SBI characteristic. When compared to the other annual and seasonal average SBI characteristics, I_{imp}, displayed the most locations with significantly different values between all the five sites (Notice the most * for I_{imp} in tables 2.3 and 2,4).

*Table 2.3: Average and Standard Deviation (in brackets) of annual inversion characteristics during the study period (1990-2016) at each of the five study sites. * means statistically different from all other locations equal to and greater than the 95% confidence level. Range of Values is the difference between the maximum and minimum average value of the five sites listed in the rows above.*

	I_z (m)	**I_{str} (°C)**	**I_{mag} (°C)**	**I_{freq} %**	***I_{imp}*** **(°C)**
Whitehorse	266 (60)*	3.4 (0.8)*	4.9 (1.2)*	33 (6.4)	1.6 (0.5)*
Fort Nelson	311 (33)	7.5 (0.8)	12 (0.9)*	43 (5.6)	5.2 (0.8)*
Fort Smith	352 (54)	6 (0.5)	9.7 (0.8)	35 (3.9)	3.3 (0.4)*
Norman Wells	374 (66)	7.2 (0.7)	10.3 (0.9)	40 (3.6)*	4.1 (0.5)
Inuvik	432 (63)*	5.9 (0.6)	9.5 (1.0)	44 (3.6)	4.2 (0.5)
Range of values	166	4.1	7.1	11	3.6

I_{str}, I_z, I_{freq}, I_{mag}, and I_{imp} were all largest on a seasonal average during the winter season (Table 2.4). For example, I_{imp} was at least twice as large in winter compared to any other season at all locations. Beyond this commonality there were many differences in seasonal inversion characteristics between the sites. For example, in Whitehorse, Fort Smith and Inuvik, spring was the season with the second highest I_{imp}, while in Fort Nelson and Norman Wells this occurs in autumn. During the summer months Norman Wells and Inuvik were the only stations having a distinctly weak I_{imp} value.

*Table 2.4: Average (Standard Deviation) of seasonal inversion characteristics across the study period (1990-2016) at each of the five study areas. The winter seasonal values are in bold. * indicates that there is a statistical difference from all the other locations at the 95% confidence level. The range (difference between max and minimum value) of each inversion characteristic between the five sites for each season is listed in the table.*

		Iz (m)	I_{str} (°C)	I_{mag} (°C)	I_{freq} (%)	I_{imp} (°C)
Whitehorse	**Winter**	**336 (101)***	**5.4 (1.7)***	**7.6 (2.3)***	**45 (11)**	**3.4 (1.4)***
	Spring	164 (43)*	2.8 (0.8)*	3.9 (0.7)*	30 (7.4)	1.2 (0.4)*
	Summer	170 (49)	2.3 (0.5)*	3.4 (0.7)*	30 (4.6)	1.0 (0.3)*
	Autumn	178 (60)*	2.3 (0.7)*	3.4 (1.0)*	28 (8.5)	1.0 (0.4)*
Fort Nelson	**Winter**	**423 (62)***	**11.6 (1.3)**	**16.9 (1.5)***	**56 (11)**	**9.5 (2.2)**
	Spring	234 (31)*	5.2 (0.9)	9.2 (1.0)	36 (5.6)	3.3 (0.5)
	Summer	239 (22)	4.4 (0.4)	8.4 (0.5)*	39 (3.7)	3.3 (0.3)*
	Autumn	305 (48)	7.0 (0.9)*	11.5 (1.0)*	42 (6.8)	4.8 (0.9)*
Fort Smith	**Winter**	**564 (107)**	**8.3 (1.0)**	**13.3 (1.6)**	**42 (7.3)**	**5.6 (1.3)***
	Spring	290 (49)	5.7 (0.8)	8.9 (1.0)	32 (4.5)	2.8 (0.5)
	Summer	224 (22)	4.6 (0.6)	7.5 (0.6)*	36 (5.1)	2.7 (0.4)*
	Autumn	269 (63)	4.7 (0.8)	7.9 (1.0)	29 (5.8)	2.3 (0.5)*
Norman Wells	**Winter**	**580 (134)**	**10.8 (1.5)**	**15.3 (2.3)***	**53 (6.3)**	**8.2 (1.6)**
	Spring	326 (77)	6.3 (1.0)	9.0 (1.2)	34 (4.1)	3.0 (0.7)
	Summer	175 (34)	4.1 (0.9)	5.8 (0.9)*	37 (4.0)	2.1 (0.5)*
	Autumn	327 (75)	6.1 (1.1)*	8.9 (1.4)*	37 (6.0)	3.3 (0.7)
Inuvik	**Winter**	**597 (105)**	**8.5 (1.1)**	**13.1 (1.7)**	**66 (5.9)***	**8.7 (1.3)**
	Spring	425 (66)*	5.7 (0.6)	9.2 (0.9)	39 (4.2)	3.6 (0.7)
	Summer	209 (30)	3.0 (0.5)*	5.1 (0.6)*	31 (3.3)	1.6 (0.3)*
	Autumn	344 (98)	4.5 (1.0)	7.4 (1.6)	40 (4.3)	3.0 (0.6)
Range	**Winter**	**261**	**6.2**	**9.3**	**24%**	**6.1**
	Spring	261	3.5	5.4	9%	2.5
	Summer	69	2.3	5.0	9%	2.3
	Autumn	165	4.8	8.1	13%	3.8

Temperature amplitude in relation to I_{imp} and I_{freq} was also reviewed. Temperature amplitude is the difference between the warmest and coldest monthly average temperature. Whitehorse had the lowest temperature amplitude, I_{imp}, and I_{freq} (Table 2.5). All of the other sites had higher amplitude of monthly average temperature with greater I_{imp}, and I_{freq}. Between these four sites however, there was no apparent pattern towards larger temperature amplitude resulting in greater I_{imp} and I_{freq} (Table 2.5).

Table 2.5: Each radiosonde site locations and the amplitude between the coldest monthly average and the warmest monthly average which was always January and July respectively. Also included is annual average I_{imp} and I_{freq}.

Location	Amplitude (°C)	I_{imp} (°C)	Frequency (%)
Whitehorse	29.5	1.6	33
Fort Nelson	37.4	5.2	43
Fort Smith	39.6	3.3	35
Norman Wells	43.0	4.1	40
Inuvik	40.1	4.2	44

All study sites had a higher number of total transient SBI events than persistent SBI events, with Whitehorse having the highest proportion and Inuvik the lowest proportion of transient events (Table 2.6). However, the sum of the SBI hours associated with persistent SBI events, accounted for the majority of the total SBI hours at Fort Nelson, Norman Wells and Inuvik. Furthermore, persistent SBI events occurred more often and accounted for more hours during the winter, while transient SBI events accounted for most of the total hours with an SBI present in the summer (not shown). Overall, persistent SBIs played a substantial role in increasing SBI hours yearly with considerable impact during the winter months for each site, especially at Inuvik. The longest persistent SBI events at three of the sites lasted for roughly 300 hours, while Fort

Smith's longest duration was only 144 hours and Inuvik's is 624 hours. The mean length of persistent inversion events ranged from 38 hours in Fort Smith to 61 hours in Inuvik. This highlighted that many of the persistent inversions lasted much longer than our minimum 24-hour threshold.

Table 2.6: Length of inversion events during the 27-year study at the five sites (1990-2016). Transient inversion events have maximum two consecutive radiosonde readings with a SBI present (<24 hrs), while persistent inversion events are those that persist in three or more consecutive radiosonde readings (≥24 hrs).

Location	SBI Event Type	Number of Events	Percentage of Total Events (%)	Total SBI Hours	Percentage of Total SBI Hours
Whitehorse	Transient	4116	92.3	26244	65.7
	Persistent	341	7.7	13692	34.3
Fort Nelson	Transient	4133	88.3	26244	48.7
	Persistent	547	11.7	27696	51.3
Fort Smith	Transient	4196	91.2	26892	63.8
	Persistent	406	8.8	15228	36.2
Norman Wells	Transient	3887	87.4	24264	45.7
	Persistent	558	12.6	28824	54.3
Inuvik	Transient	3292	81.4	20556	30.8
	Persistent	754	18.6	46164	69.2

2.4.2 TEMPORAL PATTERNS IN INVERSION CHARACTERISTICS

I_z decreased by roughly 50-150 m at each of the five sites over the 27-year period (Figure 2.5), but at Fort Nelson it decreased 2-3 times more than the other sites (p-value < 0.05). I_{str} only decreased significantly at Whitehorse and Inuvik. Whitehorse, Inuvik and Fort Smith had slightly increased inversion magnitudes over time. Although I_{freq} had a significant trend at Norman Wells, the rate of increase of occurrence was only +0.003 % year^{-1}. No other site had sinficant trends in $I_{freq.}$ I_{imp} shows weak but significant increasing temporal trends at Whitehorse, Fort Nelson, and Inuvik (p-value < 0.05).

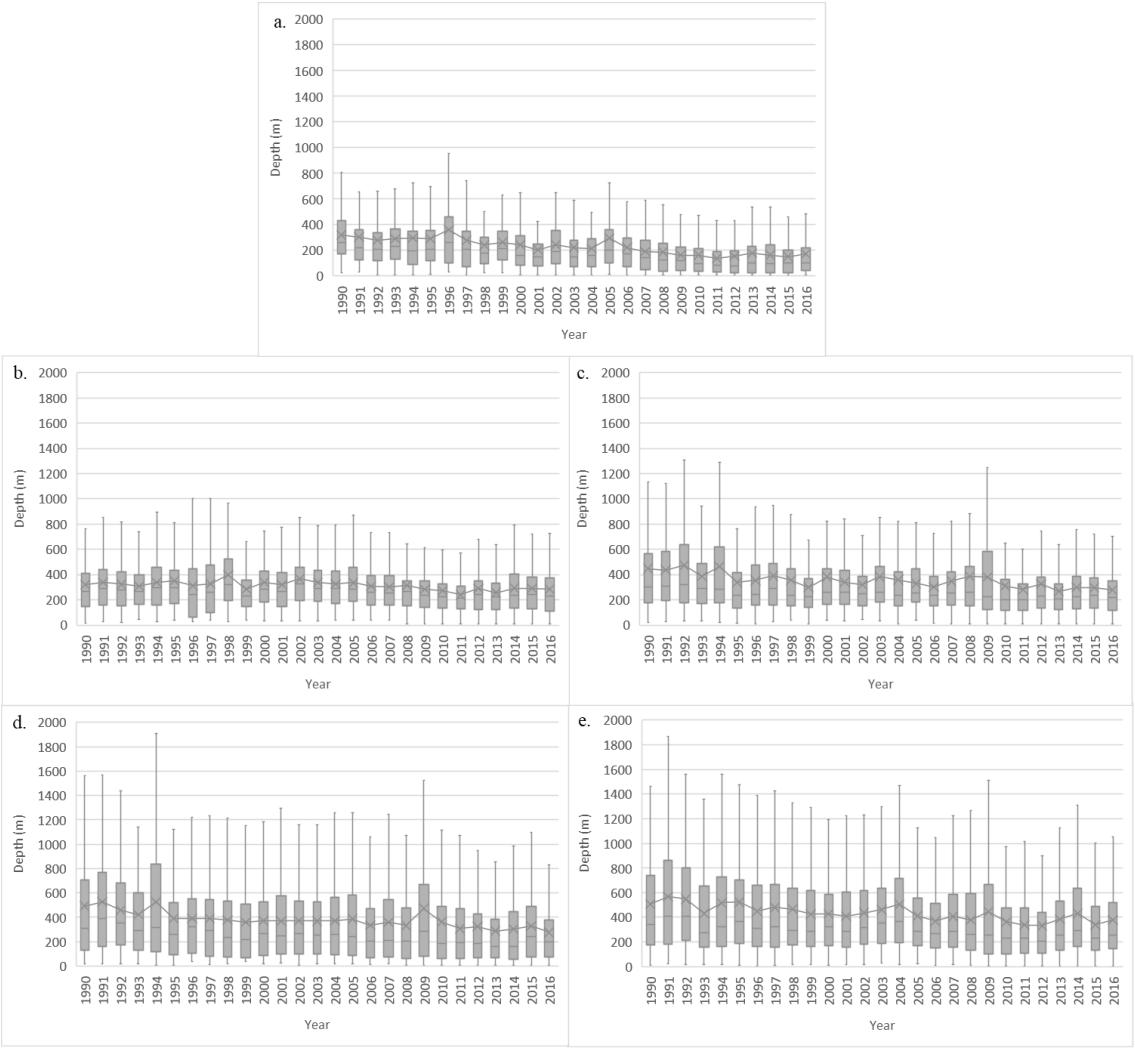

Figure 2.5: Change in annual I_z over the study period (1990-2016) for a) Whitehorse, b) Fort Nelson, c) Fort Smith, d) Norman Wells, and e) Inuvik. The boxes indicate the range of the middle two quartiles of I_z in any given year. The vertical line indicates the entire range of the I_z each year and the crosses connected by the line are the yearly mean of I_z.

Seasonal analysis of SBI metrics shows that I_{imp} was greatest during winter, with a significant (p-value < 0.05) decreasing multiannual temporal trend at Whitehorse, Fort Nelson, Fort Smith, and Inuvik (Figure 2.6). Wintertime I_{freq} showed no significant trends during the study period.

I_{imp} in seasons other than winter showed significant, but weak, trends occurring only at Whitehorse (autumn), Fort Nelson (spring), and Norman Wells (summer and

autumn). Norman Wells experienced a significant increase in I_{imp} (0.04°C yr^{-1}) in both summer and autumn. The trend in I_{imp} was negative (-0.02 to -0.14°C yr^{-1}) at Whitehorse (summer and autumn) and Fort Nelson (spring). Norman Wells recorded marginally increasing I_{freq} during summer (0.28% yr^{-1}) and autumn (0.51% yr^{-1}) while during summer only the I_{mag} was increasing. Overall, there was also a pattern of reduced year to year variability and subsequent residuals from the predicted line of best fit. The only site with statistically significant reduction in residuals (p-value < 0.05) was Fort Smith.

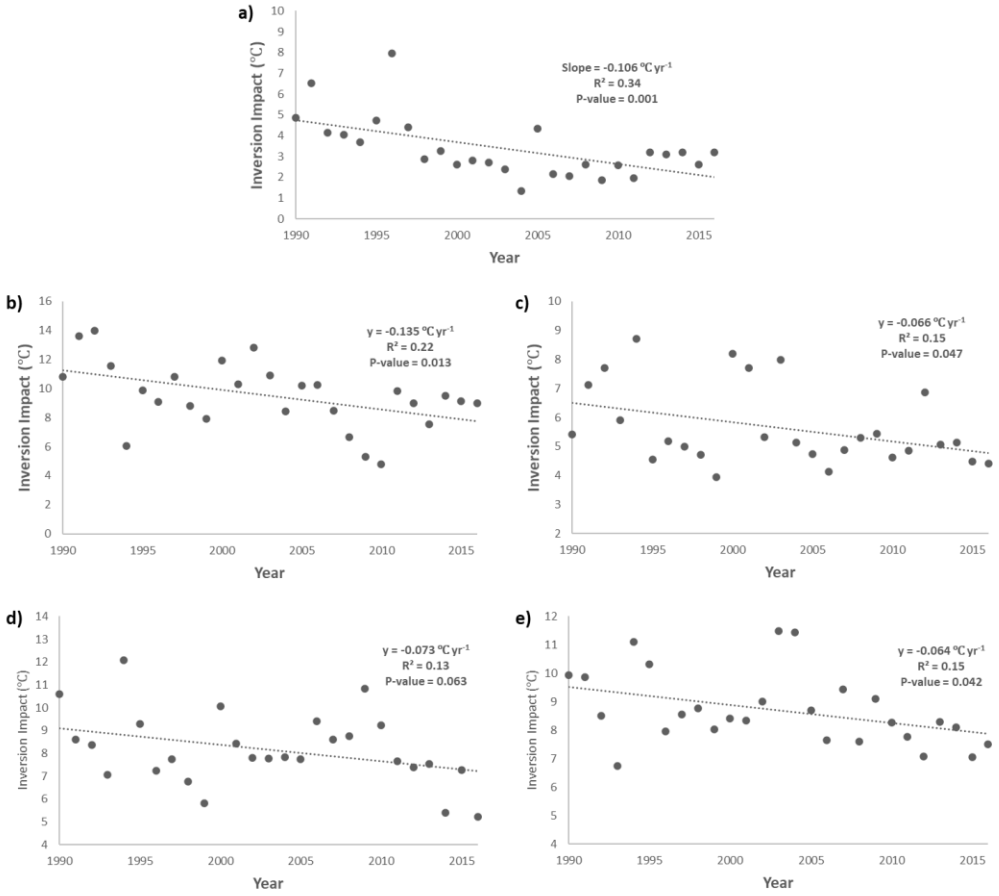

Figure 2.6: Linear trends in winter I_{imp} over the study period (1990-2016) a) Whitehorse, b) Fort Nelson, c) Fort Smith, d) Norman Wells, and e) Inuvik.

Homogeneous periods of radiosonde data were selected as described in section 2.3.5. At Norman Wells, a gradual increase in the number of vertical sounding levels

occurred throughout the study period; hence, the dataset had no well-defined homogeneous period. At Whitehorse and Inuvik, multiple step changes occurred in the number of sounding levels and all significantly correlate with I_z decrease. Meanwhile, mean I_z was reviewed for the main homogenous period based on step changes in the number of sonde soundings below the 500 hPa radiosonde depth at each location (1993-2009 for Whitehorse and 1993-2010 for Inuvik) (Figure 2.4). For each of the homogenous periods at Whitehorse and Inuvik significant decreasing trends in I_z were comparable to their annual decreasing trends across the full study period (Table 2.7). When considering data homogeneity, the decreasing trend in I_{str} only remained statistically significant (p-value < 0.05) at Whitehorse (Table 2.7).

I_{imp} at Whitehorse decreased significantly (p-value < 0.05) during the homogeneous period as well as the full study period, but at Inuvik the trend was not significant during the homogenous period. Therefore, I_{imp} trends at Inuvik were more likely linked to radiosonde instrumentation changes than climate or other temporal drivers, which, at Whitehorse, may drive the decreasing trend in I_{imp}.

At Fort Nelson and Fort Smith, the trends of I_z and I_{str} during the full study period (1990-2016) were possibly linked to radiosonde instrumentation change because there were no significant trends during the homogeneous periods. Conversely, at Fort Smith a significant (p-value < 0.05) decreasing trend (-0.15 °C yr^{-1}) in I_{imp} was found during the homogenous period though not during the full study period. However, this was based on a very short homogenous period of only 7 years. Fort Nelson had a significant (p-value < 0.05) trend of I_{imp} both during the full study period (-0.05°C yr^{-1}) and the homogeneous

period (-0.12 °C yr^{-1}), yet I_z and I_{str} on their own did not have a significant decreasing trend.

To make certain that outlier points of data during the 27-year study period were not skewing the results of the temporal trends determined through linear regression, a Theil-Sen regression with a Mann-Kendall test was completed. There were no new significant (p-value < 0.05) trends found and existing significant trends remained significant following the implementation of this statistical test. The slope of the statistically significant trends did marginally change with this alternative statistical testing (I_z < 0.7 m yr^{-1}, I_{str} < 0.3 °C yr^{-1}, and I_{imp} < 0.1 °C yr^{-1}).

Table 2.7: Trends during homogeneous periods for I_z, I_{str}, and I_{imp} compared to trends during the study period (1990-2016) for each location in the study area. Slope represents each unit of the column per year. For example, the slope value for depth has units of m yr^{-1}. Bolded values indicate statistically significant p-values.

		Homogenous Period			Study Period		
		I_z (m)	I_{str} (°C)	I_{imp} (°C)	I_z (m)	I_{str} (°C)	I_{imp} (°C)
Whitehorse	Slope	**-9.2**	**-0.11**	**-0.10**	**-6.8**	**-0.07**	**-0.04**
	R2	**0.60**	**0.36**	**0.57**	**0.78**	**0.53**	**0.35**
	p-value	**0.00**	**0.03**	**0.00**	**0.00**	**0.00**	**0.00**
	STD	54.4	0.83	0.61	61.3	0.80	0.52
Fort Nelson	Slope	-0.8	-0.05	**-0.12**	**-2.6**	-0.02	**-0.05**
	R2	0.07	0.18	**0.59**	**0.37**	0.02	**0.21**
	p-value	0.35	0.14	**0.00**	**0.00**	0.46	**0.02**
	STD	20.2	0.73	1.03	33.6	0.84	0.86
Fort Smith	Slope	-4.9	-0.10	**-0.15**	**-5.2**	-0.01	-0.01
	R2	0.18	0.29	**0.67**	**0.57**	0.02	0.05
	p-value	0.30	0.16	**0.01**	**0.00**	0.52	0.25
	STD	28.5	0.46	0.46	54.8	0.56	0.45
Inuvik	Slope	**-6.3**	-0.04	-0.01	**-6.6**	**-0.03**	**-0.03**
	R2	**0.42**	0.07	0.01	**0.65**	**0.16**	**0.21**
	p-value	**0.01**	0.32	0.68	**0.00**	**0.04**	**0.02**
	STD	45.9	0.65	0.48	64.6	0.62	0.49

2.4.3 INVERSION IMPACT COMPARED TO TRADITIONAL INVERSION CHARACTERISTICS

I_{imp} combines I_z, I_{freq}, and I_{str} into one variable that can be used to quantify the conceptual impact of SBIs on SAT. This can be useful, specifically, for determining relationships between SBI and elements of the cryosphere. We present I_{imp} as a way to bridge the atmospheric phenomenon of SBIs with the subsurface phenomenon permafrost.

Results from the ANOVA suggested that I_{imp} highlighted more statistically significant differences between the sites than any of the other inversion characteristics on their own. For example, for an annual average I_{imp} was significantly different at Whitehorse, Fort Nelson, and Fort Smith from any of the five sites. Meanwhile, annual averages of I_{str}, I_z, and I_{freq} did not have a single site recorded to be significantly different from all the other locations (Table 2.3). This suggested that I_{imp} combined other traditional inversion characteristics together in a way that highlighted the subtle differences of SBIs between the five sites. Similar patterns were observed for seasonal inversion characteristics (Table 2.4).

2.4.4 INVERSION IMPACT AND WINTER TEMPERATURE ANOMALIES

Winter climate anomalies are the difference between observed winter SAT and the 1981-2010 average winter SAT based on the WMO normal. These anomalies quantify the degree to which winter temperature was above, below, or near climatological normal in any given winter season. Since I_{imp} was influenced predominantly by winter SBIs we examined the correlation between winter I_{imp} and winter regional climate anomalies over the study period (Figure 2.7). Statistically significant, negative correlation between climate anomalies only occur at the most northern location, Inuvik (Figure 2.7). At the three other sites no correlation between winter temperature anomalies and average winter I_{imp} was found (not shown). On an annual basis, only Inuvik had a significant negative correlation between I_{imp} and annual climate anomalies (not shown). These results implied that accelerated winter warming likely tied to Arctic Amplification in the northernmost location was correlated with weakened I_{imp}. This may contribute to a further rise in SAT,

thus generating a positive feedback mechanism. This additional warming is particularly important to permafrost in this region.

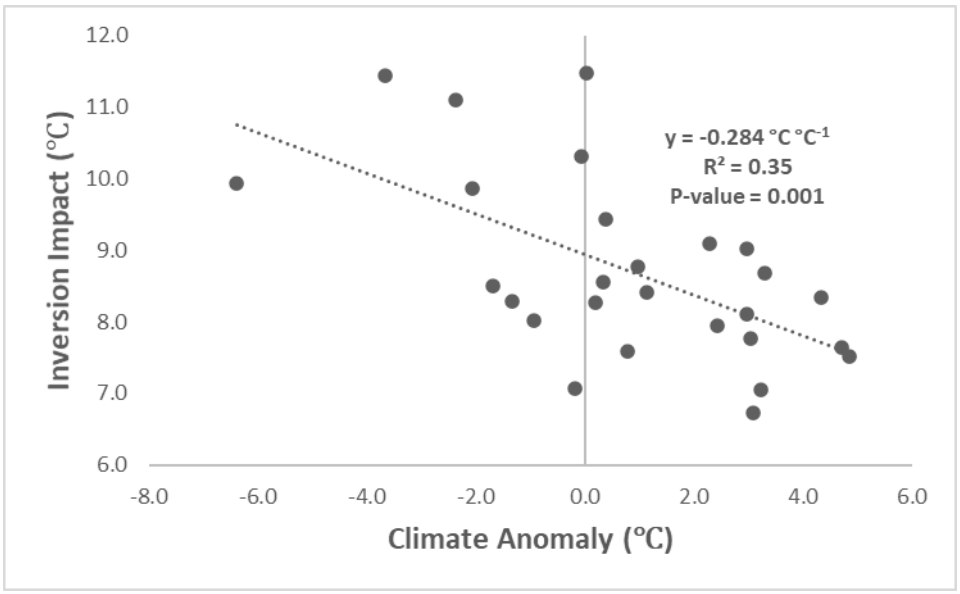

Figure 2.7: Winter inversion impact on surface air temperatures (SAT) as a function of winter climate anomalies for Inuvik.

2.4.5 INVERSION IMPACT AND LARGE-SCALE CLIMATE OSCILLATIONS

I_{imp} at each of the sites displays interdecadal oscillations (Figure 2.6). In this section, we investigate whether these I_{imp} oscillations are driven by large-scale climate oscillations, as suggested by Bourne et al. (2010). To achieve this goal, we statistically tested the correlation between I_{imp} and the indices of the PDO, NPI, and the AO.

No significant relationship between PDO and I_{imp} transpired. At Norman Wells, we found a significant, although weak, inverse relationship between I_{imp} and PDO index, both on annual average (-0.23°C index value^{-1}) and during the winter season (-0.82 °C index value^{-1}). Although the correlation was stronger and more significant during winter, R^2 remained low (Table 2.8). The only statistically significant correlation we found was,

again, observed in Norman Wells, where I_{imp} increases with NPI (0.26°C index value^{-1}: Table 2.8). I_{imp} in northwestern Canada was typically lower during negative periods of the AO and higher during more positive periods of AO (Table 2.8), but the only location with a significant correlation between I_{imp} and AO was Fort Nelson (0.84°C index value^{-1}, 0.12 R^2, and $p = 0.04$).

Table 2.8. Correlation statistics between mean annual surface-based inversion impact and mean annual climate oscillation indices. Slopes are given in °C per index value. Bolded values indicate statistically significant p-values.

		Pacific Decadal Oscillation *(°C index value^{-1})*	North Pacific Index *(°C index value^{-1})*	Arctic Oscillation *(°C index value^{-1})*
Whitehorse	Slope	0.143	0.01	0.090
	R^2	0.06	0.00	0.00
	p-value	0.22	0.91	0.73
Fort Nelson	Slope	0.328	-0.091	0.836
	R^2	0.12	0.04	0.15
	p-value	0.08	0.31	**0.04**
Fort Smith	Slope	0.009	-0.044	0.374
	R^2	0.00	0.03	0.11
	p-value	0.93	0.36	0.09
Norman Wells	Slope	-0.229	0.134	0.270
	R^2	0.16	0.26	0.05
	p-value	**0.04**	**0.01**	0.28
Inuvik	Slope	-0.099	0.014	0.007
	R^2	0.03	0.01	0.00
	p-value	0.37	0.56	0.78

2.4.6 INVERSION IMPACT AND SEA ICE AREA IN THE BEAUFORT SEA

I_{imp} in Inuvik, Whitehorse, Fort Nelson, and Fort Smith were significantly positively correlated with mean annual sea ice area in the Beaufort Sea, though with a relatively low R^2 value (Table 2.9). On a seasonal scale I_{imp} and sea ice coverage were similarly positively correlated at Inuvik, reflecting the closer proximity between Inuvik and the Beaufort Sea than the other sites in northwestern Canada.

Table 2.9: Correlation statistics between mean annual I_{imp} and mean annual sea ice area in the Beaufort Sea.

		Beaufort Sea ice area *(°C/10³ km²)*
Whitehorse	Slope	0.0037
	R^2	0.20
	p-value	**0.02**
Fort Nelson	Slope	0.0062
	R^2	0.21
	p-value	**0.02**
Fort Smith	Slope	0.0030
	R^2	0.17
	p-value	**0.03**
Norman Wells	Slope	0.0002
	R^2	0.00
	p-value	0.88
Inuvik	Slope	0.0039
	R^2	0.25
	p-value	**0.01**

2.4.7 INVERSION IMPACT AND SURROUNDING TOPOGRAPHY

Hypsometric curves indicate that in both flat lying and mountainous areas there is a significant I_{imp}. In mountainous areas with relief in the order of 1000 m, such as Whitehorse and Norman Wells, SATs in valley bottoms are significantly impacted by SBI but ~ 50% of the terrain is above the mean I_z (Figure 2.8). In flat lying areas such as Fort Smith and Inuvik significant I_{imp} is occurring across the landscape as the average top of inversion layer is roughly 250 to 300 m higher than any of the surrounding topography. Fort Nelson is also mountainous but the average top of SBI layer falls roughly 50 m above the highest surrounding mountain peaks.

At Inuvik, Fort Nelson, and Fort Smith, 40 - 60 % of the land surface in the surrounding 25 km radius has an elevation lower than the elevation of the radiosonde

launch site (Figure 2.8). This indicates that the I_{imp} determined at these sites may underrepresent the actual impact of SBIs on SATs in the low-lying areas which may be greater than determined from the sonde readings.

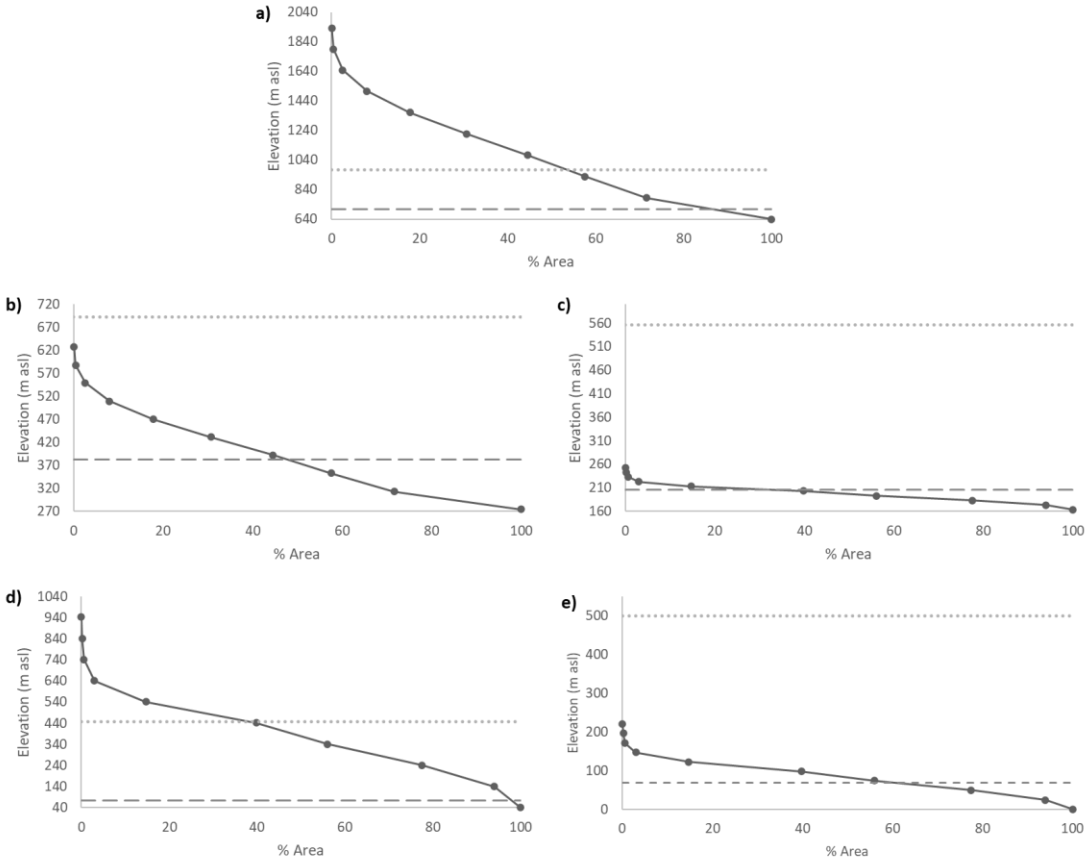

Figure 2.8: Hypsometric curves (solid line) for the 25 km radius surrounding a) Whitehorse, b) Fort Nelson, c) Fort Smith, d) Norman Wells, and e) Inuvik. Dashed and dotted lines represent the site elevation and the average top of SBI, respectively.

2.4.8 ADJUSTED INVERSION IMPACT

I_{imp} when adjusted for the potential of lapse rates not being as strong as the assumed ELR is reduce roughly by a magnitude of 2.2 (Table 2.10). For example, annual average I_{imp} is reduced by the most to 2.4 °C (reduced by 2.8 °C) at Fort Nelson. Like all variables and models there is limitations due to assumptions made when calculating I_{imp}.

Understanding what the Lapse rates are when SBIs are absent needs to be undertaken to increase the accuracy and predictive power of this new inversion characteristic.

Table 2.10: I_{imp} compared to adjusted I_{imp} when lapse rates are assumed to be gentler than the ELR.

	I_{imp}	Adjusted I_{imp}
Whitehorse	1.6	0.7
Fort Nelon	5.2	2.4
Fort Smith	3.3	1.5
Norman Wells	4.1	1.9
Inuvik	4.2	1.9

2.5 DISCUSSION

Results presented in this study have been focused into two broad categories of spatial and temporal results. Each category of result is discussed in the context of previous literature regarding high-latitude SBI research. Then, possible macroclimatic mechanisms behind dominant patterns observed in SBI are reviewed with a final discussion of the actual implications of I_{imp} on different topographies.

2.5.1 SPATIAL PATTERNS OF INVERSION CHARACTERISTICS

I_z across northwestern Canada ranged from 266-432 m during the study period. This is somewhat lower than in the High Canadian Arctic, where *Iz* in the northwestern Arctic Canada were 700-800 m and in the northeastern Arctic deepening to 1000-1100 m (Kahl et al., 1992). Like Kahl et al. (1992), Zhang et al. (2011) found that I_z were greater in central and eastern parts of northern Canada than in northwestern Canada, but for the latter they report a 300-500 m depth range, which agrees with our results. Alaska Coastal

areas also had similar I_z ranges to our study, with values ranging from 300-500 m in Southern Alaska Coastal Areas to 400-600 m in the Interior Ranges (Bourne et al., 2010).

I_{str} in northwestern Canada ranged from 3.4 °C to 7.5 °C which is similar to the value found in regions surrounding northwestern Canada (Zhang et al., 2011). I_{freq} in northwestern Canada ranges from 33-44% of the time during the year which is comparable to the values of Zhang et al. (2011) for northwestern Canada. I_{freq} was much higher in Alaska and northeastern Canada than in northwestern Canada (Zhang et al., 2011). In the case of Alaska, Bourne et al. (2011) found that interior locations, such as Fairbanks, had annual inversion frequencies around 70-80% of the time while many other locations had annual inversion frequencies > 50% of the time. This confirms a higher I_{freq} throughout much of Alaska than in northwestern Canada.

The main observed spatial pattern in inversion characteristics in the northern Canadian Arctic was an increase in depth, strength, and frequency of SBI with increased latitude (Kahl et al., 1992). Increased SBI frequency has more broadly been observed at higher latitudes in both the Northern and Southern Hemispheres (Seidel et al., 2010). Zhang et al. (2011) found that in locations with higher I_{freq} there was also a correlation to both stronger and deeper SBI. On a regional scale, SBI frequency was observed to increase along a north-easterly gradient across southern and central Yukon related to increased continentality and distance from the influence of the Pacific Ocean (Lewkowicz & Bonnaventure, 2011).

Our results do not confirm this latitudinal and continental gradient across the entire study region. Some locations of northwestern Canada that did follow this predicted pattern included both of the most north-easterly sites, Norman Wells, and Inuvik, which

had some of the greatest I_z, I_{str}, and I_{freq} while Whitehorse, the most southwestern site, had SBI characteristics that were significantly lower than all other sites in northwestern Canada. Fort Nelson was an outlier in relation to these north or north-easterly gradient patterns in SBI characteristics and had the greatest inversions strength, depth, and I_{imp}, even though this location is the most southern site in the study region.

A significant pattern deemed responsible for the SBIs gradient discussed in Lewkowicz and Bonnaventure (2011) was greater amplitude between the warmest and coldest monthly average temperatures correlating to the stronger influence of SBIs on an annual basis. Across northwestern Canada, amplitudes and subsequent inversion impacts do not verify this pattern strongly (Table 2.5). While Norman Wells, Inuvik, and Whitehorse fit this pattern well, Fort Nelson had abnormally high I_{imp} and I_{freq} for a location with a relatively low monthly average temperature amplitude. Fort Smith also had a higher amplitude than Fort Nelson but significantly reduced I_{freq} and I_{imp}. A notable difference in these studies, however, is that Lewkowicz and Bonnaventure (2011) utilized 2 m height surface logger transects rather than free-air measurements.

Other regional studies of SBI have taken place in Greenland (Gilson et al., 2018a; Shahi et al., 2020), the Central Arctic (Palo et al., 2017), Europe (Palarz et al., 2018) and China (Guo et al., 2020). Similar to findings in this study, significant spatial variability of inversion characteristics was observed in each of these regions, pointing to both influences of local surface conditions (incl. snow or ice coverage, proximity to a water body, surrounding topography), larger scale atmospheric circulation (seasonal dominant synoptic air pressure systems, climate variability driven by ocean oscillations, etc.) (Bourne et al., 2010; Palarz et al., 2018), and local or regional synoptic conditions (such

as fog) (Gilson et al., 2018a). Therefore, SBI characteristic variability across a region has both microclimatic influences and larger scale regional and macroclimatic influences. The scope of this paper includes understanding the spatial patterns of SBI broadly across northwest Canada and thus how regional or macroclimate conditions is driving SBI characteristics. Thus, spatial variability is a central focus of the remainder of this discussion.

2.5.2 INVERSION IMPACT

I_{imp} was developed not to replace the traditional inversion characteristics but rather consolidate them into one new inversion characteristic that would be useful in conceptualizing the impact SBIs have on SATs. While I_{imp} is considered theoretical and has not yet been quantified beyond the level that we do in this chapter, it provides evidence that SBIs play a significant role in defining SATs in this high-latitude region. This signifies that permafrost distribution is influenced by the impact of SBIs on SATs in northwestern Canada. Further refining and development of this variable in the future will prove invaluable to permafrost science in these SBI prone environments. The remainder of the discussion will centre on I_{imp} and factors that may be driving spatial and temporal patterns of I_{imp}.

2.5.3 LARGE-SCALE CLIMATE OSCILLATIONS INTERACTIONS WITH INVERSION IMPACT

Each of PDO, NPI, and the AO indices have been linked to variations in precipitation and temperature from climatological means in the western Canadian Arctic and Subarctic and surrounding regions (Trenberth and Hurrell, 1994; Morison et al.,

2000; Rigor et al., 2000; Bourne et al. 2010; Fleming and Whitfield, 2010; Dong et al., 2015). Although NPI and PDO are correlated, there are both negative and positive correlations between the two climate oscillations and the systems they are influencing (Newman et al., 2016) and, therefore, we investigate them separately in our analysis.

SBIs have been observed to be influenced at times by warm air advection above the stable layer. The strength of the SBI could be magnified by Pacific warm air advection aloft (Bradley et al., 1992) over high mountain ranges. In contrast, further south, along the Columbia Basin of Washington, warmer and more humid airmasses from the Pacific Ocean have been directly observed to erode and break up SBI (Whiteman et al., 2001). Changes to sea surface temperatures (SST) and sea level pressure (SLP) over the East Pacific can influence warm air advection from the East Pacific into northwestern Canada (Trenberth & Hurrell, 1994). Furthermore, multiple studies have highlighted the connection between the occurrence of cold, dry Arctic air masses and more frequent, stronger, and persistent inversions (Blandford et al., 2008; Fridley, 2009; Lu & Zhong, 2014). Therefore, any altering synoptic scale weather systems and their frequency could significantly influence SBI characteristics. For example, the negative phase of AO is associated with a weaker jet stream (Cohen et al., 2014) and is correlated with an increase in the number of blocking patterns that persist in the upper atmosphere (Hassanzadeh and Kuang, 2015). Blocking patterns result from quasi stationary synoptic weather patterns and are associated with persistent surface weather conditions leading to extended periods of abnormal heat or cold (Röthlisberger et al., 2019). Thus, interdecadal oscillations of I_{imp} may be linked directly to ocean oscillations and resultant oscillations in global atmospheric circulation.

PDO describes monthly variation in sea surface temperature anomalies (SSTA) from 20-70° N (Newman et al., 2016). Negative (positive) PDO is typical of colder (warmer) than normal SSTs in the East Pacific along the west coast of North America (Dong and Dai, 2015). During positive PDO phases, higher air temperatures and precipitation totals are typically observed in much of Yukon and Northern British Columbia (Fleming and Whitfield, 2010). The general lack of connection between PDO and inversion characteristics is consistent with findings from Bourne et al. (2010) in Alaska for the 1990 – 2007 time period. However, they found that more than half of their sites had a significant link between PDO and inversion characteristics over the period 1957 - 1989. We are unable to verify such a link at our study sites for this period because of the unreliability of radiosonde data prior to the 1990s (see Section 2.3.1).

NPI is the area weighted measure of the surface pressure level to define the strength of the wintertime Aleutian Low (Bourne et al., 2010). During the positive periods of NPI, the semi-permanent Aleutian low-pressure system weakens, reducing warm air that is advected northwards into Alaska (Trenberth & Hurrell, 1994). There is no apparent relationship between NPI and I_{imp} across northwestern Canada, much the same as PDO index and I_{imp}. Similarly, Bourne et al. (2010) found that positive NPI phases did not have any significant correlation with SBI characteristics.

Despite Norman Wells being more continental it was the only site to have a significant relationship between I_{imp} and PDO/NPI. Diurnal valley wind cycles dominate at Norman Wells (Klock et al., 2002). It is possible that local or small-scale conditions such as these local winds may be shaping I_{imp} in a way that differs from other locations in northwestern Canada leading to the unique pattern observed here. These findings warrant

further review in research of local influences on SBI in high-latitude mountainous locations

AO is defined to be the difference in normalized SLP from 35-65° N (Zeng et al., 2018). Northern Hemisphere Jetstream position and variability is influenced by AO and its position results in changes to precipitation and temperature anomalies through manipulation of the storm track (Belmecheri et al., 2017). Positive phases of AO are associated with a stronger jet stream that keeps storms moving from west to east in the mid-latitudes rather than deflecting northwards and displacing cold Arctic air at high-latitudes southwards (Devasthale et al., 2012). Weak and mostly insignificant tendencies between I_{imp} and AO indicate that this macroclimatic metric has little to no influence in shaping SBI characteristics in northwestern Canada.

Overall, while there are ample mechanistic reasons why correlations between these anomalies and I_{imp} might be found, the observed oscillations in I_{imp} during the study period (1990-2016) are not explained well by the large-scale climate oscillations associated with PDO, NPI, and AO.

2.5.4 INVERSION IMPACT INTERACTIONS WITH BEAUFORT SEA ICE EXTENT

General decreasing trends of sea ice extent, concentration, thickness, and age are driven by current climate change, although extent can vary considerably from year to year in part due to variable atmospheric stability and regional wind patterns (Serreze and Meier, 2019). Amplified changes to climate are influenced by a strong positive feedback loop driven by changes in albedo because of diminishing snow and ice cover (Serreze & Barry, 2011; Cohen et al., 2014; Overland et al., 2014). Chapman and Walsh (1993) first discussed the possibility of a link between SBI and sea ice coverage in Arctic areas, while Deser et al. (2010) found a direct connection between the reduction of Arctic sea ice and the loss of lower-level atmospheric stability, thus reducing the development of SBI.

Statistically significant (p-value < 0.05) tendencies at all sites except for Norman Wells indicate that there is a pattern of I_{imp} being correlated with sea ice coverage in the Beaufort Sea. If these patterns do indicate a functional relationship between the two variables, they may be indicative of the broader scale weather and climatic patterns associated with the reduction of sea ice in the Arctic Ocean. Sea ice and I_{imp} patterns may not be directly linked, but they could both be affected by the same atmospheric conditions such as the strength of the Beaufort High pressure system (Serreze and Barrett, 2011) or changes to water vapor levels in the lower atmosphere (Serreze et al., 2012).

2.5.5 INVERSION IMPACT AND TOPOGRAPHY

In mountainous areas stable SBI layers most often form from cold-air pooling in the valley due to a radiative imbalance on the slopes leading to cold-air drainage (Serafin

et al., 2018). As a result, the lower atmosphere can become decoupled due to cold-air pooling in the valley bottom and a subsequent SBI often develops (Whiteman and Richland, 2000). Near the top of the SBI layer, a thermal belt develops at the focal point for reversal of surface lapse rates (SLRs) from inverted back to normal (Lundquist and Cayan, 2007; Lute and Abatzoglou, 2021). This inflection point of SLRs and subsequent thermal belt has been theorized and observed in some areas of Yukon to occur around treeline (Wahl, 2004; Lewkowicz and Bonnaventure, 2011; Lewkowicz et al., 2012). I_{imp} is likely reduced on an annual basis above the average free-air top of SBI (as measured from the valley bottom). The strong and persistent infuence of SBI in valley bottom locations in high-latitude mountainous areas of northwestern Canada have been observed to alter expected SAT patterns associated with heterogeneity in elevation (Lewkowicz and Bonnaventure, 2011). Similar influence of SBI in lower lying areas has been observed in other studies of cold-air pooling and subsequent SBI development (Whiteman et al., 2001; Wei et al., 2013; Frei, 2014). Changes to SAT patterns in high-latitude mountainous areas subsequently influences permafrost distribution (Bonnaventure and Lewkowicz, 2013).

To understand this pattern more completely it could be helpful to compare free-air lapse rates from these radiosonde readings with SLRs (Lewkowicz & Bonnaventure, 2011) collected from elevational transects set up from valley bottom to mountain top. Previous work collecting SLRs in mountain valleys in northwestern Canada suggests that SBIs have less influence on SAT at higher elevations than at lower elevations (Taylor et al. 1998; Cote, 2002; Lewkowicz and Ednie, 2004; Bonnaventure and Lewkowicz, 2013). Hence, to accurately predict SAT and subsequent influence on cryospheric elements such

as permafrost distribution, I_{imp} variability across elevations needs to be quantified and understood.

At Fort Smith and Inuvik, locations with limited relief, most of the terrain is well below the top of the average top of the SBI. Therefore, in these areas, I_{imp} may influence a higher percentage of the landscape than in regions of greater relief. This was contrary to the hypothesis made that I_{imp} would be strong in mountain valleys, while weak over flat lying areas due to the higher potential for cold air pooling in valley bottoms. This finding highlights the potential for significant I_{imp} that occurs across the entire landscape to have wide reaching consequences if it has a decreasing trend over time. This signifies that temporal trends of I_{imp} in flat lying areas experiencing strong I_{imp} needs to be accurately quantified due to their influence on future temperature patterns in these regions.

2.5.6 INVERSION CHARACTERISTIC TRENDS AND RADIOSONDE DATA INHOMOGENEITY

Temporal trends were found to be present in our radiosonde data, much like in other SBI studies conducted around the world (Kahl et al., 1992; Bourne et al., 2010; Palarz et al., 2018; Ji et al., 2019; Shahi et al., 2020). Kahl et al. (1996) found that Arctic inversions were increasing in strength and frequency between 1950-1990 but fewer were considered SBIs, as more were recorded to be elevated inversions. Bourne et al. (2010) observed that SBI in Alaska from 1957-2008 had an initial decrease in I_z and I_{freq} but that from 1990-2007 both inversion characteristics were increasing significantly at most of their sites. In contrast, our findings indicate that at each of the five locations in northwestern Canada there was a significant and relatively rapid (>5 m yr^{-1}) reduction of I_z between 1990 and 2016. These trends, however, were only significant at Inuvik and

Whitehorse during the homogeneous periods of radiosonde data within the study period. Overall, trends during homogenous periods within the study period suggest that there is a reduction of I_{imp} across parts of northwestern Canada including Whitehorse, Fort Nelson, and Fort Smith. If these downward trends are part of long-term patterns of I_{imp}, then there could be significant changes to elevationally controlled SAT patterns across the region. The accelerated warming of lower elevation areas due to breakdown of I_{imp} could contribute significantly to unique climate warming patterns such as Arctic Amplification in this high-latitude region (Chang et al., 2017). Furthermore, SBIs and changes to them can have strong implications on permafrost distribution and thaw patterns (Bonnaventure & Lewkowicz, 2013). In summation, the accurate quantification of trends in SBI characteristics is essential for gaining better understanding of climate change and permafrost thaw in high-latitude regions.

While these temporal patterns may indicate that I_z and I_{str} are decreasing time, data inhomogeneities need to be considered. Zhang et al. (2011) found that decreasing trends in I_z and strength existed across the Arctic from the 1970s to early 2000s were related to an increase in vertical resolution of the radiosonde soundings. Therefore, these inhomogeneities may ultimately produce a false temporal decrease in I_{imp}. I_{freq} is less sensitive to inhomogeneities than I_{str} (Zhang and Seidel, 2011) and our analysis revealed only one significant near-zero trend of I_{freq} during the study period at Norman Wells. Here, we used a simple approach to account for data inhomogeneities (section 2.3.5) which revealed that some trends in SBI characteristics were directly linked to instrumentation changes while others may conceivably be climatological. More advanced methods of addressing radiosonde data homogeneity have been put forward (e.g.,

Lanzante, 1996; Waldon et al.,1996; Zhang & Seidel, 2011; Zhang et al., 2011; Zhou et al., 2020) and while these were beyond the scope of this study, they provide opportunities for radiosonde data homogenization in northwestern Canada for a study period that extends back to the earliest radiosonde observations (1950's).

2.6 SUMMARY AND CONCLUSIONS

The purpose of this research was to present the spatial and temporal variation of SBI characteristics across the vast region of northwestern Canada and examine if changes in SBI characteristics have occurred in conjunction with the current rates of climate change in Arctic regions. SBI characteristics were reviewed for five locations distributed throughout the study region. To obtain a conceptual measure of how much inversions are influencing SAT a new variable, inversion impact (I_{imp}), was created. I_{imp} combines SBI characteristics of I_{str} and I_z with I_{freq} and was shown to be a strong alternative measure to directly conceptualize the influence of SBI on SAT which is particularly useful for permafrost science. Our main results can be summarized as follows:

- Between the five sites average annual ranges for SBI characteristics are an I_z of 266-432 m, I_{str} of 3.4-7.5 °C, I_{freq} of 33-44%, and an I_{imp} of 1.6-5.2 °C.
- On annual and seasonal scales, I_{imp} was highest at the Fort Nelson and lowest at the Whitehorse site.
- I_{imp} is significantly higher during the winter when SBI events are the longest and most persistent.
- The new I_{imp} variable and conceptual framework suggests that the SBI have a substantial impact on SAT in high-latitude areas of northwestern Canada. Theoretical influence of I_{imp} on SAT, defined as the difference between measured

SAT during an SBI and expected SAT without an SBI, was on annual average > 5°C and on seasonal average ~10°C (wintertime) at the locations most impacted by SBI.

- There are indications of a reduction in I_{imp} over the study period (1990-2016) at some locations (Whitehorse and Fort Nelson) independent of radiosonde sensor resolution change. Potential change to I_{imp} over time is worth investigating further using more advanced radiosonde data homogenization methods, which, alongside climate reanalysis data can aid in extending the SBI records further back in time.
- Due to the relatively limited average vertical extent of SBI relative to the full relief in the mountainous regions, the impact of SBI on SAT may be variable. Low relief landscapes likely have a more persistent impact of SBI on SAT. In both cases, further understanding of the spatial variation of I_{imp} needs to be ascertained in future research.

The results from this study indicate the need for further analysis of SBI impact on SAT in high-latitude regions. The new inversion characteristic I_{imp} defined in this research is recommended for future use in the study of SBIs. This metric provides details regarding the spatial variation of SBI characteristics across a region such as northwestern Canada that were not observed by any one traditional characteristic on their own. Furthermore, I_{imp} provides a conceptualization of how much SATs are impacted by the presence of SBIs over a period of time which is invaluable to understanding how SBI influence surface phenomena such as permafrost. Research into the relationship between SBIs and patterns of macroclimate and sea ice extent was largely inconclusive. Correcting for data inhomogeneities, insofar this is possible for the five radiosonde records presented

here, is essential so that analysis of both macroscale and local-scale climatic effects could be explored in future research, since SBI can be modified by local topographic shading (Colette et al., 2003), wind patterns (Anquetin et al., 1998), vegetation (Bader & McKee, 1985), cloud cover (Sedlar et al., 2012), water vapor (Johansson et al., 2017), and fog occurrence (Gilson et al., 2018a).

2.7 ACKNOWLEDGMENTS

We acknowledge that this work was completed on the traditional territory of the Kwanlin Dün First Nation, Fort Nelson First Nation, Salt River First Nation, Smith's Landing First Nation, Sahtu Dene People, and the Inuvialuit People. We acknowledge Robert G. Way for consult and inspiration in the initial stage of research conceptualization. This research was supported by funding from the NSERC Canada Graduate Scholarships-Master's program, NSERC Discovery Grant Program, and the University of Lethbridge. Computational resources outside the University of Lethbridge were provided by the supercomputing facilities of the Université catholique de Louvain (CISM/UCLouvain) and the Consortium des Equipements de Calcul Intensif en Fédération Wallonie Bruxelles (CECI) funded by the Fonds de la Recherche Scientifique FRS/ FRNS.

Chapter 3

Surface Temperature Inversion Characteristics in Dissimilar Valleys, Yukon Canada

Manuscript planned for submission to: Arctic Science

Authorship: *Nick C. Noad[1], & Philip P. Bonnaventure[1]

[1]Department of Geography and Environment, University of Lethbridge, Lethbridge, AB, T1K 3M4, Canada

*Corresponding Author email: nick.noad@uleth.ca

Key words: Surface-based inversions, Surface Air Temperature, Permafrost Distribution, Dissimilar Valleys

3.0 ABSTRACT

Permafrost distribution in high-latitude continental mountainous areas has an intersection between latitudinal and elevationally controlled permafrost. This is related to the occurrence of surface-based temperature inversions (SBIs) which significantly modify surface lapse rates (SLRs) on an annual basis. We aim to identify and quantify patterns of SBI characteristics in two proximal yet dissimilar central Yukon valleys. Elevational transect analysis (ETA) is applied by using sensors in valley bottoms and 100 m up slope to determine in-situ SLRs. Data from downscaled climate reanalysis products (GlobSim and ClimateNA) almost entirely missed the presence of strong SBIs which produce annual average SLRs that range from 0.46 °C $100m^{-1}$ to 1.2 °C $100m^{-1}$. The magnitude of these hyper-inversions was grossly underpredicted by previous surface air temperature (SAT) modelling that attempted to account for SBI across Yukon of surface air temperatures in this region. Previous assumptions of normal SLRs in valleys above treeline were found to be inaccurate for the treeless valley, though SLRs were more gently inverted than in the treed valley. A significant relationship, though not known if causal or covariant, exists between SLRs and microclimate conditions of valley bottom wind speed, air temperature, and incoming solar radiation. These SBI differences contribute substantially to complex patterns of permafrost distribution as have been previously conceptualized for this region.

3.1 INTRODUCTION

As the impacts of climate change continue to be realized, it is more and more evident that high-latitude areas are undergoing complex and accelerated warming (Serreze & Barry, 2011; Johannessen et al., 2016). Although this is well known, less

study and attention have been paid to cold regions in mountainous and high-elevation terrain, which also display similar accelerated warming patterns (Wang et al., 2013; Pepin et al., 2015; Williamson et al., 2020). High-latitude mountainous areas, including those of northwestern Canada, represent a particularly complicated environment in which to assess trends in climate due to limited accessibility and lack of climate observation locations (Palazzi et al., 2019). Further complicating this is that these environments are subject to the influence of the aforementioned warming phenomenon. Warming in northwestern North America is currently occurring at rates not seen in the Holocene period (Porter et al., 2019). What is less evident however, is precisely how the spatial distribution of this warming is manifested over areas of complex topography. Additionally, these areas also show considerable heterogeneity in vegetation, landform, and snow distribution, which all influence air and ground temperatures. These in turn prominently contribute to the spatial distribution of permafrost, which can have a profound impact on ecosystem services (Schuur & Mack, 2018), community infrastructure and water security (Hjort et al., 2018), landform structure and stability (Wang et al., 2009; Ward Jones et al., 2019), hydrology (Quinton et al., 2011; Vonk et al., 2015), and act as a reservoir for carbon (Olefeldt et al., 2016) and exotoxins including mercury (Schuster et al., 2018; Schaefer et al., 2020).

Riseborough et al. (2008, p. 145) highlights that "the overall magnitude of the effect of topography on ground temperature conditions can be as high as 15 °C within a horizontal distance of 1 km — comparable to the effect of a latitudinal distance of 1000 km in polar lowland areas." As a result, permafrost distribution and thermal state, can be highly variable and difficult to predict across mountainous landscapes (Etzelmüller, 2013). Principally, this stems from the often-non-linear surface variability of climatic and

surface influencing attributes, including Mean Annual Air Temperature (MAAT) (Smith & Riseborough, 2002; French & Williams, 2013), snow depth (Garibaldi et al., 2021), substrate composition, and moisture level (Smith et al., 2010b), and vegetation cover (Shur & Jorgenson, 2007; Kropp et al., 2020) all of which interact and impact ground temperatures uniquely.

Perhaps the largest climatological difference regulating permafrost distribution in lower-latitude mountains compared to those in high-latitude continental areas, involves the intersection of latitudinal and elevationally controlled permafrost (Bonnaventure et al., 2012). This results from the occurrence of persistent Surface-Based Temperature Inversions (SBIs), which influence MAAT across the landscape on an annual scale (Chapter 2; Lewkowicz & Bonnaventure, 2011; Lewkowicz et al., 2012). SBI can occur frequently in high-latitude regions of northwestern Canada, particularly in the winter months, where they can persist for more than 80% of the time (Zhang et al., 2011). Bonnaventure and Lewkowicz (2013) conceptualized that persistent annual SBIs play a considerable role in permafrost distribution in these areas as Surface Lapse Rates (SLRs) can be gentle or inverted on an annual average. This can result in permafrost having no lower limit and being nearly continuous in valley bottoms and mountain tops, while subsequently absent at mid slope and approaching treeline (Lewkowicz & Bonnaventure, 2011).

SBI research in northwestern Canada is limited in high-latitude remote locations as weather and climate monitoring apparatus are often sparse and unevenly distributed (Urban et al., 2013; Pepin et al., 2015). Therefore, traditional methods of measuring and monitoring SBIs utilizing radiosonde sensors (Bradley et al., 1992; Bourne et al., 2010;

Zhang et al., 2011; Mayfield & Fochesatto, 2013; Chapter 2) only cover small portions of these immense regions, leaving vast areas between locations of detailed data collection. The use of remote sensing techniques (Liu & Key, 2003; Liu et al., 2006; Devasthale et al., 2010; Chang et al., 2018) or climate reanalysis models (Palarz et al., 2018; Akperov et al., 2019; Luo et al., 2019; Shahi et al., 2020) have begun to fill these gaps. Climate reanalysis datasets, specifically, offer a potential way to examine a first-hand assessment of past, current, and future SAT/SLR patterns in remote locations (Compo et al., 2011). Permafrost distribution modelling relies on the use of these datasets to understand past, present, and future MAAT (Obu et al., 2019; Tao et al., 2019; Qin et al., 2020), but there are limitations to the accuracy of both remote sensing and climate reanalysis methods, particularly in mountainous areas due to their coarse spatial and temporal resolutions (Etzelmüller, 2013).

This research applies an increasingly popular alternate method to evaluating SBI characteristics and influence across topography through the set up of elevational transects of sensors from valley bottom up surrounding mountain slopes. We will term this methodology elevational transect analysis (ETA). These methods have allowed for expansion of research on SBIs in remote areas of Finland (Pike et al., 2013; Williams & Thorp, 2015), portions of Nunavut (Smith & Bonnaventure, 2017; Garibaldi et al., 2021), and southern and central Yukon (Cote, 2002; Lewkowicz & Bonnaventure, 2011; Lewkowicz et al., 2012; Bonnaventure & Lewkowicz, 2013). ETA gives a view of SBI conditions up a slope with a resolution not seen in other products or analysis. Unfortunately, both set up and data retrieval require considerable effort and time (e.g.,

Bonnaventure et al., 2012) and thus there is a limit as to how many and where these transects can be logistically set up.

The objectives of this study include: First, to identify and quantify patterns of SBI characteristics in neighboring central Yukon valleys that are dissimilar by using ETA. Where previous studies have generalized impact of SBIs on SLRs, we aim to highlight how this impact can differ even over short distances. Second, to compare observed SLRs with previously assumed SLRs for this region. Third, to investigate correlations between microclimatic conditions and SLRs in the two valleys to identify possible driving factors behind SLR variability on local valley-to-valley scales. Fourth, to assess the limitations of using downscaled climate reanalysis data in valleys with strong and frequent SBIs and how use of ETA can supplement these limitations.

3.2 STUDY REGION AND AREA

3.2.1 STUDY REGION

The study region includes roughly 120 km^2 area of complex mountainous terrain along approximately a 50 km stretch of the Dempster Highway in Yukon (Figure 3.1). The Dempster Highway begins in a boreal forest ecoregion along its southern end and transitions quickly to a treeless tundra environment due to elevational and latitudinal climatic influences (Wahl, 1987). Dominant species in the Boreal Forest portion of the region include black spruce (*picea mariana*), and shrubby vegetation including dwarf birch (*betula glandulosa*) and willow (*Salix spp*.), while tundra vegetation is dominated by mosses, lichens, and grasses on flatter lying areas with substantial hummocky terrain (Stanek et al., 1981; Scudder, 1997). This portion of the Dempster Highway is found within the Ogilvie Mountains, which is characterized by a series of narrow valleys

predominantly covered with colluvium and alluvium surficial materials (Burn et al., 2015). The terrain in the study region was last glaciated during the Pre-Reid Glaciation (2.6 Ma – >200 Ka) but remained unglaciated in the subsequent more recent glaciations (Duk-Rodkin, 1999). The study region is located northeast of the Tintina Trench, with rock type being mostly sedimentary, dominated by limestone and shale (Hart, 2002). Most soils in the study region are classified as static cryosols (mineral soils without evidence of cryoturbation) (Scudder, 1997). Permafrost in this region is classified as continuous (90-100%), with low to moderate (<10-20 %) ground ice content (Heginbottom et al., 1995). More recently, O'Neill et al. (2019), found that segregated and wedge ground ice were low to negligible in this area. Bonnaventure et al. (2012) modelled permafrost in this region at 30 x 30 m resolution. They found that permafrost probability in this study area ranges from being roughly 75%-100% at high elevations while permafrost was least likely at mid-elevations, particularly on south facing slopes where permafrost probability was 40-50%. Meanwhile the valley bottom locations had a permafrost probability of around 60-80% (Figure 3.1). The study region has a subarctic continental climate, with modifications from intense cold-air drainage into valley bottoms that result in amplified cold winter temperatures (Burn et al., 2015).

The closest Environment Canada (EC) climate station to the study region is at Dawson, Yukon (~160 km to the southwest). The MAAT climate normal at Dawson from 1981-2010 was -4.1 °C with annual precipitation averaging 324.4 mm with 38% of precipitation falling as snow (Environment Canada, 2020a).

3.2.2 STUDY AREA

The study area consists of two mountain valleys located roughly 10 km from each other in the same subrange of the Ogilvie Mountain range (Figure 3.1). The two valley locations were selected as they have multiple differences between them, including vegetation cover, orientation, geometry, and fetch length. South Valley (SV) is located on the southern edge of the subrange of mountains that surround Distincta Peak (Figure 3.1). The up-valley orientation is aligned in a west-northwest direction with a curve towards the north in the upper part of the valley. The SV valley bottom is at an elevation of 980 m a.s.l. with surrounding ridges that are 450 m higher in elevation to the north and 200-250 m higher in elevation to the south. SV is V-shaped and narrow with a gently sloping valley floor, approximately 250-300 m wide, running between the steep slopes (25-30° on the south face slope and 30-40°on the north face slope) (Figure 3.2). Valley fetch length from top to bottom is 4.4 km. The south face slope (SFS) in the SV consists of bedrock that is black weathered shale and laminated siltstone while the north face slope (NFS) comprises of grey and buff-weathering dolostone and limestone (Yukon Geological Survey, 2020). Vegetation cover consists primarily of open boreal forest mostly consisting of Black Spruce (*Picea mariana*) with thick mosses, lichens, Labrador tea (Rhododendron groenlandicum), and grasses at the surface in the valley bottom and roughly 100-150 m up the SFS (moss thins substantially on the steeper valley walls). The slopes are covered with felsenmeer with patches of mosses, lichens, and grasses above the forested area on the SFS and up the entire NFS. The NFS has a vegetation cover of thin mosses and lichens with some patches of Labrador tea. Most the surrounding surface lacks vegetation and consists of exposed bedrock at the surface.

NV is located on the north part of the subrange with the up-valley orientation facing south (Figure 3.2). The NV bottom has an elevation of 1090 m a.s.l with surrounding ridges roughly 300-350 m higher in elevation to the west and roughly 250-300 m higher in elevation to the east. The NV is U-shaped with a relatively flat 500-550 m wide valley floor between the steep slopes (30-40°). The valleys fetch length is 5.7 km. The valley floor is comprised of bedrock of black, weathered shale as well as laminated siltstone with the surrounding slopes consisting of bedrock which is grey and buff-weathered dolostone and limestone (Yukon Geological Survey, 2020). Valley bottom has no trees and the vegetation is tundra-like with thick mosses and lichens on the gentle slope (below 1140 m a.s.l.). Felsenmeer covered slopes surround the valley bottom with patches of mosses and lichen located near springs.

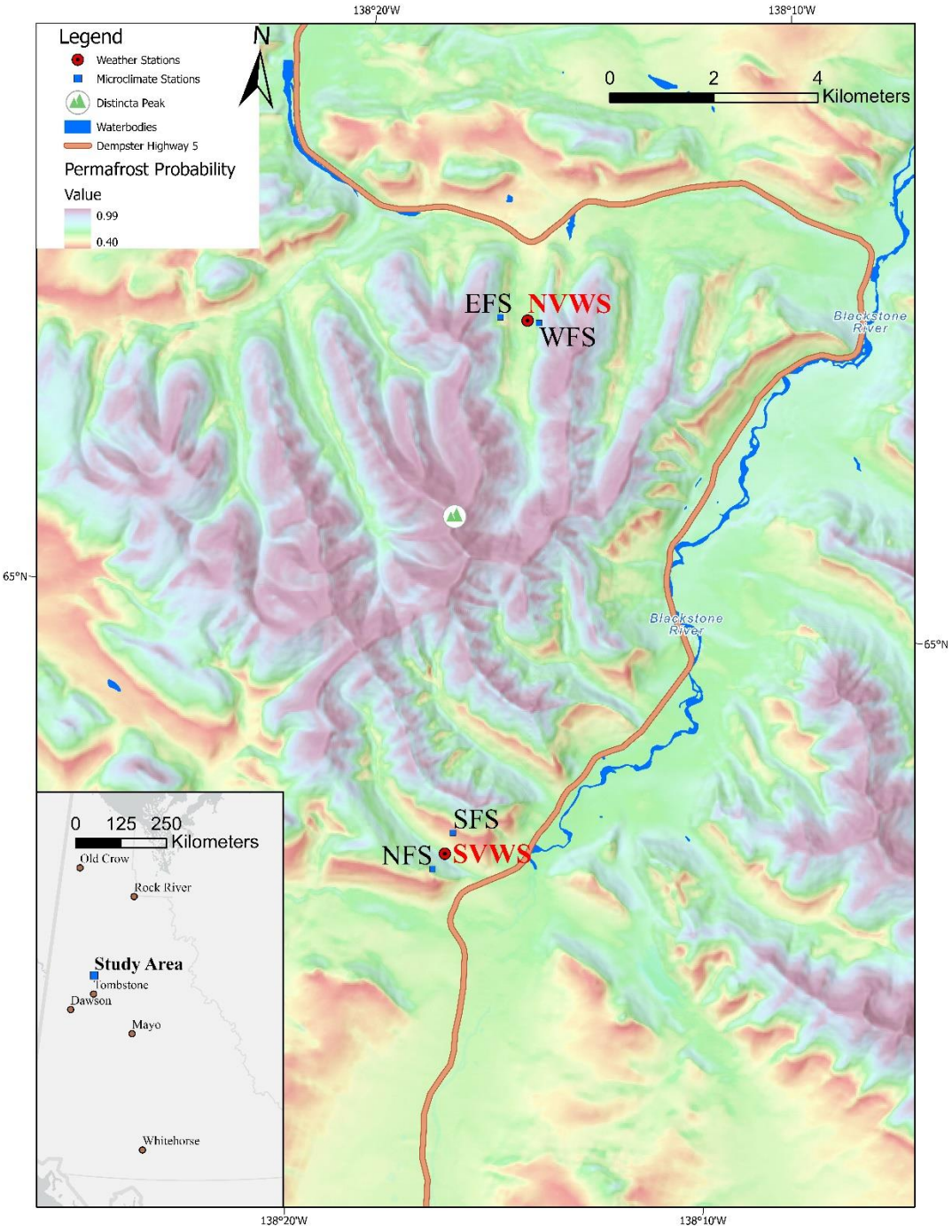

Figure 3.1: Map of the subrange (≈120 km^2) of the Ogilvie Mountains where the two valleys are located (≈10 km apart). The two valleys include, the north valley (NV) and the south valley (SV). In the NV there are three sensors called north valley weather station (NVWS), east facing slope (EFS), and west facing slope (WFS). In the SV there are three sensor locations called south valley weather station (SVWS), north facing slope (NFS), and south facing slope (SFS). Overlain on the map is the 30 x 30 m grid of permafrost probability as outlined in Bonnaventure et al. (2012).

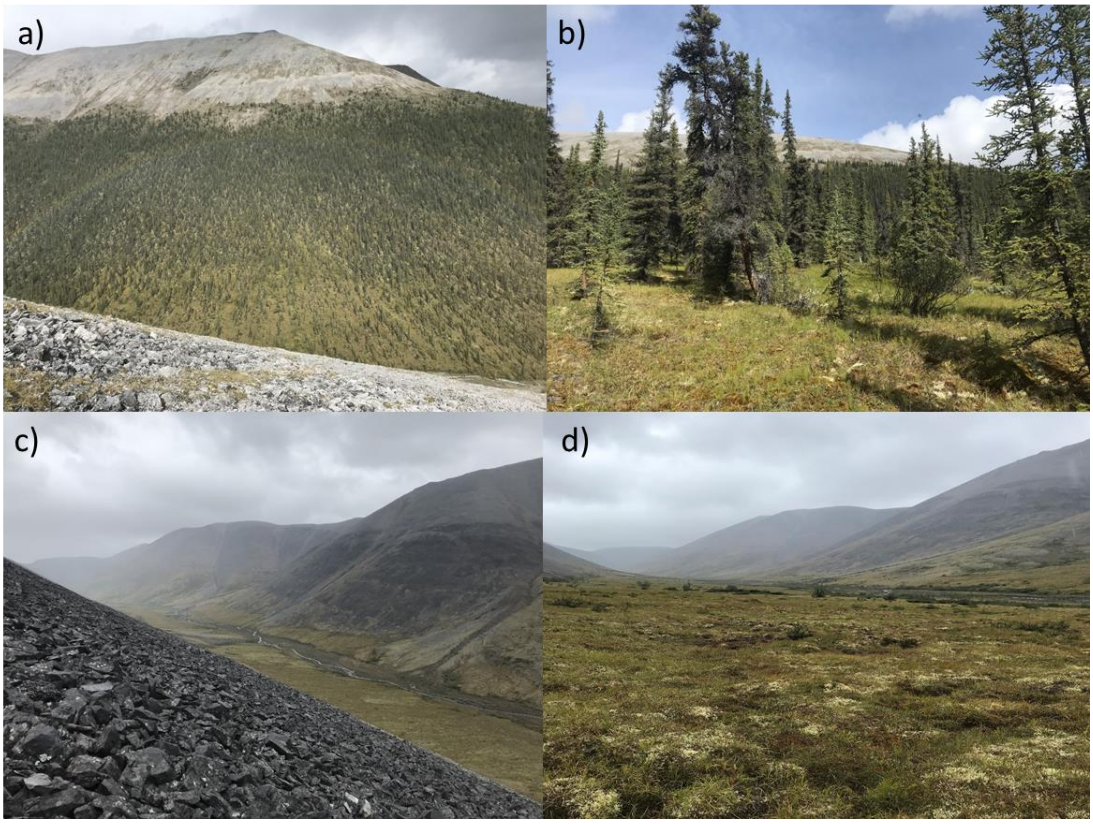

Figure 3.2: Photos of each valley taken in August 2019. a) is taken in the SV from the NFS and is of the treed SFS. b) is taken from the valley bottom of the SV looking towards the SFS. c) captures the NV valley from the view of the WFS and is taken looking up-valley to the south. d) is a view of the relatively flat valley bottom of the NV also looking up-valley to the south.

3.3 METHODOLOGY

3.3.1 STATION DEPLOYMENT AND DATA COLLECTION

To examine the objective of quantifying the unique microclimatic variability in SLRs over local valley-to-valley scales in this region, two valley locations were selected using an initial search in Google Earth Pro. Initially, the design of this experiment was inspired around testing the differences between SBIs in valleys with and without trees. Previous research suggests that SLRs are strongly inverted on treed slopes while reversing back to more normal SLRs above treeline (Wahl, 2004; Bonnaventure et al.,

2012; Lewkowicz et al., 2012). Therefore, this research aimed to observe the influence of forested area on SLRs but expanded from there to include other dissimilarities between the valleys. These dissimilarities include valley orientation, geometry, fetch length, and elevation. Multiple locations were initially chosen where treeless and forested valleys were spatially proximal, while directly adjacent to the Dempster Highway. This requirement was important as deployment and data retrieval was to be done on foot. The pair of valleys selected fit the selection criteria, were close to each other, and were the easiest to access of the candidate locations. In each valley, three sites were chosen to set up sensors (Table 3.1). Weather stations (HOBO USB Micro Station Data Logger - H21-USB; Table 3.2) were set up in each valley bottom roughly 1000-1500 m away from the Dempster Highway. This distance assured that measurements were outside of the influence of anthropogenic effects from the highway including snow clearing. Microclimate stations (U23-001 HOBO sensors in a solar radiation shield – RS1; Table 3.2) were positioned roughly 100 vertical m up each slope nearest to the weather station (Figure 3.3). This position on each surrounding slope was selected as treeline in the SV was located at roughly 100-150 m up from the valley bottom, while there were no trees in the NV. Treeline was defined as the elevation at which the presence of trees became isolated to absent. The methodological set up for data collection in this study is similar to that of Williams and Thorp (2015).

Table 3.1: Study area valley station geographic coordinates, elevation, and vegetation characteristics.

Sensor Site	Latitude	Longitude	Elevation (m a.s.l)	Vegetation
South Valley (SV)	64.95854°	-138.2803°	993	Boreal Forest
South Face Slope (SFS)	64.96209°	-138.2771°	1132	Treeline
North Face Slope (NFS)	64.95583°	-138.2846°	1133	Felsenmeer Slope
North Valley (NV)	65.0498°	-138.2634°	1103	Tundra
West Face Slope (WFS)	65.04954°	-138.2588°	1195	Felsenmeer Slope
East Face Slope (EFS)	65.05003°	-138.2744°	1195	Felsenmeer Slope

The SV bottom weather station location has ground covered by deadfall and thick mosses. The sensor is in a position where there is little shading from the trees throughout the day as the forest canopy in this valley is not thick but rather open. The logger location on the SFS is also in an open black spruce forested area roughly at treeline. The NV bottom weather station location has surface vegetation cover dominated by mostly grasses with patches of mosses. The EFS and WFS microclimate stations are both on a strip of grass and moss surrounded by exposed bedrock at the surface.

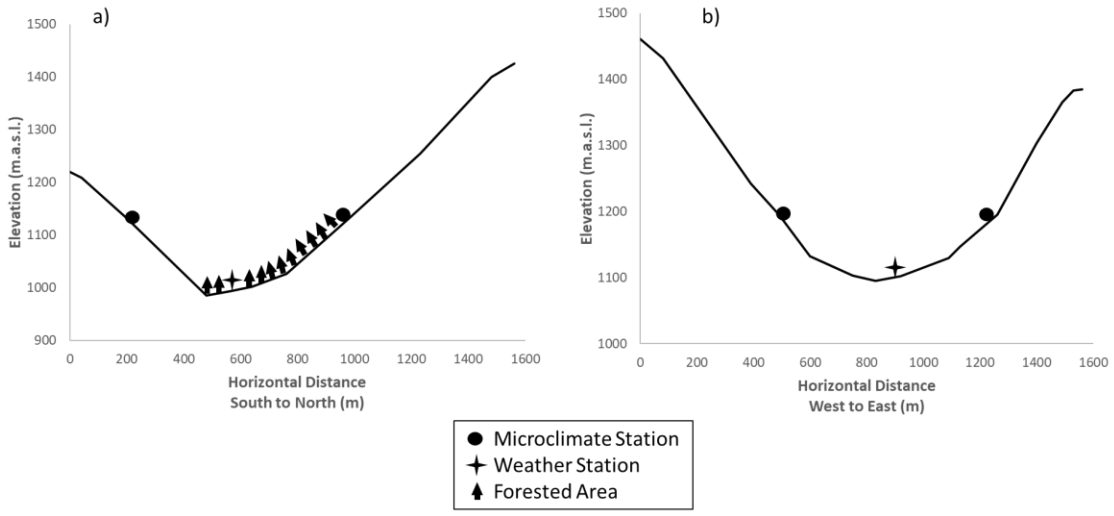

Figure 3.3: Schematic representation of the set-up of the elevational transect in valley locations. a) represents setup in the SV whereas b) represents setup in the NV where there are no trees present. Each elevational transect was graphed by taking sample points of coordinates and elevations on Google Earth Pro.

Weather stations comprised sensors that recorded wind speed and direction, atmospheric/relative humidity, incoming solar radiation, 2 m air temperature, ground temperature, and temperature at depth sensors (Figure 3.4a; Table 3.2). In addition, air, ground and depth temperatures and relative humidity data are the sole observations collected at the four microclimate stations (Figure 3.4b). Depth sensors were positioned at a best approximation of the depth of the top of permafrost layer to collect the temperature at the top of permafrost (TTOP) (range from 25 cm – 70 cm). The sensors were set up by inserting a probe downwards into the substrate until the frost layer was reached by the tip of the probe. Due to the coarse substrate at some locations, as well as the time of year field work was conducted (August 2017), these were the maximum achievable depths or frost table locations. Thus, particularly at the slope locations TTOP is not likely to have been reached due to the coarse substrate so this term will be referred to as mean annual ground temperature at depth (Depth MAGT).

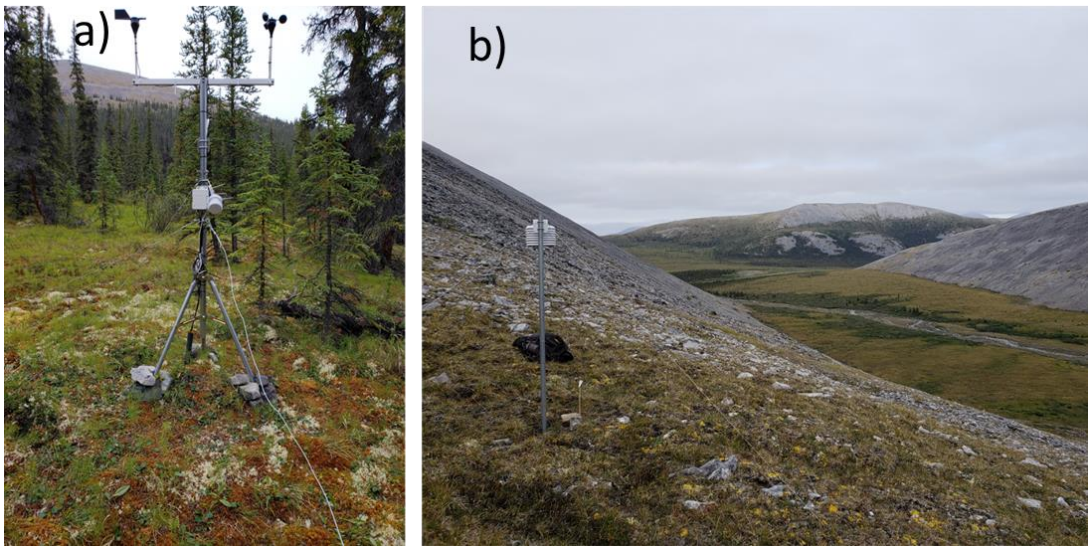

Figure 3.4: a) is the weather station sensor setup in the SV and b) is a microclimate station set up on the EFS.

At each sensor location, data were collected at a sampling interval of two-hours beginning at 000 PST on August 28th, 2017 and finished recording on 2200 PST on July 31, 2019. This means that data was collected in a momentary reading every two hours. Data were collected for the same sampling period at each transect including the north face transect (NFT), south face transect (SFT) and the west facing transect (WFT). The east facing transect (EFT) was the exception as it was not deployed until August 15th, 2018, and the first reading was collected at 0:00 PST of that day.

Table 3.2: Uncertainties and resolution of sensors used at microclimate and weather stations in each valley as listed by Onset HoboWare Loggers.

Sensor	Measurement type (Units)	Accuracy	Resolution Interval
U23-001 HOBOware	Air, Ground and Depth Temperatures	0.25 °C	0.02 °C
U23-001 Hoboware	Relative Humidity	2.5%	0.03%
HOBOnet Wind	Wind Speed	The greater of 1.1 ms^{-1} or 5% of total wind speed	0.5 ms^{-1}
HOBOnet Wind	Wind Direction	7 °	1.4 °
HOBOnet Silicon Pyranometer	Incoming Solar Radiation	10 Wm^{-2}	1.35 Wm^{-2}

3.3.2 INVERSION CHARACTERISTICS USING CLIMATE REANALYSIS MODELS

Three main platforms of downscaled reanalysis data were downloaded using the GlobSim program described by Cao et al. (2019). The three reanalysis models include ERA5, MERRA, and JRA55. SAT data from these models were downscaled through an empirical-statistical method to 2-hour increment instantaneous data at point locations (more specifically to a 10 x 10 m grid) for the study period (August 2017- July 2019) to match our in-situ sensor locations for direct comparison. The GlobSim program first downloads the original gridded coarse resolution climate reanalysis data for the study region as projected by each of the three reanalysis models. Then the original gridded climate data are interpolated to point location time series datasets. The climate reanalysis datasets are vertically interpolated through pressure levels present for each climate variable in the original dataset to match the input point location's elevation. Each climate reanalysis dataset has vertical resolutions that vary model to model based on the number

of vertical pressure levels of data that are projected by each model. Downscaled climate reanalysis datasets of SATs are then scaled temporally to match the desired 2-hour incremental datasets. A second program called ClimateNA Version 6.3 was used to downscale a 4 x 4 km baseline grid-cell cluster with monthly climate averages to scaleless point data. Elevations for the nearest 8 surrounding cells are used to estimate generalized lapse rates in a region. The creators of this program acknowledge that estimations of lapse rates using their downscaling product has challenges predicting variation of lapse rates across a region (Wang et al., 2016).

3.3.3 CALCULATION OF SURFACE-BASED TEMPERATURE INVERSION CHARACTERISTICS

For the in-situ and downscaled climate reanalysis data SLRs were calculated from the raw temperature data by using the LINEST function in Microsoft Excel 2013 to determine a slope of the linear line representing temperature change between the valley bottom and higher elevation stations on each slope. Using these data, SBI metrics were calculated including strength, which is converted into the inverted surface lapse rates (ISLRs) and frequency. Strength is the difference of temperature between the lower and upper station during an SBI (Bradley et al., 1992) which is converted to ISLR by scaling that temperature change to °C/ 100 m, whereas SBI frequency (I_{freq}) is the proportion of time that inversions are present (Bourne et al., 2010). When SLRs become ≥ 1 °C/ 100 m we considered them to be hyper-inverted. Using these methods, SLR and SBI characteristics were calculated for every 2-hour interval for each of the four elevational transects. Each Inversion characteristic was calculated and averaged for monthly, seasonal (based in meteorological seasons e.g., winter is December, January, and

February), annual, and two-year study period time periods. These characteristics were compared within and between the valleys in search of any patterns that are present in one or both valleys on a monthly, seasonal, annual, and two-year study period basis (EFT in the NV was excluded in the statistical testing between the valleys for the two year study period due to only 1 year of data available).

Another set of SBI characteristics were included in the analysis for this study based on SBI event length. The classification system used was developed by C. D. Whiteman et al. (2001) and modified in chapter 2. In this system inversion events are classified as either transient or persistent based on how long inversion events last. Persistent inversions are defined to last 18 hours or longer without reversal of lapse rates back to normal, thus no SBI break-up event. Transient inversions refer to events that are less than 18 hours in length. Classifying SBI using this system aids in understanding how length of inversions varies spatially. The assumptions made while classifying the length of inversion events is that the inversion does not break-up and redevelop within a 2-hour increment and thus is missed by the 2-hour incremental readings. The result of such an assumption may be the overprediction of how long some persistent inversions are.

Daytime and nighttime readings were selected based on the sunrise and sunset time calculated for each day of the year using the NOAA sunrise and sunset calculator (NOAA, 2021). The coordinates of WS01 were inputted into the calculator to represent both valleys. Due to their close proximity, the times for their daily sunset and sunrise are similar and showed no difference in the calculator. These sunrise and sunset times do not account for topographic shading as they were aimed to represent times where substantial indirect or direct solar radiation was reaching each valley bottom. The output sunrise and

sunset values were then used to select whether the reading was taken before/after sunrise or sunset, thereby separating all SLR datapoints into nighttime or daytime readings. Then annual and seasonal averages of SLRs were compared and then tested for significant differences between the SLRs during the night and day readings using a Mann-Whitney U test.

3.3.4 IN-SITU DATA COMPARISON TO LOCAL MODELLED INTERPOLATIONS

In-situ AMAT data were compared to a modelled surface of MAATs that was developed using a series of logger transects and records from 18 EC weather stations across the central Yukon and northern British Columbia (Lewkowicz et al., 2012). This 30 x 30 m resolution MAAT surface was input into permafrost modelling for this region that was used to predict permafrost probability while accounting for dominant SLR patterns across the region. In the creation of this MAAT surface, SLRs were defined using ETA from transects set up across south and central Yukon. The surface is not a perfect comparison, as it was constructed for the 1981-2010 climatic normal and was applied using various assumptions. The most notable of these include interpolated surfaces for the position of treeline (where SLR changes sign and magnitude). As a result, even small deviations in these variables between the modelled and the observed data at the valley scale, will result in substantially different annual temperature values. This analysis aimed to not only examine the predicted and actual absolute temperature between the modelled MAAT surface and the in-situ reading, but more specifically predicted assumed SLRs compared to observed SLRs. Comparison of this MAAT surface with our in-situ data will expose limitations in accounting for SBIs influence in this region for

permafrost probability mapping. By finding limitations of previous model assumptions for this study region, future improvements to permafrost modelling in the region can be made.

Additionally, Lewkowicz et al. (2012) made observations using in-situ measurements regarding the amplitudes of temperature between the coldest and warmest monthly average surface air temperature (SAT) at low elevation sites compare to treeline locations. Their findings showed that annual temperature amplitudes were substantially smaller at treeline locations. Using our in-situ valley bottom and treeline data, amplitudes were also compared in the treed valley to those of the treeless valley to establish if this pattern exists most intensely in the treed SV.

3.3.5 ASSESSMENT AND COMPARISON OF VALLEY MICROCLIMATE CONDITIONS

Data collected in both valleys for each meteorological condition on a microclimatic scale were compared. Wind speed, wind direction, incoming solar radiation, and relative humidity were averaged across the study period on annual and seasonal scales. This allowed for a direct comparison of variation of each microclimate condition between the two-valley bottom weather station locations. Statistical testing was utilized to determine if differences exist between microclimate characteristics through a Mann-Whitney U test as data for each of these variables from the 2-hour sample frequency was not normally distributed. SLR data for two weeks prior and two weeks following the estimated onset or loss of snow cover at each transect were compared for differences.

For each dataset including wind speed, relative humidity, and solar radiation, readings were collected for the instantaneous observation immediately prior to each SBI event breakup then to the instantaneous observation immediately following each SBI breakup. By reviewing these instantaneous moments directly before and following SBI breakup, patterns of microclimate conditions, if any, could be identified. Furthermore, observations of all data with an SBI present and without an SBI present were reviewed. Overall, the purpose of this section of analysis is not to definitively define the microclimatic conditions influence on SBI characteristics but rather to highlight any apparent connections between them that can direct future study on the topic.

3.3.6 STATISTICAL ANALYSIS

All statistical analyses were undertaken in SPSS version 27 to test a series of hypotheses (Table 3.3). Much of the data on the two-hour interval seasonally and annually were not normally distributed, thus a non-parametric statistical test, such as the Kruskal-Wallis test was needed (Ostertagová et al., 2014). The Mann-Whitney U test was used to determine if there is a significant difference in the median SLRs between each of the four transects.

In some cases, seasonal and monthly averages of ISLRs, I_{freq}, and SLRs lacked homogeneous variance between the four transects. Therefore, a Welch's analysis of variance (WANOVA) test with a post hoc Games-Howell test was utilized to test for significant difference between the groups means as there is no assumption of homogeneous variability of the data (Ruxton & Beauchamp, 2008). The other monthly average inversion characteristics had equal variance and normal distribution and were

compared between the transects using ANOVA analysis and Tukey post hoc statistical testing (Abdi & Williams, 2010).

Univariant linear regression is utilized to determine if any significant correlation between an inversion characteristic and each of the microclimate variables observed in the two valleys exists. This was used to identify any potential relationships between microclimate variability and spatial variability of SLRs. Finally, use of linear mixed-effects models were also utilized, however, residuals between SLRs and microclimate data were not normally distributed, which is an assumption of these models, although this issue does not completely nullify modeled results, so they were included (Schielzeth et al., 2020).

Table 3.3: Null hypotheses for each objective of study that required a statistical test and the type of statistical test used to test for significance ($p<0.05$).

Null Hypothesis	STATS Test
I_{freq}, ISLRs, and SLRs are the same between all 4 transects	Mann-Whitney U test
Monthly and seasonal average I_{freq}, ISLRs, and SLRs are the same between all 4 transects (Normally Distributed/ Homogeneous Variance)	ANOVA and Tukey post hoc test
Monthly and seasonal average I_{freq}, ISLRs, and SLRs are the same between all 4 transects (Normally Distributed/ Inhomogeneous Variance)	WANOVA and Games-Howell post hoc test
I_{freq}, ISLRs, and SLRs are the same during both night and day readings	Kruskal-Wallis test
SLRs are not correlated with variability in microclimate conditions between the valleys	Univariant linear regression and linear mixed-effects models
In-situ measured SLRs are same as SLRs predicted by downscaled climate reanalysis models	Kruskal-Wallis test

3.4 RESULTS

3.4.1 STUDY PERIOD CLIMATIC CONDITIONS

To better understand how the current climate of the region (including the dissimilar valleys) has varied from the 1981 to 2010 climatic normal, the residuals of the MAAT are examined. August 2018-August 2019 was the warmest year examined when compared to the 1981-2010 climate normal at Dawson, Mayo, and Old Crow (+1.9 °C, +1.2 °C, and +2.8 °C respectively) (Table 3.4) (Environment Canada, 2020a; Environment Canada, 2020b). Recent amplified climate warming on an annual average (upwards to 3.25 °C) has been observed in the region from 1948-2016 (Zhang et al., 2019). When our temperatures were compared to a compiled 10-year record (2010-2019) from the nearest EC stations, our observations were not skewed by a few extreme years (Table 3.5) (including Rock River station installed in 1994) (e.g. Garibaldi et al., 2021).

Table 3.4: Climate data for the three closest Environment Canada climate stations (1981-2010) (Environment Canada, 2020a).

	Distance/ Direction from Study Valleys	Elevation (m a.s.l)	MAAT (°C)	Precipitation (mm)	% Precipitation as Snow
Old Crow	290 km NW	250	-8.3	278.6	44.4
Dawson	115 km SW	370	-4.1	324.4	38.0
Mayo	190 km SE	504	-2.4	313.5	35.0

Table 3.5: Decadal AMAT (2010-2019) at Environment Canada climate stations in the study region (Environment Canada, 2020b) compared to study period years (2017-2019). At Rock River indicates that climate data from 2010-2015 was incomplete with several months of data missing each year. For Old Crow * indicates that due to extensive missing climate data in 2010 and 2011 they were excluded from the 2010-2019 average MAAT.*

	Site Information			AMAT °C			
	Longitude (°)	Latitude (°)	Elevation (m a.s.l)	2010-2019	2017	2018	2019
Old Crow	-139.84	67.57	250	-6.2	-6.2	-6.4	-5.5
Rock River*	-136.22	66.98	731	-4.5	-3.9	-4.7	-4.5
Dawson	-139.13	64.06	370	-3.2	-3.8	-3.2	-2.2
Mayo	-135.87	63.62	504	-1.7	-2.4	-2.0	-1.2

3.4.2 MEAN ANNUAL SITE TEMPERATURES

AMAT between the different valley and slope sensor locations varied considerably ranging 2.2 °C between the warmest site (WFS sensor) and the coldest site (SV weather station) (EFS excluded due to only 1 year of data) (Table 3.6). Each of the three sensors in the SV location had colder AMATs than the three sensors in the NV. In both valleys, valley bottom locations had the coldest AMAT while the upslope locations were all warmer. Mean annual ground surface temperature (MAGST) between the sites followed a different pattern than the AMAT. MAGST in the SV were generally warmer than the MAGST in the NV. The depth sensors were somewhat colder in the NV than the SV with the NV bottom location being the coldest. All depth sensors at slope locations were cooler than the valley bottom locations except for the depth sensor on the SFS. Five of the six locations showed average annual depth temperatures below 0 °C supporting the notion of permafrost below the station. The one exception to this was the SF sensor at around treeline were based on the depth temperature (Depth MAGT = 1.6 °C) it appears permafrost is absent.

Table 3.6: Annual Mean Air Temperatures (AMAT), Mean Annual Ground Surface Temperatures (MAGST), and Mean Annual Ground Temperature at Depth for each of the 6 sensor locations in °C. Also included are the depths from the surface each Depth MAGT sensor is positioned at (indicates that the site was installed in August 2018 rather than August 2017).*

	AMAT (°C)	MAGST (°C)	Depth MAGT (°C) (Depth cm)
SV	-5.1	0.0	-1.0 (55)
SFS	-3.4	1.6	1.6 (72)
NFS	-3.8	-0.8	-1.2 (67)
NV	-3.3	-2.0	-2.5 (61)
WFS	-2.9	-1.8	-1.9 (25)
EFS *	-2.3	-0.9	-1.1 (55)

3.4.3 STUDY PERIOD, ANNUAL, SEASONAL AND MONTHLY INVERSION CHARACTERISTICS FROM IN-SITU SENSORS

The highest I_{freq} of SBIs occurs in the SV and as a result the valley bottom had a substantially colder AMAT than the surrounding higher elevation sites (Table 3.7). SBIs in the SV persisted for longer durations on average, which led to a lower total number of separate SBI events throughout the study period. Inversion strength measured by ISLR was closely comparable between all the sites as it ranged only 0.22 °C $100m^{-1}$ between the four elevational transects. SLR in the SV had a considerably more inverted SLR on average than the NV.

*Table 3.7: Total number of distinct inversion events, the I_{freq}, the average length of inversion events, the average SBI strength measured through the mean inverted surface lapse rates (ISLRs), and the average SLR in each valley across the study period (Aug 2017 to July 2019). The * indicates that the averages across the study period are estimated based on one year of data from Aug 2018- Jul 2019.*

Transect	Total SBI Events	I_{freq}	Inversion Length (hours)	ISLR (°C $100m^{-1}$)	SLR (°C $100m^{-1}$)
SFT	731	0.62	14.3	2.40	1.21
NFT	620	0.55	15.0	2.63	0.89
WFT	798	0.43	9.0	2.20	0.46
EFT*	783	0.44	9.5	2.41	0.49

Both I_{freq} and SLRs are larger during year two of the study (September 2018-July 2019) (Table 3.8). ISLRs were to a lesser degree larger in the second year but this is only marginal compared with the other two characteristics. The monthly averages for each characteristic do not differ significantly (P-value> 0.05) from year one to year two. This is likely, at least in part, due to the large variation in monthly averages of each inversion characteristic within the year, producing a large standard deviation from the mean which masks any interannual variation between the two years. When comparing the seasonal averages for all characteristics between the two years, only wintertime I_{freq} on the SFS has a significant difference.

A Welch ANOVA test and a Games-Howell Post Hoc test was used to test the hypothesis that there are significant differences between the monthly mean SLRs on each transect. The only significant difference occurred between the SFT and the WFT (P-value = 0.00). ISLRs were similar between each of the four transects and there were no statistically significant differences found between the monthly means. ANOVA testing

between the grouping of the three transects (EFS excluded) indicates that only I_{freq} in both years had significant difference of means between the three transects (P-value ≤ 0.02). In both cases I_{freq} at the SFT was the outlier from the other transects and was only related to the mean I_{freq} observed at the NFT (both in the SV). Like findings across the entire study period, attributes of SLR and SBI characteristics indicate that SBI were more frequent and thus had a more defined influence on monthly mean SLRs in the SV.

Table 3.8: Annual SBI characteristics at each of the four elevational transects set up between the two valley locations. Annual SLRs, ISLRs, and I_{freq} are included.

	Year	ISLR (°C 100m^{-1})	I_{freq}	SLR (°C 100m^{-1})
SFT	2017-2018	2.23	0.60	1.17
	2018-2019	2.31	0.68	1.41
NFT	2017-2018	2.43	0.54	0.88
	2018-2019	2.55	0.59	1.04
WFT	2017-2018	2.01	0.41	0.38
	2018-2019	2.23	0.47	0.66
EFT	2017-2018	#N/A	#N/A	#N/A
	2018-2019	2.35	0.46	0.56

For each of the two SBI characteristics of ISLR and I_{freq}, magnitudes were greatest in the winter (Dec-Feb) (Table 3.9). This resulted in subsequent SLRs being most inverted during the winter season. Moreover, the range of I_{freq} and SLRs between the four elevational transects is greatest during the winter season. The SLRs are only normal on a seasonal average in the summer (Jun-Aug) at three of the four transects. The one exception was the SFT which had neutral (0.0 °C/ 100 m) SLR in the summer season. In all other seasons at each transect, SLRs were on average inverted. One exception to this pattern was a neutral SLR on the EFT during the spring season. At no point did the SLR conform to the assumed ELR of -0.65 °C/ 100 m.

The mean I_{freq} between the transects were significantly different in the winter, spring, and autumn seasons (p-values < 0.05). Tukey Post Hoc test indicated that the SFT, and WFT had a significant difference between their means in all seasons except for the summer season. The only other statistically significant finding was for the mean SLRs between the transects during the winter season. Post Hoc Tukey test indicated that both the SV transects were significantly different from the WFT in the NV.

Table 3.9: Seasonal SBI characteristics at each of the four elevational transects set up between the two valley locations. Seasonal ISLRs, I_{freq}, and SLRs during the duration of the study period (August 2017-2019) are included. The winter season is bolded to highlight that inversions are strongest and most frequent in the winter (Dec-Feb). The range of each SBI characteristic seasonally between the sites is also included.

	Season	ISLR (°C 100m^{-1})	I_{freq}	SLR (°C 100m^{-1})
SFT	**Winter**	**3.2**	**0.80**	**2.4**
	Spring	2.0	0.61	0.9
	Summer	1.4	0.39	0.0
	Autumn	2.4	0.66	1.4
NFT	**Winter**	**3.2**	**0.78**	**2.3**
	Spring	2.4	0.47	0.2
	Summer	1.8	0.33	-0.3
	Autumn	2.5	0.60	1.1
WFT	Winter	**2.6**	**0.54**	**1.1**
	Spring	1.9	0.44	0.3
	Summer	1.6	0.28	-0.2
	Autumn	2.3	0.43	0.6
EFT	**Winter**	**2.7**	**0.61**	**1.4**
	Spring	2.0	0.37	0.0
	Summer	2.0	0.26	-0.2
	Autumn	2.5	0.49	0.8
Range	**Winter**	**0.6**	**0.26**	**1.3**
	Spring	0.5	0.23	0.9
	Summer	0.6	0.13	0.3
	Autumn	0.2	0.23	0.8

There were different months of peak ISLRs between the two valleys (Figure 3.5). In the SV, ISLR showed a well-defined peak in February (SFT = 3.70°C $100m^{-1}$; NFT = 3.67°C $100m^{-1}$). In the NV ISLR had a peak ISLR that occurs in November (WFT = 2.78°C $100m^{-1}$; EFT = 2.99°C $100m^{-1}$). Minimum monthly ISLR clearly occurred in the month of August in both valleys (0.84 – 1.22 °C $100m^{-1}$).

In the SV the I_{freq} lacked a well-defined peak. There was a weak peak in December (SFS = 0.82; NFS = 0.81), with November and February lagging closely behind (0.80-0.77) (Figure 3.5). In the NV there are two monthly peaks in I_{freq}. One peak occurred in November (0.63 on the WFS) and the other in February (0.69 on the EFS). During December I_{freq} in the NV is substantially lower than any of the surrounding months. Thus, there was a wide gap (~ 0.35) between SBI frequencies between the two valleys in December. The SV had a minimum I_{freq} in June (SFS = 0.34; NFS = 0.28) which was closely followed by another minimum in August. The NV had a clearly defined minimum I_{freq} in August.

Monthly SLRs were shaped by a combination of SBI strength and frequency. The SV had a maximum peak of SLR occurring in February (SFT = 2.77°C $100m^{-1}$; NFT = 2.63°C $100m^{-1}$) (Figure 3.5). In the NV there was a peak of SLR in November (WFT = 1.49°C $100m^{-1}$; EFT = 1.76°C $100m^{-1}$). Both sites had the most normal SLRs occur in August (-0.11°C $100m^{-1}$ - -0.68°C $100m^{-1}$) with a second peak in June (-0.09°C $100m^{-1}$ - -0.52°C $100m^{-1}$). In the SV SBI shaped the monthly SLRs resulting in hyper inverted results (>1 °C/ 100 m) from November through March. The NV had on average a strongly inverted SLR from November through February excluding December on the WFT. SLRs were consistently positive between all the elevational transects only during

June and August. The month with the largest range between values in the two valleys was December due to less inverted SLRs than surrounding months in the NV.

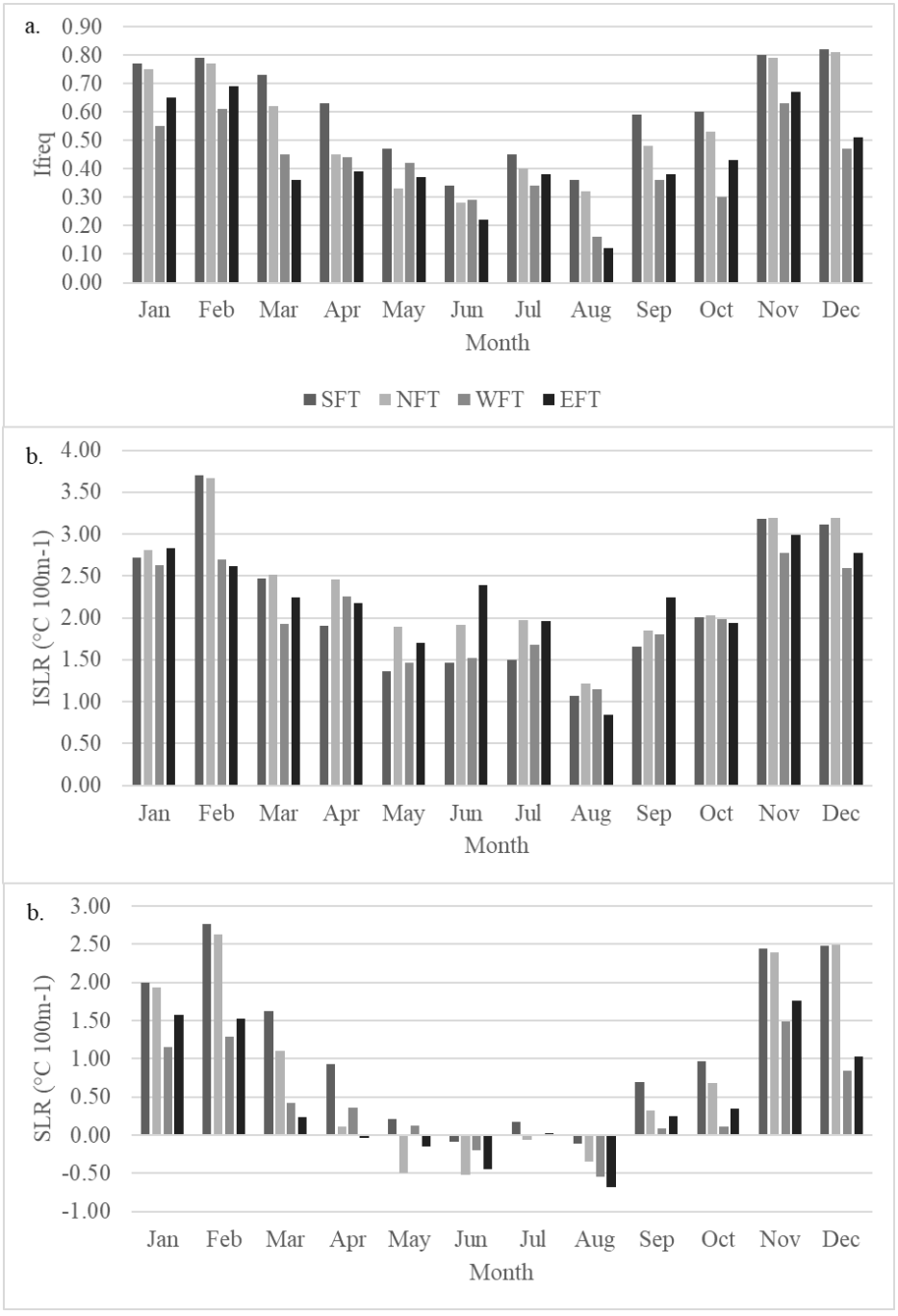

Figure 3.5: Monthly a) I_{freq}, b) ISLR, and c) SLR displayed for each elevation transect. Note that the EFS only represents one of the two years in the study period (Aug 2018-2019).

3.4.4 INVERSION EVENT LENGTH CLASSIFICATION

For each of the transects in the two valleys there were more individual transient SBI events than persistent events (Table 3.10). These made up the vast majority of the proportion of the total number of SBI events in both valleys during the study period (August 2017-July 2019). Persistent SBI events dominated the proportion (≥55%) of the total SBI hours in the SV while they made up nearly half of the total SBI hours in the NV.

*Table 3.10: SBI are defined by event length as transient (<18 hours) or persistent (≥18 hours) events. This table includes the number of transient and persistent SBI events, the proportion of total SBI events each classification of SBI length classification made up, the total SBI hours attributed to each classification of SBI event, and the proportion of total SBI hours attributed to each SBI length classification for the four elevational transects during the study period (August 2017 - July 2019, * denotes that the East Facing Slope transect consists of data only from August 2018 – July 2019).*

Location	Inversion Events	Events	Proportion of Total Events	Hours	Proportion of Total SBI Hours
SFT	Transient	582	0.80	3884	0.37
	Persistent	**149**	**0.20**	**6596**	**0.63**
NFT	Transient	502	0.81	4200	0.45
	Persistent	**118**	**0.19**	**5100**	**0.55**
WFT	Transient	672	0.84	3908	0.54
	Persistent	**125**	**0.16**	**3278**	**0.46**
EFT*	Transient	342	0.87	2044	0.55
	Persistent	**49**	**0.13**	**1672**	**0.45**

Likewise, to patterns observed on an annual scale, persistent SBI events remained less frequent than transient SBI events on a seasonal scale, even in the winter season. Though they represented a much lower proportion of the total SBI events, the persistent SBI events did account for a substantial number of total hours with an SBI present. During the winter the highest number of persistent events and peak proportion of hours (up to 86 % in SV) with an SBI present that were associated with SBI events classified as persistent. Similarly, in the autumn season persistent SBIs also, to a lesser degree, dominated the proportion (60-70 % in the SV) of total hours with an SBI present. Spring and summer seasons saw a dramatic drop in the number of persistent SBI events and subsequent proportion (≤31%) of hours represented by these events. In the spring, the WFT in the NV had a slightly higher proportion of total hours with an SBI present attributed to persistent SBI events than the transects in the SV. In every other season the SV transects had a larger proportion of the total hours with an SBI present attributed to persistent SBI events than the transects in the NV.

The longest SBI events each lasted for roughly 12 days (based on two-hour temporal resolution) and these events occurred in the SV (Table 3.11). In the NV the WFT had an SBI event last roughly 9 days and the EFT roughly 4.5 days. The mean persistent SBI event duration was substantially longer on the SV transects. Mean SBIs were much greater than the median SBI lengths and thus were skewed to be longer by a few outlying lengthy SBI events. The median values imply that most of these persistent inversion events are most often approximately one day long.

Table 3.11: Attributes of persistent SBI events are described including the maximum length of persistent SBI events, the mean length of persistent SBI events, and the median length of persistent SBI events during the study period (Aug 2017 - Jul 2019).

Persistent Events	Max Length (hr)	Mean Length (hr)	Median Length (hr)
SFT	292	44.3	26.0
NFT	288	43.2	24.0
WFT	216	36.0	22.0
EFT	112	34.1	20.0

3.4.5 NIGHT VS DAYTIME INVERSIONS

SLRs during the daylight hours on an annual average were gently inverted or gently normal depending on the transect (Figure 3.6). During the night SLRs were hyper-inverted, averaging over 2 °C/ 100 m in the SV while averaging closer to 1 °C/ 100 m in the NV. This strong diurnal pattern of SLRs is exemplified by the summer average SLRs during the night and day hours where they were normal (-0.17 – -0.58 °C/ 100 m) during the day and inverted (0.5 – 0.8 °C/ 100 m) at night. This diurnal pattern breaks down with low sun angles and short days in the winter when inversion most frequently persist beyond the normal diurnal pattern observed in the summer. This is characterised by similar SLRs between both nighttime and daytime readings in the winter season on average. On the SFT daytime SLRs are slightly more inverted than nighttime SLRs. A statistically significant difference was found between median SLRs during the night and day after the Kruskal-Wallis test was completed (P-value = 0.00). In the winter season the only site with statistically significant differences between the median SLRs in the day and night was SLRs calculated for the SFT (P-value = 0.03).

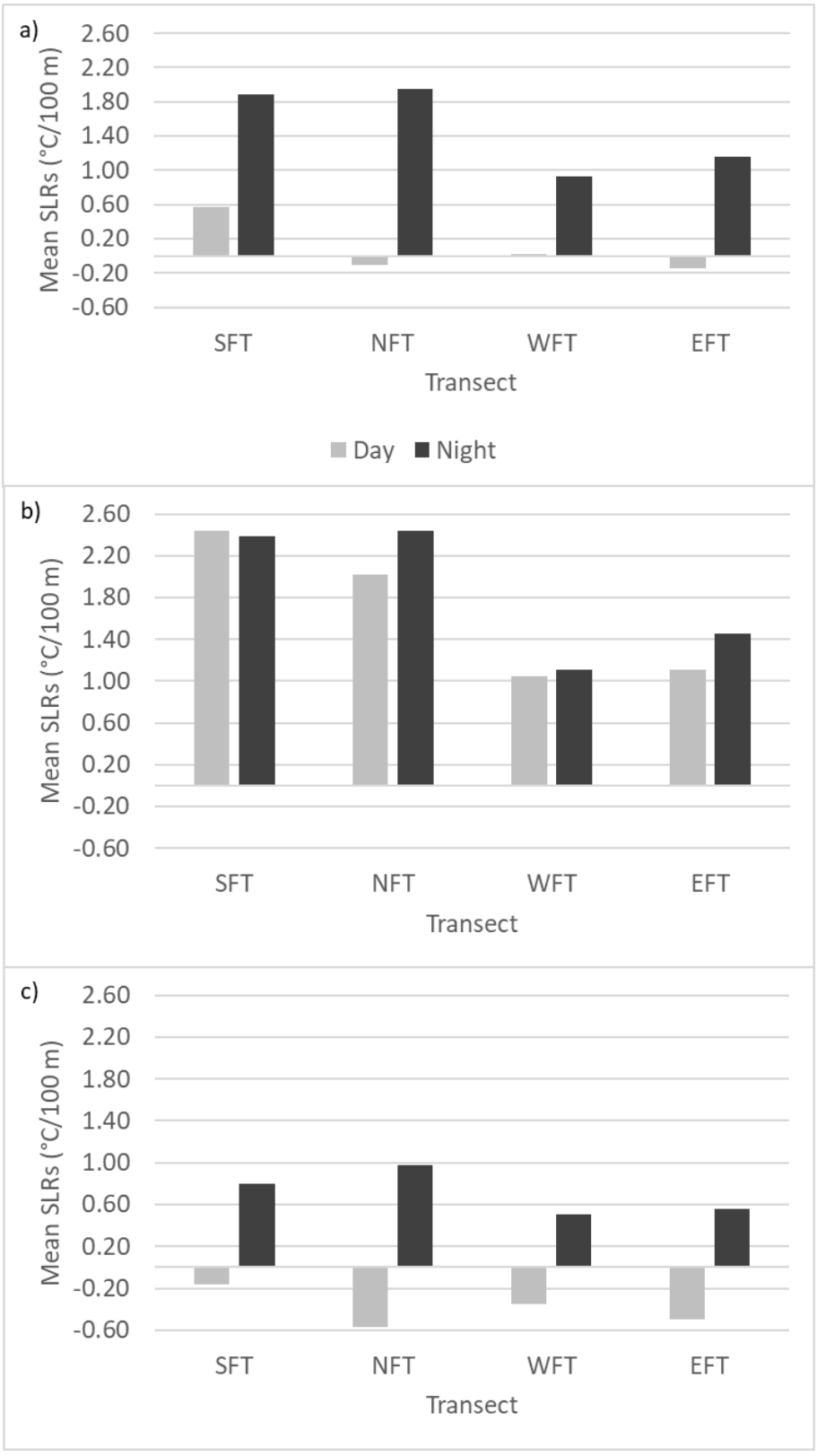

Figure 3.6: SLRs on each transect during night and day readings a) annual b) winter c) summer.

3.4.6 MICROCLIMATE IN EACH VALLEY

On an annual average the peak incoming solar radiation at both sites occurred at 14:00 PST with values of 232 and 253 Wm^{-2} in the SV and NV respectively (Figure 3.7). The only exception to this pattern seasonally occurred during the summer in the SV when incoming solar radiation was greatest during the 16:00 PST reading. Minimum solar radiation on annual average occurred at both weather station locations during the 2:00 PST reading. Overall solar radiation was greater on annual average in the NV with an annual average incoming solar radiation of 81.7 Wm^{-2} compared to 78.3 Wm^{-2} in the SV. Mean solar radiation had roughly the same difference between the valleys with the NV having a mean incoming solar radiation that was roughly 3 - 6 Wm^{-2} greater than the SV in the winter, autumn, and spring. Meanwhile in the summer the mean incoming solar radiation was roughly 3 Wm^{-2} greater in the SV. On annual and seasonal average, according to a Mann-Whitney U test, median solar radiation differs significantly between each weather station location (P-value < 0.05).

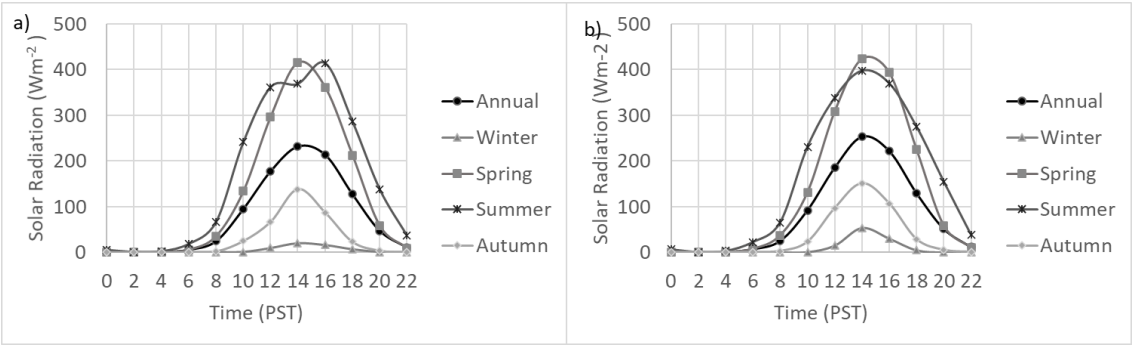

Figure 3.7: Annual and Seasonal average solar radiation by two-hour increments during the day a) weather station in the SV b) weather station in the NV.

Dominant wind conditions in the SV were light (≤1.5 m/s) and blowing from the southwest (Figure 3.8a). Whereas in the NV wind was most frequently from the south at speeds ≥ 1.5 m/s. The highest wind speeds recorded in the SV were from the north and

northwest (≈5.5 m/s) while in the NV were from the south and southeast (≈13 m/s) (Figure 3.8b). Typically, the wind was much lighter in the SV with wind speed averaging 0.07 m/s across the study period compared to the NV which averaged 1.97 m/s. In the SV wind was calm (<0.5 m/s) over 90% of the time while in the NV valley was only calm roughly 25% of the time. This large difference in wind speeds were observed in each season and for both annual and seasonal averages there were statistically significant differences in median wind speed between the valleys based on Mann-Whitney U tests (P-value ≤ 0.00). On a seasonal average, wind speed in the NV was highest in the winter while the opposite was true in the SV where wind speed was greatest in the summer.

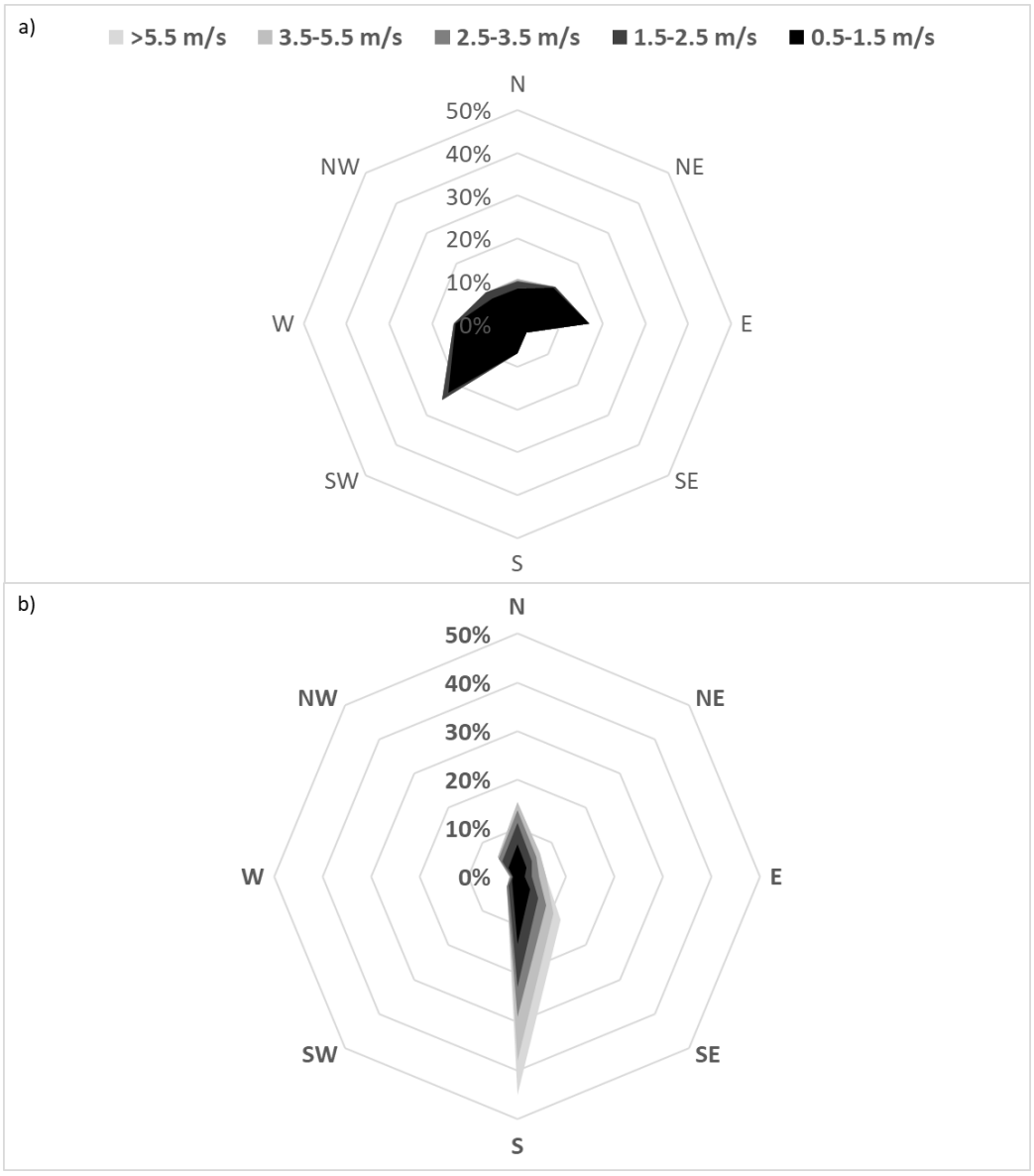

Figure 3.8: Wind rose diagrams for each weather station valley location a) SV weather station b) NV weather station.

Relative humidity (RH) was highest in the SV with an annual average of 77.4% while the NV averaged 71.1%. This difference in RH readings was also recorded in each season with the NV having lower RH. In both valleys the highest RH occurred in the autumn season followed closely by the winter season. The lowest RH occurred during the summer; however, spring RH was very close in value. Overall, these seasonal RH averages ranged from around 84% (76%) to 70% (68%) in the SV (NV).

3.4.7 MONTHLY AVERAGE AIR TEMPERATURE AMPLITUDE

Amplitude between the warmest and coldest average monthly SAT temperatures based on our in-situ sensors was calculated. In the SV amplitude was 34.3 °C while 31.5 °C and 31.2 °C at the NFS and SFS respectively. In the NV monthly average temperature amplitude was 30.8 °C at the weather station in the valley bottom while 30.0 °C and 30.7 °C at the EFS and WFS respectively. The EFS may not be representative because it only consists of one year of data (2018-2019) compared to the other sites 2 years (2017-2019) of data.

3.4.8 IN-SITU MEASURES COMPARED TO MODELLED MEAN ANNUAL AIR TEMPERATURES

Examining the modeled surface developed by Lewkowicz et al. (2012) MAAT at each site was predicted. In the SV MAAT was predicted to be -4.58 °C. At the SV slope locations MAATs were predicted to be -4.45 °C on the SFS while -4.41 °C on the NFS. Using the MAATs predicted by the model SLRs would be roughly 0.2 °C/ 100 m. Thus, the influence of the SBIs on SLRs in this valley were grossly underpredicted. The actual annual SLRs in this portion of the valley as measured by in-situ sensors were 0.8-1.2 °C/ 100 m. The NV was positioned above treeline in reality but not according to the MAAT model (treeline predicted to be 1170 m a.s.l in the NV and 1180 m a.s.l. in the SV). Thus, part way up each slope SLRs were predicted to be inverted on annual average while above 1170 m a.s.l. SLRs reversed back to normal (-0.65 °C/ 100 m). As a result, MAAT were predicted by the model to be -4.78 °C at the NV bottom weather station, -4.83 °C on the EFS, and -4.90 °C on the WFS. Therefore, SLRs between the sites would have been roughly -0.05 to -0.12 C/ 100 m. According to our in-situ data, SLRs on these two

transects were roughly 0.45-0.5 °C/ 100 m meaning that they were inverted, while somewhat less intensely than the SV, inverted on an annual average. This indicates that again, the influence of SBIs on SLRs in the NV were neglected by the model but in this case, it was due to the prediction of normal SLRs in a valley above treeline which was not recorded in our measurements.

3.4.9 PREDICTED SURFACE LAPSE RATES USING CLIMATE REANALYSIS DATASETS

On annual and seasonal scales each of the climate reanalysis datasets ERA5, JRA-55, and MERRA-2 had SATs that were predicted to be nearly the same between all sites including the local high point, Distincta Peak (1760 m a.s.l.) (Figure 3.1). Thus, little variability across these small horizontal distances with substantial elevational heterogeneity are being observed in the climate reanalysis datasets. This is exemplified as winter seasonal SLRs for each model were on average near 0 °C/ 100 m for each transect (Figure 3.9). A large elevational transect from the SV valley bottom to Distincta Peak with vertical distance of around 700-800 m was similarly predicted to be near 0 °C/ 100 m. ClimateNA predicts annual average SLRs that are closest to being representative on the WFT and the SV bottom and Distincta Peak transect. These SLRs are still predicted to be roughly ten times smaller than the actual observed SLRs. No seasonal pattern of more strongly inverted winter SLRs were observed in the predicted SLRs.

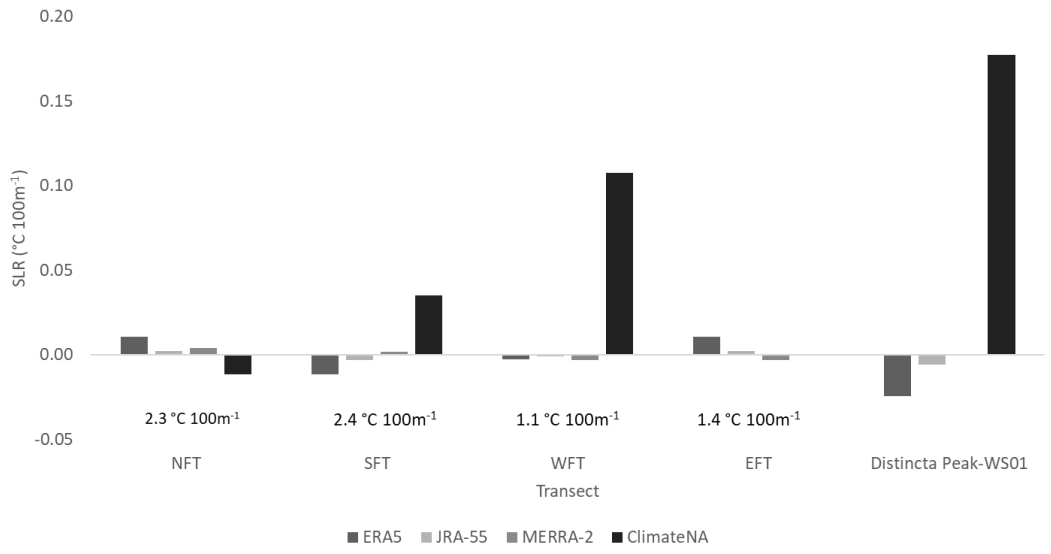

Figure 3.9: Comparison of winter season SLRs predicted using downscaled climate reanalysis data. Listed below the bars for each elevation transect is the actual average in-situ measured wintertime SLRs.

Both measured and downscale modelled SLRs between each transect were graphed to test for the correlation between SLR values. Results of this process give an indication into how well moments with inverted SLR are being predicted by each climate model in relation to what is actually being measured in each valley. If predicted accurately, it would be expected that there would be a significant positive linear relationship between the modelled SLRs and the observed SLRs if there was an accurate accounting of when SLRs were inverted. For each transect there was little to no relationship between the SLRs. On each transect both ERA5 and JRA-55 models had significant p-values (P-value ≤ 0.05) but the R^2 of the linear relationship between the two was low (<0.11). The relationships that were observed were not only weak, but they also indicated that at times during observed inverted SLR there was a trend towards prediction of more normal SLRs. In the end, with no consistent patterns and low R^2 values, indications are that the models do not accurately account for the timing of inversion events on a two-hour temporal resolution scale. Another finding important to note from

this analysis was the extra ordinarily high variability in minimum and maximum SLR values predicted by the MERRA-2 model. The ranges on the graph for the other two models never even approached 1 or -1 °C while on the MERRA-2 model graph the minimum and maximum range values for SLRs was upwards to 30 or 40 °C on the transects located in the NV.

3.5 DISCUSSION

3.5.1 SURFACE-BASED TEMPERATURE INVERSION CHARACTERISTICS BETWEEN THE VALLEY ELEVATION TRANSECTS

Inversion strength (represented by ISLRs) and I_{freq} was greatest in the winter season which is consistent with other research completed on high-latitude SBIs (Seidel et al., 2010; Zhang et al., 2011; Mayfield & Fochesatto, 2013; Shahi et al., 2020). This pattern suggests the dominance of anticyclonic conditions in the region during the winter months (Mayfield & Fochesatto, 2013) and the prevalence of cold-air drainage resulting in cold pooling due to net negative radiative balances (Daly et al., 2010). Similar to findings in Shahi et al. (2020), the spatial variation of SBI ISLRs and I_{freq} between the two valleys was greatest during the winter months. This means that the focus of variation in SBI characteristics between the four transects should be the winter months. Furthermore, during the nighttime hours throughout the study period, SBIs were significantly more frequent than daytime readings resulting in inverted SLRs. This pattern is also consistent with findings observed in other literature regarding SBI characteristics on a diurnal scale (Whiteman & Richland, 2000).

Diurnal and seasonal variation of SBI frequency drive SLR variations spatially and temporally between the four sites. For example, I_{freq} on the NFT was roughly 40%

during the nighttime readings across the study period compared to roughly 18% during the daytime readings (Figure 3.6). In comparison, ISLRs during the night on the NFT were 2.8 °C $100m^{-1}$ during the night and 2.4 °C $100m^{-1}$ during the day. While there is a difference between ISLR values in night and day readings these were much less defined than the variation in I_{freq}.

One finding that stood out as abnormal was that I_{freq} and SLRs were greater during the second year of the study period even though temperature on an annual average was warmer during the second year (Aug 2018-2019). While temperatures on annual average were warmer in the second year, on a seasonal average they were colder in the second winter (December 2018 – February 2019) (SV =-19.4 °C and NV = -14.5 °C) than the first (December 2017 – February 2018) (SV =-17.0 °C and NV = -13.0 °C). Since winter has the most frequent and strongest SBIs, winter season SBI characteristics have the most influence on defining annual average SBI characteristics of any season. Increased prevalence of cold-air drainage and subsequent SBIs could follow a pattern of wintertime SATs that are colder in the second year (Bourne et al., 2010; Chapter 2). This potential relationship was signified by SLRs in the second winter that were more inverted by ~0.65 °C $100m^{-1}$ in the SV and ~0.47 in the NV °C $100m^{-1}$ than in the first winter.

I_{freq} was linked to the average length of SBI events in each valley. In the SV the two transects had average SBI event lengths of 14 to 15 hours while in the NV SBI event length on average lasted only between 9 and 9.5 hours. Between the four transects, persistent SBIs were longer and more frequent in the SV leading to more regular occurrence of inverted SLRs. Thus, these persistent SBIs play an important role in

shaping SBI frequency and the variability of SLRs spatially on these valley-to-valley local scales.

Research on the evolution of persistent cold pooling and subsequent SBI events has been undertaken in multiple studies (Whiteman et al., 2001; Pigeon and Jiskoot, 2008; Barry, 2013; McCaffrey et al., 2019; Sun & Holmes, 2019). What is lacking is a study of the development and evolution of persistent cold pooling events in high-latitude areas, particularly those in the mountainous areas of northwestern Canada. Due to the significance of these persistent cold pooling events in shaping the variability of SLRs spatially, there is a need for more comprehensive review of persistent SBI events. Furthermore, it is essential to obtain a deeper understanding regarding why it is that SBIs persist past a normal diurnal cycle more readily in one valley compared to the other.

3.5.2 MICROCLIMATE INFLUENCES ON LOCAL SCALE SURFACE LAPSE RATE VARIATION

SBI development, persistence, and breakup is linked to weather conditions in locations where they occur (Daly et al., 2010; Pike et al., 2013; Williams & Thorp, 2015). On valley-to-valley scales, microclimatic condition variance between the valleys becomes an important aspect to review when assessing why there is variability of local weather conditions and subsequent SBI characteristics (Whiteman, 1982; Sakiyama, 1990). It is difficult to ascertain if a climate condition is covarying with an SBI characteristic or if the microclimatic condition is defining variability of SBI characteristics. In this section any relationship between microclimate conditions and SLRs resulting from SBI characteristics will be identified. The aim of this will be to assist in future work of understanding why SBIs vary on local valley-to-valley scales in high-latitude regions.

3.5.3 SURFACE LAPSE RATES AND WIND SPEED/DIRECTION

Wind speed was found to be substantially greater in the readings immediately following SBI breakup compared to the readings directly before SBI breakup (Table 3.12). The linear mixed-effects model analysis indicates that wind speed does indeed have a significant correlation with SLRs between each of the four transects during the study period. In the literature, debate exists whether increased wind speed is responsible for inversion breakup or if increased wind speed is the result of destabilization of the lower atmosphere following SBI breakup. The results of this research cannot answer this question; however, similar to other studies findings indicate that wind speed and SLRs are correlated in valleys of northcentral Yukon.

Synoptic wind speed aloft is related to the erosion of an SBI from the top down (Whiteman & Doran, 1993; Pepin et al., 2009). The ability of the winds aloft to mix down to the surface has been linked to the longer persistence and the eventual breakup of lengthy persistent inversion events on some locations (Pepin et al., 1999; Lundquist & Cayan, 2007; Wei et al., 2013; Lu & Zhong, 2014; Lareau et al., 2015). Specifically, C. D. Whiteman et al. (2001) found that the cold pool did not persist after wind speeds at their lowest sites were above 3.1 m/s. While this is an example of a potential wind speed threshold used in previous research there are no consistent estimations for wind speed at which SBI most often cannot persist through in the literature. In our findings, SBIs were present with and without the presence of wind. An attempt was made to see if a wind speed threshold existed however, no definite conclusions could be reached. SBI were recorded while wind was roughly 11 m/s and even during the heaviest winds (≈ 13 m/s,

NV). The SV rarely had wind recorded to be ≥2 m/s and when it did SBI were still recorded to be present during some readings.

When synoptic winds aloft at ridgetop level are weak the valley atmosphere becomes decoupled from the free-atmosphere (Daly et al., 2010) and thermally driven mountain valley wind systems develop and dominate (Whiteman & Doran, 1993; Whiteman et al., 2004; Lundquist & Cayan, 2007). The development of local valley wind systems through unequal heating or cooling of the surface (Pielke, 2002) can drive both the formation of cold pools and their eventual dissipation (Anquetin et al., 1998). Downslope winds dominate during cold-air drainage that can lead to the formation of strong SBIs (Gustavsson et al., 1998). Previous research suggests that cold-air pooling can be more intense in forested valleys compared to unforested (Gross, 1987; Gustavsson et al., 1998). This is consistent with our findings for these two valleys. The SV has trees which increase surface roughness reducing wind speeds. This results in decoupling of the sub-canopy atmosphere producing strong vertical stratification of temperature near the surface (Launiainen et al., 2007). This idea was theorized in Yukon by Wahl (2004), while measurements in A. G. Lewkowicz et al. (2012) suggest that above treeline SLRs in high-latitude Yukon valleys reverse back to normal due to reduced surface roughness.

Valley depth, width, and length all contribute to the strength at which along valley and cross valley flows can develop (Wagner et al., 2015) and can influence cold-air pooling in the valley bottom (Kiefer & Zhong, 2015). When there is a bend in the valley the wind speed associated with the along-valley flow can be significantly altered (Kossmann & Sturman, 2003). These factors may all play a role in the development of unique thermal wind systems in each valley. For example, in the SV the wind was light

and more variable. Valley orientation would suggest large temperature gradients between the SFS and the NFS resulting in across valley thermal winds that can dominate through more significant proportions of the day, whereas winds in the valley bottom remain light and variable (Weigel et al., 2006). Furthermore, this valley is shorter and curved meaning along-valley winds would likely be weaker.

Most commonly SBI are associated with down-valley winds in the form of cold-air drainage (Gustavsson et al., 1998). When SLRs were compared with wind direction in the NV a strong pattern was observed where SLRs were substantially more inverted during southerly down-sloping winds (Table 3.13). This same pattern was not observed in the SV. Another note of this wind direction and SLR comparison is that in both valleys SLRs are predominantly inverted during calm wind conditions (wind speed <0.5 m/s) which solidifies the conclusion made regarding lighter winds to increased SBI activity.

There is still much opportunity to verify the connection between wind speed and local SBI characteristics in this region. Future incorporation of wind-speed modelling in valleys could be imperative to increasing the accuracy of predicting SLRs for permafrost modelling in the future. Thresholds of wind speed if they exist, need to be found in future research to be added into future modelling of SLRs and SATs in this region for more accurate accounting of SBI impact.

3.5.4 SURFACE LAPSE RATES AND SOLAR RADIATION

One major component to both the development (Gustavsson et al., 1998) and breakup (Whiteman et al., 2001) of SBI is the presence or lack of solar radiation to warm the surface. As the surface warms from incoming solar radiation, the convective boundary

layer (CBL) begins to erode the SBI from the surface upwards. This eventually, if strong enough, entirely mixes out the SBI layer resulting in a recoupling of the near-surface atmosphere with conditions aloft (Whiteman, 1982).

Statistical testing using a linear mixed-effects model indicated that at each transect SLRs are significantly related to solar radiation (P-value < 0.05) across the study period except for the SFT (P-value = 0.613). Furthermore, when SBI are present compared to when SBI are absent the mean incoming solar radiation is substantially less (Table 3.12). In readings directly before inversion breakup solar radiation is also sharply less than the reading immediately following SBI breakup. This confirms the concept in the two valleys that solar radiation has a close relationship to SBI breakup (Leukauf et al., 2015).

Topographic shading and slope aspect can shape patterns of SBI breakup (Colette et al., 2003; Williams & Thorp, 2015). In the case of our research, topographic shading and aspect played a particularly important role in the SV. The SFS location would receive much more incoming radiation throughout the year than even the SV valley bottom location. Meanwhile the NFS would have the least annual average incoming solar radiation. On the SFT, SBIs were significantly more frequent than the NFT. This led to SLRs that were significantly more inverted on annual average than the NFT, whereas SLRs were near neutral in the summer while being much closer to normal on the NFT. We hypothesize that incoming solar radiation warmed the SFS while the valley bottom had little to no direct incoming solar radiation and thus minute warming of the surface resulting in an SBI on the SFT. As suggested by Colette et al. (2003), this pattern would be most prevalent during times when there is a lack of clouds and the SFS is in direct sunlight while the valley bottom is shaded by topography. An example of where this

similar situation was observed in Central Yukon valleys is discussed in Cote (2002). Thus, these inversions were not always linked to CAP but could occur due to differential heating of the slope based on aspect. This may also explain why there was no significant relationship between solar radiation in the SV bottom and SLRs on the SFT. In this case, SBI were formed through the presence of solar radiation rather than the absence of it, as frequently occurs in cases linked to cold-air pooling. Conversely, the NFT should show the opposite effect of aspect on SBIs. The NFS location has lower incoming solar radiation than the valley bottom due to topographic shading. Warmer valley bottom temperatures due to direct solar radiation would expel any existing SBIs or inhibit formation of SBIs on the NFT. Further evidence of this is that SFT had considerably higher presence of SBIs with non-calm winds than the NFT (Table 3.13) which would suggest that SBIs can remain present or develop due to aspect and topographic shading on the SFS when wind speeds are greater. Trees also can play a role in reducing ground level solar radiation however, the forest in the SV lacks a thick canopy. Where the SV weather station is set up there are no trees in the direct vicinity shading the station throughout the day.

3.5.5 SURFACE LAPSE RATES AND SURFACE AIR TEMPERATURES

SBI are often associated in mountain valley areas with the presence of a cold pool of air near the surface (Whiteman & Richland, 2000). These cold air events can become intense and produce extremely cold conditions in low lying areas (Harris, 1982; Clements et al., 2003; Whiteman et al., 2004). SBI have also been observed to occur when synoptic weather conditions include cold, dry, and stable Arctic airmasses (Serreze et al., 1992; Blandford et al., 2008; Vitasse et al., 2017) where surface conditions are cold.

The results of our in-situ SLR data indicate that SATs are significantly colder while SBI are present during the study period (Table 3.12). The issue with this conclusion is that most SBI occur during the winter months. Thus, due to seasonality in the SATs at these valley locations the results may be skewed to being colder during inverted SLR readings compared to normal SLR readings. Seasonally winter was examined to determine if SBI correlated with colder SAT. In the SV (NV) valley bottom SAT when SBI were present average -20.1 °C (-16.5 °C) compared to -12.1 °C (-10.6 °C) when SLRs were normal. Furthermore, in the readings directly before inversion breakup SATs were substantially colder than the moment immediately following inversion breakup.

Extreme cold events and SBI presence were compared by observing SLRs for each reading with a SAT at or below -30 °C. In the SV every single reading with temperatures at or below -30 °C had inverted SLRs on both transects. In the NV the SLRs were inverted roughly 75% of the time on both transects in extreme cold conditions. This highlights that extremely cold SATs in the SV were connected to the presence of SBIs with a similar but less defined pattern in the NV. What may contribute to this pattern is microclimatic conditions such as wind speed. These differed significantly between the valleys, thus perhaps driving SBI breakup even during extreme cold conditions in the NV.

Table 3.12: Each microclimate condition across the study period (Aug 2017 to July 2019) for the entire dataset, readings with SBIs present, readings without SBIs present, the last reading before breakup of each SBI event, and the first reading immediately following breakup of each SBI event.

		Entire Dataset	Inversion Present	Inversion Absent	Post Inversion Breakup	Just prior to Breakup
Solar Radiation (Wm^{-2})	SFT	78.3	35.5	148.6	183.7	123.4
	NFT		10.4	161.7	122.7	40.2
	WFT	81.7	30.6	119.7	111.9	60.9
	EFT	82.7	16.3	135.1	117.2	41.5
Wind Speed (m/s)	SFT	0.07	0.01	0.15	0.09	0.06
	NFT		0.00	0.14	0.03	0.01
	WFT	1.97	1.05	2.66	2.35	1.77
	EFT	1.96	1.06	2.68	2.53	1.9
SAT (°C)	SFT	-5.0	-10.0	3.1	2.3	-0.1
	NFT		-11.4	2.8	-0.6	-3.9
	WFT	-3.3	-7.8	0.1	-0.7	-2.7
	EFT	-2.7	-7.9	1.3	-1.0	-3.2

Table 3.13: Percent of hours with a recorded wind direction, average SLRs during that time, and percent hours an SBI is present during each wind direction. Each of these are totaled for the entire dataset form August 2017 to July 2019.

Wind Direction (WD)	Transect	N	NE	E	SE	S	SW	W	NW	Calm
SV % Hours of WD		1.0	1.2	1.6	0.3	0.7	2.4	1.4	1.0	90.4
Average SLR (°C $100m^{-1}$)	NFT	-1.5	-1.9	-2.2	-2.6	-2.1	-1.5	-1.5	-1.1	2.4
	SFT	-0.3	-0.3	-0.5	-0.9	-0.8	-0.9	-0.9	-0.6	2.2
% Hours SBI Present	NFT	2.3	1.0	0.0	0.0	0.0	1.0	1.7	6.0	83.6
	SFT	11.6	35.0	26.7	8.3	7.3	4.5	7.5	17.9	84.7
NV % Hours of WD		11.3	5.0	4.6	9.6	35.5	2.3	1.1	4.2	3.1
Average SLR (°C $100m^{-1}$)	EFT	-0.6	-0.5	-0.4	-0.2	0.6	-0.4	0.0	-0.8	1.0
	WFT	-0.3	-0.2	-0.4	-0.1	0.5	-0.1	0.0	-0.4	0.8
% Hours SBI Present	EFT	15.3	16.3	6.5	29.5	49.8	27.3	31.0	14.4	58.4
	WFT	21.7	21.9	16.8	26.4	46.2	30.3	28.3	17.6	52.7

3.5.6 ASSUMED ANNUAL AVERAGE SURFACE LAPSE RATES

Minder et al. (2010) highlighted the errors that came when predicting SAT in complex terrain using assumed average SLRs in the Cascade Mountains of Washington, USA based on the ELR (-0.65°C $100m^{-1}$). In these valleys using ELR to interpolate SATs in the valleys, slope temperatures are predicted to be much colder than observed by in-situ sensors (Figure 3.10). SLRs were assumed to have a maximum annual average inverted rate of 0.1°C $100m^{-1}$ in previous MAAT and permafrost distribution modelling for this region (Lewkowicz et al., 2012; Bonnaventure et al., 2012). In comparison 0.1°C/ 100 m is still significantly less inverted than the average annual SLRs of ≥0.46 °C $100m^{-1}$ recorded on each elevational transect. Error in predicted temperatures across this mountainous landscape would be produced if SLRs were assumed to average the ELR or even if assumed to be gently inverted on an annual basis. This error is also magnified in the SV where SBI are more prevalent and intense throughout the year.

Pidgeon and Jiskoot (2008) found that lapse rates during days with an SBI present there was much higher variance of lapse rates then days when there was no SBI. One solution proposed in areas with frequent SBIs was to review median lapse rates on a seasonal or annual scale to better represent lapse rates in the region. The median on an annual scale in the two valleys is 0.67 °C $100m^{-1}$,0.39 °C $100m^{-1}$, -0.31 °C $100m^{-1}$, and -0.30 °C $100m^{-1}$ on the SFT, NFT, WFT, and EFT respectively. Taking the median in this case greatly reduces the extent of the inverted SLRs in the SV while reversing the SLRs to being normal in the NV (though still nearly 0.35 °C $100m^{-1}$ much gentler than the ELR). Though these values are closer to some of the previous model projections there is still substantial spatial variability of SLRs that are missed and assumptions that are made

that miss the strong influence of SBIs in the SV. Using the median or the mean SLRs based on regional in-situ measures could be an option for modelling moving forward. By applying these values to models, assumptions previously made for these regions can be adjusted and more accurate representations of SATs can be made in these mountain valley locations.

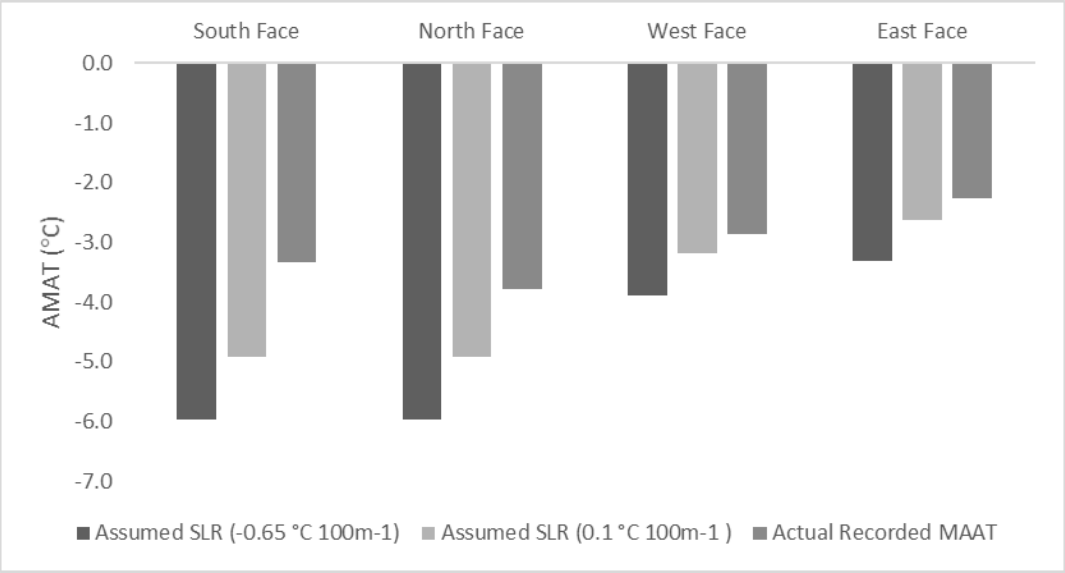

Figure 3.10: Presumed MAATs at each slope location based on SLRs being assumed to be 1) the Environmental lapse rate 2) annual average SLRs used for this study region in Bonnaventure et al. (2012) for permafrost probability modelling that aimed to account for SBIs that dominate throughout the year.

3.5.7 SURFACE LAPSE RATES FROM DOWNSCALED CLIMATE REANALYSIS DATASETS

GlobSim nearly entirely missed the impact SBIs had on SLRs (Figure 3.9). In most cases SLRs on annual and seasonal averages were predicted to be near zero for the lowest 100 m of the atmosphere. The main question linked to these findings is whether vertical temperature resolution of these models allows for prediction of SLRs at this scale or if the data only accounts for horizontal variation in temperature at these scales.

Each reanalysis product used for GlobSim has a different number of model levels for vertical readings, but these are typically interpolated into pressure levels that increase in altitude/elevation in 25 hPa increments for the lowest part of the atmosphere (1000-700 hPa) (Martineau et al., 2018; Graham et al., 2019). Vertical interpolation between the pressure levels of each reanalysis dataset by calculating the geopotential height of each reading and situating it to the elevation of the local point is used to interpolate lapse rates. Using the NOAA (2021) Pressure Altitude Calculator, rough estimates for the predicted elevations/altitudes at each pressure level were made. Increments of elevation/altitude gain began at around 210 m and that increment slowly grew until the 725 to 700 hPa pressure level, where the increment was around 275 m. The valley and slope locations fall in between the pressure level of 900 hPa and 875 hPa which are predicted to be at roughly 990 m a.s.l and 1220 m a.s.l. Distincta peak is at an elevation of 1760 m a.s.l. so SLRs between the SV bottom (993 m a.s.l.) span across pressure levels 900 hPa to a little higher than pressure level 825 hPa. This means that this transect incapsulates roughly four pressure levels. Therefore, this transect was selected and included to assess differences in SLR prediction by these downscaling products when more than two pressure levels separate the low and high site of the transect. Again, there was a near zero component to the SLRs recorded between these sites using GlobSim. This indicates that there is a lack of accounting for SBI or normal lapse rates in the atmosphere. A possible alternative to this hypothesis could be inverted SLRs in the lower parts of the atmosphere and more normal SLRs higher up cancelling each other producing near zero SLRs between these pressure levels. Though this is possible, the main finding here is that intensely inverted SLRs near the valley bottom are being altogether missed by this downscaling model. This could be a result of model accuracy or limits in vertical resolution of the models.

The authors of GlobSim acknowledge that other scaling methods could be integrated to the program to improve interpolation of point location climate conditions, based on elevation in complex mountainous terrain (Cao et al., 2019). An alternative method to calculate finer scale lapse rates in downscaled data is based on interpolation of temperature differences between the pressure levels then taking those lapse rates and adding them to SAT predicted by reanalysis datasets based on the elevation and surrounding topography of the point location (Gao et al., 2012). Gao et al. (2017) discussed different methods of correcting for elevationally controlled temperatures in the Alps produced by downscaled climate reanalysis data and found this method was by far the most effective. Thus, this method could be applied within mountain valleys for GlobSim type downscaling climate reanalysis datasets, to attempt to better account for the actual SLRs occurring on these mountain slopes. A model that deploys this methodology was recently developed by Cao et al. (2017) called REanalysis Downscaling Cold Air Pooling Parameterization (REDCAPP). This model was used to correct for limitations of predicting temperatures on fine scales in complex terrain where cold pooling frequently occurred as is observed in the two Yukon valleys of this study. Immense opportunity exists to apply this model in northwestern Canadian valleys prone to cold air drainage, to improve the prediction of SLR patterns using downscaled climate reanalysis data. What is absent from the REDCAPP program is the climate variables, other than air temperature, that are needed for many permafrost models including the northern ecosystem soil temperature (NEST) model (Chen et al., 2003; Yu Zhang et al., 2003). Furthermore, this model uses only the ERA-Interim climate reanalysis dataset (Cao et al., 2017). There is a need for integrating GlobSim and REDCAPP products in these high-latitude mountainous areas for modeling permafrost distribution.

ClimateNA predicted some SLRs that are closer to measured SLRs though still being ten times less in magnitude. ClimateNA may be representing SLRs of these transects slightly closer to in-situ measures due to predicted temperatures across the landscape based on empirically derived regional lapse rates which are assumed to remain invariant across the region (Wang et al., 2016). This is particularly problematic for the study area as there is little to no observational climate data within close vicinity. This means assumptions of lapse rates in this region are based on limited data and do not vary on the fine scales reviewed in this research.

Assessment of climate reanalysis data has seldom been completed in complex terrain (Roberts et al., 2019) as seen with GlobSim and ClimateNA. GlobSim has been observed to work reasonably well in predicting climate variables necessary for permafrost distribution modelling in a non-mountainous area of the Northwest Territories, Canada (Cao et al., 2019). ClimateNA has been applied in mountainous areas across North America with some success, particularly when projected over long periods of time (Wang et al., 2012). These climate data downscaling products are extraordinarily useful in broadly understanding climate conditions, particularly when observational data is unavailable for an area. That said, due to isolation of this study area and the complexity of the topography and associated cold-air pooling there were major issues in the predictive power of these models to project local temperature variation with elevation. Future work on improving these programs and incorporating other already developed datasets and models should be the aim moving forward in the mountainous regions of northwestern Canada. Currently, the use of downscaled temperature data for permafrost modelling

where SBI dominate will result in complex patterns of permafrost distribution being missed.

3.5.8 REGIONALLY MODELLED MEAN ANNUAL AIR TEMPERATURES AND SURFACE LAPSE RATES

Modelled MAAT and associated SLRs (Lewkowicz et al., 2012) grossly underpredicted the influence of SBIs in these valleys. This resulted in valley slope locations being significantly cooler than actual measurements indicate. The valley bottom MAATs were predicted in the SV to be roughly 0.6 °C warmer than were recorded by in-situ sensors. Furthermore, the model was based off the 1981-2010 climate normal which was shown in our analysis of climate to be outdated. This would conceivably result in MAATs predicted to be colder than the current climate of this fast-warming region. cold-air pooling is intense in the SV. Studies have indicated that there is at times a susceptibility of interpolated temperature grids to underrepresent local cold-air pooling (Lundquist et al., 2008; Frei, 2014). Valley locations susceptible to this phenomenon can be predicted to be substantially warmer than they are. Thus, the SV looks to be modelled to be warmer than in-situ data suggests.

Another measure that has been associated with SBI influence on SAT patterns in mountainous areas of northwestern Canada is monthly average temperature amplitude between the coldest and the warmest months (Lewkowicz & Bonnaventure, 2011). Similarly, high amplitude of maximum and minimum temperatures was observed in the Alps to indicate locations prone to cold-air pooling and frequent SBI presence (Rist et al., 2020). Lewkowicz and Bonnaventure (2011) found a significant linear relationship between the amplitude of monthly average temperature between the warmest and the

coldest months and measured SLRs. This relationship predicted the strongest annual SLRs they recorded (0.1 °C $100m^{-1}$) to be correlated with amplitudes of about 40-45 °C. Amplitudes measured in our valleys at the six sites was between 30-35 °C while the SLRs were between 0.46 and 1.2 °C $100m^{-1}$ on annual average. Thus, the pattern projected in this article is not confirmed by our results. However, the authors acknowledge that our valleys are possibly outside of the geographic constraints of this assumption. Additionally, these patterns were also generated from amplitudes in lower elevation EC stations and not actually tested on the surrounding slopes where summer conditions are not likely to be as warm, lowering the amplitude. More recently amplitude of monthly average temperatures was studied across the region of northwestern Canada at radiosonde stations (Noad et al., *In Progress*). The pattern of monthly temperature amplitude indicated that lower temperature amplitudes had more gently inverted annual average lapse rates while higher amplitudes led to more strongly inverted annual average lapse rates. When the amplitude was high enough there was not a continuing pattern of more strongly inverted SLRs. This means that there is a point where increased amplitude of monthly average temperatures does not result in continued increase of SLRs to be more inverted. Overall, our results suggest that the valley that is more prone to SBIs and inverted SLRs is the valley with higher amplitude of monthly average temperatures.

Intense cold-air pooling and subsequent SBI development and persistence is resulting in temperature patterns where low-lying and high-elevation locations are coldest and mid-elevations are warmest. EDW is predicted to occur as climate change is accelerated in high elevations faster, and more intensely than lower elevations (Pepin et al., 2015). These patterns have recently been observed in Southern Yukon (Williamson et

al., 2020). What has not been discussed is the potential for low-lying areas prone to cold-air pooling to also experience rapid warming. Recent research regarding trends I_{imp} on SATs in northwestern Canada highlighted some evidence for reduction of inversion impact on SAT over time (Chapter 2). While this pattern is far from confirmed, much future care and research into this topic is essential. If change in the vertical structure of the atmosphere is occurring, then valley bottom locations could be susceptible to accelerated warming much like higher elevations as is associated with EDW.

Overall, quantification of SAT patterns associated with dominant SBIs in complex mountainous terrain is needed so predictions can be made regarding how they might change. This phenomenon drives much of the temperature variation across mountain valley landscapes where elevation is highly variant across small horizontal distances (Chapter 2*)*. Many aspects of research need an accurate representation of temperature across a surface. For example, any ecological studies in this region will need an accurate representation of temperature conditions across the landscape, and how they will change with time (Turner et al., 1989). Similarly, the study of cryospheric elements in mountainous areas including glaciers, icings and permafrost need the same accurate temperature surface to project their current state and future change (Gardner et al., 2009; Mernild & Liston, 2010; Morse & Wolfe, 2015; Smith & Bonnaventure, 2017). The main focus of this paper has been on the influence of dominant SBI on SAT patterns in northwestern Canadian valley locations and how they influence permafrost.

3.5.9 IMPLICATIONS OF INVERSIONS ON PERMAFROST DISTRIBUTION IN THE VALLEYS

Ground depth temperature data observed at each of the valley bottom and slope locations indicate that permafrost is present at each site excluding the SFS site (Table 3.5). According to the model developed by Bonnaventure et al. (2012) the SFS site is predicted to have the lowest permafrost probability (46 %) (Figure 3.1). Permafrost probability is greatest across ridgetop locations (75-100%) and second highest in valley bottom locations (60-80%). Mid-slope locations at the elevation of treeline predicted permafrost probability was lowest (40-50%). Therefore, this model, and conceptualizations (Bonnaventure & Lewkowicz, 2013) in SBI dominated valleys explain permafrost findings at these point locations well. With only 6 data collection sites included in this study, there still exists the need for work to be done including ground truthing and monitoring of permafrost temperatures on slope locations to further confirm this conceptualization.

Permafrost temperatures and probability is defined not only by SAT but also by other factors including snow depth (Garibaldi et al., 2021), substrate composition and moisture level (Smith et al., 2010b) and vegetation cover (Shur & Jorgenson, 2007; Kropp et al., 2020). Therefore, SBI can impact permafrost distribution however, this impact must be viewed through the lens of additional factors also shaping permafrost distribution. For example, the NFS air temperature was significantly warmer than in the valley bottom however, temperature at depth was colder on the above slope. This may be a result of lack of solar radiation warming the ground temperatures on the NFS due to topographic shading. Additionally, deeper snow cover in the valley bottom location

because of trees capturing snow, could insulate the ground surface from wintertime SATs (Way & Lapalme, 2021). While this conclusion is not confirmed, this example illustrates that SBI contribute to SAT patterns in valleys but that these patterns do not always translate to permafrost temperature patterns.

Another significant factor that was observed is that SBI dominate throughout the cold months of the year and during the night hours. This indicates that the pattern of warmer conditions taking place at slope locations more often occurs during times where temperatures are freezing. This is especially important when analytically determining permafrost distribution through empirical models such as the TTOP model which includes thawing and freezing degree-days (Riseborough et al., 2008). During the freezing season permafrost temperatures are dominated by freezing n-factors that are related to the snow depth reducing the interaction between SAT and TTOP (Garibaldi et al., 2021). If SBI influence SAT most in the winter season when freezing degree-days dominate, then permafrost distribution is most likely influenced by SBI in areas with less snow cover. In the summer, thawing degree-days are influenced by vegetation cover restricting surface warming through shading of incoming radiation (Way & Lapalme, 2021). In this case, SBI are much less frequent and consequential as the SLRs on average are much more normal with the slope locations often being colder than the valley bottom location. Therefore, SBI are much more noteworthy in shaping SAT patterns during the cold portions of the year when the active layer is refreezing or remaining frozen. This is an essential concept to understand while moving forward with research on the impact SBIs are having on shaping current and future permafrost distribution.

Strongly inverted SLRs on seasonal and annual scales were found within the lowest 100 m of the valley locations. This pattern has been found to have an influence on permafrost distribution in the lower parts of the valleys, particularly at and below treeline. Data collected and assumptions made in other studies suggest that annual average SLRs reverse back to normal above treeline (Wahl et al. 2003; Lewkowicz & Bonnaventure, 2011; Lewkowicz et al., 2012) so this was incorporated into permafrost probability modelling (Bonnaventure et al., 2012; Bonnaventure & Lewkowicz, 2013). Our results only confirm hyper-inversions below treeline resulting in strongly inverted annual average SLRs. SBI influence while not as strong in the treeless valley remains significant in producing inverted SLRs on an annual basis. This finding raises questions regarding the generalized assumption of annual SLR reversal to normal above treeline especially for above treeline valleys. One recommendation we suggest may improve modeling developed by Lewkowicz et al. (2012) is inclusion of the Topographic Position Index to assist in accounting for continued cold-air pooling and subsequent inverted SLRs in valleys that entirely fall above treeline. Overall, to verify existing assumption regarding SLRs in this region, these transects need to be replicated and extended higher to test at what elevation, if any in the valley, there is a reversal of SLRs back to normal.

3.6 SUMMARY AND CONCLUSIONS

Fine-scale spatial and temporal variation in SBI characteristics in near-proximity dissimilar high-latitude valleys were reviewed in this chapter. The implications of these variations on SLR patterns and subsequent permafrost attributes have been discussed. There were several key findings that include:

- Strongly inverted annual average SLRs led to SATs at each of the higher elevation sites that were significantly warmer, particularly during the winter season. Ground surface temperatures and ground depth sensors were warmer at all higher elevation sites except for the NFS. Ground depth temperature on average was above 0°C across the two-year study period at the SFS location. This indicates that permafrost is likely absent at this site while being present in the valley bottom. This depends on the time lag between remaining permafrost and the thermal lag of warming climatic temperatures. Thus, permafrost distribution is likely impacted by SBIs supporting the results modelled by Bonnaventure et al. (2012) and conceptualized in Bonnaventure and Lewkowicz (2013).
- Annual average nighttime SLRs were hyper-inverted averaging over 2 °C/ 100 m in the SV while averaging closer to 1 °C/ 100 m in the NV. Annual average daytime readings, were on average ≥0 °C/ 100 m on each transect except for the SFT where SLRs were around 0.5 °C/ 100 m.
- SBIs in the region were found to be much more frequent and stronger than anticipated from previous research. The resulting annual average SLRs were inverted on each elevational transect (0.46-1.21 °C $100m^{-1}$) and were much more strongly inverted in the SV, particularly on the SFT. Observed SLRs were much more intensely inverted than those predicted in modelling created by Lewkowicz et al. (2012) which predicted average annual SLRs that were inverted to a maximum of 0.1°C $100m^{-1}$.
- Statistical testing indicated significant relationships between SLRs and various microclimatic conditions were related to terrain attributes and valley orientation

and subsequent aspects. This included wind speed, solar radiation, and SATs however, it remains unknown if they are causal relationships or covariant. Wind speed differed significantly between the valleys, possibly linked to valley geometry, length, orientation, and surface roughness due to vegetation differences.

- Previous research and modelling by Lewkowicz et al. (2012) in southern and central Yukon predict and assume that SLRs reverse back to normal above treeline. Our findings did observe warming towards treeline, but also showed that in the treeless valley SLRs are also inverted in the first 100 m off the valley floor. The assumptions made by Lewkowicz et al. (2012) must be reviewed to determine when and if there is an inflection point of SLRs in treeless valleys. Furthermore, it the hypothesis that there exists an inflection point of SLRs back to normal above treeline in the treed valleys must be tested. Thus, ETAs need to be extended up higher in each valley to review these assumptions.
- SLRs calculated for each transect using the climate reanalysis downscaling programs of GlobSim and ClimateNA were close to being neutral (0.0 °C/ 100 m). This indicates that these programs do not capture the hyper-inversions that occur frequently in the lowest parts of the valley. This signifies a major limitation to utilization in complex mountainous areas where SBIs dominate. Thus, ETA is an important tool to quantify the influence SBIs have on annual average SLRs in these remote valley locations.

Overall, this research implies that there is indeed a significant impact of SBIs on SATs and subsequent permafrost temperatures in complex mountainous high-latitude terrain. Most importantly, these findings indicate that SBI significantly vary valley-to-valley and

that they play a central role in defining elevational SAT patterns throughout each valley. These patterns may be substantially altered in the future as local warming reduces I_{imp} and if so, valley bottom locations may warm quicker than anticipated. As such, this could imply a needed adjustment to the concept of EDW in order to be more inclusive of SBI prone terrain. It will be imperative to understand how any future variation in these patterns will contribute to permafrost degradation. Immense opportunity exists to continue study of SBIs interaction with permafrost on these scales.

CHAPTER 4: CONCLUSIONS

4.0 CHAPTER OUTLINE

The central objective of this thesis was to review the impact inversions have on elevational SAT patterns and how those patterns define the distribution of permafrost. The central question driving this objective was to determine how the variability of SBIs influences assumed SATs spatially and temporally in northwestern Canada and what implications this has on permafrost distribution? Both small and large scales were studied to answer this question. The study examined in chapter two reviewed this objective on a regional scale across northwestern Canada using radiosonde data from 1990-2016 at five stations. The second study fulfilled this objective on a local scale by examination of in-situ temperature data from elevational transects in neighboring dissimilar valleys. In this chapter, main findings from each study will be summarized, then implications of the findings and future directions of research will be discussed.

4.1 SUMMARY OF MAJOR FINDINGS

In chapter two inversion characteristics were found to be significantly different between the five radiosonde sensors on annual and seasonal scales during the study period of 1990 to 2016. SBI were strongest at Fort Nelson on annual average while being deepest and most frequent at Inuvik. Consistently, Whitehorse had the most shallow, weak, and least frequent SBIs during the study period. To provide an extension of these traditional SBI characteristics and attempt to conceptualize how much SBI influences SAT over a given period of time, a novel variable called inversion impact (I_{imp}) was defined. When comparing this variable to the other inversion characteristics of depth, strength, and frequency it was found that three sites, Whitehorse, Fort Nelson, and Fort Smith had I_{imp}

values that were significantly unique from each other. For each of the traditional SBI characteristics no one site showed a statistically unique difference from the other sites such as that observed with I_{imp}. Thus, I_{imp} garnered a clearer understanding of the subtle differences of SBI characteristics spatially by combining traditional SBI characteristics into one metric. Furthermore, I_{imp} provided an opportunity to theorize how much SATs are defined by the presence of dominant SBIs in northwestern Canada. This conceptualization provides an invaluable variable to the field of permafrost study. Some areas of northwestern Canada had high annual average I_{imp} on SATs such as Fort Nelson (5.2 °C), Inuvik (4.2 °C), or Norman Wells (4.1 °C) while other areas such as Whitehorse showed a significantly lower I_{imp} on SAT (1.6 °C). I_{imp} varied temporally, inter-seasonally and inter-annually but trends across the study period were skewed by radiosonde instrumentation inconsistencies. Seasonally, I_{imp} was consistently and significantly greatest during the winter season. This led to a lack of ability to confidently attribute downward trends of I_{imp} observed at some locations in northwestern Canada to changing climate. There was a lack of evidence suggesting that spatial and temporal variability of I_{imp} were directly linked to macroclimate oscillations such as PDO, AO, and NPI. One macroclimate feature that did have some tendency to vary with I_{imp} across northwestern Canada was sea ice area in the Beaufort Sea. This indicated that there may be some connection between near surface atmospheric stability in northwestern Canada and loss of sea ice on the Arctic Ocean. Spatial variability of I_{imp} extended from the site locations to surrounding topography. Mountainous areas (Whitehorse, Fort Nelson, and Norman Wells) were predicted to have much more variable I_{imp} across the landscape as higher elevations extend above the average top of SBI layer. Areas with flatter surrounding topography (Fort Smith and Inuvik) had much less spatial variability of I_{imp} as low lying

flat areas fell within the full impact of SBI on SAT across the landscape. Overall, findings from this portion of the thesis indicate that across the region of northwestern Canada there is indeed a large impact of SBIs on SATs and that this impact varies spatially and temporally.

SBIs in chapter three of this thesis were found to alter SAT patterns on an elevational gradient (known as SLRs). Valley bottom temperatures were substantially colder than 100 m up each surrounding slope because of strong and persistent SBIs. Permafrost on some slopes is warmer than the valley locations due to SBI influence. On the SFS, aspect and SBIs combine to produce conditions where permafrost is absent at this site while being present in the valley bottom. Thus, permafrost distribution is impacted by SBIs supporting the results modelled by Bonnaventure et al. (2012) and conceptualized in Bonnaventure and Lewkowicz (2013). The SBI characteristics that were measured using in-situ data from elevational transects differed significantly between the two valleys. The SV had more significantly frequent SBIs leading to more inverted SLRs on seasonal and annual averages. SBI were found to be most frequent, strong, and each event was much longer in duration during the wintertime. SBIs were also much more commonly present during nighttime readings than in the daytime. Higher wind speeds increased incoming solar radiation, and warmer SATs were all related to more normal SLRs. These microclimatic variables were found to have an influence on SLRs by producing conditions necessary for SBI to develop and persist. Conversely these conditions were also driving factors of SBI breakup. Whether these variables are covarying or are more intricately related through a causal relationship remains unanswered, but clearly there is variable interaction. Furthermore, assessment of

modelled or assumed SLRs were made using the in-situ data. This unique dataset allowed for an evaluation of both climate reanalysis, downscaled models and assumed SLRs based on observed data in the region. First the downscaled climate reanalysis data did not account for strong and persistent SBIs measured in the lower parts of each valley. Thus, limitations were identified for the use of these downscaling programs in complex mountainous terrain where SBIs dominate. Assumed SLRs across the study area based on regional assumptions also had substantial limitations as they missed accounting for variability of SBIs between the valleys. Previous modelling of MAATs that regionally accounted for SBIs bellow treeline (Lewkowicz et al., 2012) underrepresented the intense impact hyper-inversions had on SLRs in the study area. Furthermore, SLRs were assumed to be normal above treeline in this model based on past research in the region. In-situ sensors in the NV, which was above treeline, indicate that annual average SLRs are inverted, though more gently than the valley below treeline. To improve on previous modelling of MAATs in the region we suggest that Topographic Position Index be used as a variable in the model to aid in accounting for valleys that are above treeline but that remain susceptible to cold air drainage and subsequent annual average SLRs that were inverted. Prediction of the impact of SBIs on the state of permafrost at fine-scale resolution remains difficult if in-situ sensors are not present across the complex terrain and between valleys. Overall, this research demonstrated local scale variability of SBI characteristics in two near proximity but dissimilar valleys. This local scale variability, while most often ignored, indicates limitations to understanding completely how permafrost distribution and thermal state is varying from valley-to-valley based on elevational gradients.

Both studies provided background on how SBI characteristics vary on regional and local scales in northwestern Canada. In both studies SBI are most influential in the winter season, an indication that permafrost temperatures are impacted most during the cold or freezing season. Findings from both chapters two and three suggest that there is a significant influence of SBIs on SAT patterns, particularly in mountainous areas where elevation varies greatly over small horizontal distances. In these landscapes, elevation is an important defining factor to the observed MAATs, and these patterns are shaped by SBIs that dominate through large proportions of the year. There are distinct differences between the findings in the two manuscripts regarding SBI characteristics. SBIs were much more prevalent in the Yukon valleys located along the Dempster highway in the Ogilvie Mountains than at any site where radiosonde sensors were released. It is difficult to directly compare these datasets because radiosondes measure free-air lapse rates and elevational transects measure SLRs. Finally, both studies outlined the role of SBIs in defining the current state of permafrost. Furthermore, there is a focus of discussion in both chapters about how this SBI impact on permafrost may alter due to climate change.

4.2 IMPLICATIONS OF FINDINGS

The linkage between atmospheric SBI to permafrost, a sub-surface phenomenon, have independently been studied extensively. Previous research bridges atmospheric studies related to SBI presence and permafrost probabilities and distributions (Lewkowicz & Bonnaventure, 2011; Bonnaventure et al., 2012; Bonnaventure & Lewkowicz, 2013; Smith & Bonnaventure, 2017). Conclusions acquired from each chapter of this thesis have extensively furthered the bridging of these phenomena in northwestern Canadian landscapes. Findings of this thesis will define future studies of permafrost in high-latitude

regions by recognizing the need for an accounting of SLRs when modelling permafrost in SBI dominated regions.

Wintertime and nighttime SBIs dominate which could imply that areas with thicker snow cover will have substantially lowered inversion impact on permafrost temperatures. Furthermore, while thaw seasons do not experience nearly as high of an inversion impact the temperature of permafrost is a product of MAAT. If permafrost freezes to colder temperatures during the winter, then it will take more energy to warm in the thaw season. Therefore, SBIs have implications on defining temperature of permafrost, although mostly during the cooling phase.

The main implication of this research is that permafrost temperatures and distribution can be defined by the presence of dominant SBIs. The intertwining of these topics of research from two different earth systems allows for new directions in future research of permafrost providing better accuracy in modelling permafrost distribution. SBIs become another variable to consider when modelling permafrost, particularly in mountainous areas of northwestern Canada. Thus, the main implication of this research is to firmly establish SBIs as an influential variable for permafrost science in northwestern Canada.

4.3 FUTURE CONSIDERATIONS

Several areas of future research were identified due to time constraint, field accessibility owed to normal and extraordinary circumstances as a result of COVID-19, and discovery of limitations during the research while working on this thesis. These items of future research include:

- Ground truthing through physical checks of permafrost presence is needed to verify where permafrost is found and where it is not found in these complex mountainous valleys dominated by SBIs. Furthermore, ground temperature networks need to be used to monitor how frequently inverted SLRs influence ground surface temperature patterns throughout the valley. Included in this analysis could be boreholes at various elevations to determine any elevational patterns associated with the thermal state of permafrost.
- Ground temperature sensor networks and boreholes, and the modelling of these, could effectively allow for an understanding of the implications and impacts of SBI during cold parts of the year.
- A direct comparison of SLRs and free-air lapse rates in northwestern Canada needs to be undertaken. This will assess differences between the two assessing the linkages, if any, exists for comparing radiosonde data directly to in-situ data.
- Major limitations were found in predicting hyper-inversions observed in the lowest part of the atmosphere by downscaled climate reanalysis data from two programs, GlobSim and ClimateNA. Other programs including REDCAPP should be assessed using in-situ data. This will involve partnerships with the program developers to understand how well these products account for strong and persistent SBIs in this region.
- In-situ sensors need to be extended to higher elevations on each slope to determine the vertical extent of SBI in each mountain valley. Additionally, a better understanding of the location where SLRs reverse back to normal in both treed and treeless valleys needs to be studied further.

- Findings of this research suggest an influence of microclimate conditions on the development, persistence, and breakup of SBIs. This relationship needs to be explored for possible causation and thresholds of microclimate variables in driving SBI development, persistence, and breakup patterns.
- I_{imp} conceptualizes how much SATs are being influenced by persistent SBIs throughout the year. I_{imp} needs to be quantified through the measure of the difference between actual SAT and air temperatures at different pressure levels. How much warmer is the upper atmosphere than the lower atmosphere near the surface? This should be quantified as at the moment I_{imp} is limited by the assumption of reversal of the lapse rates back to the normal ELR when not inverted.
- A closer look into macroclimatic influence of synoptic weather conditions on SBIs would be useful in northwest Canada. This should be conducted over an extended study period to confirm trends and relationships between these two phenomena.
- Empirical gaps now exist as this research is only applied to northwestern Canada. Other locations where this type of research could be useful is Alaska USA, the Canadian Arctic, Russia, Mongolia, Scandinavia, and Chile (Figure 4.1). Whether these patterns of SBI impact on permafrost extend to other high-latitude mountain areas should be answered.
- Not only can this research be applied to other high-latitude areas, but I_{imp} could be applied to midlatitude regions. This will aid in determining how the influence of SBIs on SATs might be different between high-latitude and mid-latitude locations. Furthermore, with many more radiosonde data collection locations, opportunities

to test this new variable may present themselves with research in mid-latitude areas.

- A major component moving forward will be to accurately predict trends of SBI characteristics and subsequent SBI impact on SAT into the future as climate changes. This is needed to identify any possible unseen consequences of climate change in this high-latitude region. These findings must be understood alongside EDW as defined by recent research (Pepin et al., 2015; Williamson et al., 2020).

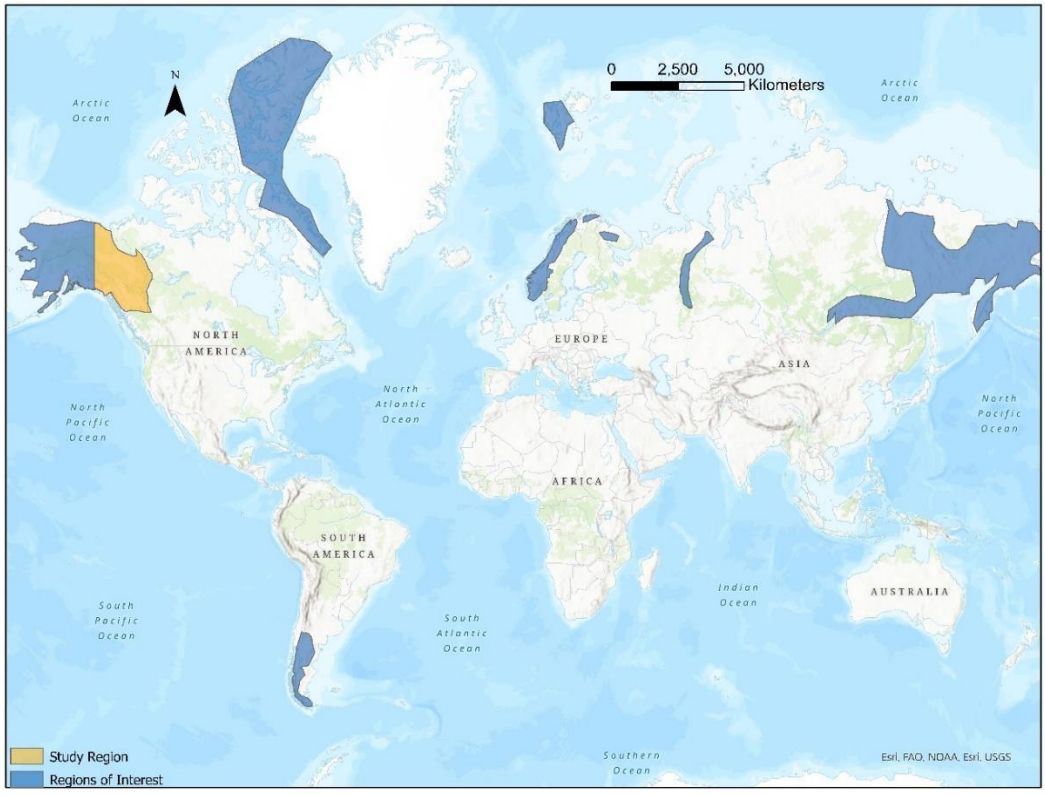

Figure 4.1: Regions of interest for high-latitude mountainous areas possibly prone to dominant SBI development and persistence.

Overall, by integrating research of the atmospheric phenomena of SBI with the subsurface phenomena of permafrost many avenues of future research have been uncovered. There is still much to be done to integrate these two phenomena and

understand how they interact. Eventually with better integration through research an accurate representation of the influence of SBI on permafrost distribution can be better accounted for in modelling. Use at finer scales however, hinges on understanding the variability of SBI development, persistence, and breakup in high-latitude regions. This thesis represents an early attempt to integrate these phenomena with each other and inaugurates future research in these fields. It is highly recommended that work continues at integrating these phenomena and verifying the influence SBIs have on the thermal state of permafrost. This is critical to understanding the role future climate change will play as environmental conditions evolve, and permafrost increasingly thaws.

4.4 BIBLIOGRAPHY

Aalto, J., and Luoto, M. (2014). Integrating climate and local factors for geomorphological distribution models. *Earth surface processes and landforms*, **39**(13), 1729-1740. doi:10.1002/esp.3554

Abdi, H., and Williams, L. (2010). Newman-Keuls Test and Tukey Test. *Encyclopedia of Research Design*, **2,** 897-902. doi: 10.4135/9781412961288

Akperov, M. G., Mokhov, I. I., Dembitskaya, M. A., Parfenova, M. R., and Rinke, A. (2019). Lapse Rate Peculiarities in the Arctic from Reanalysis Data and Model Simulations. *Russian meteorology and hydrology*, **44**(2), 97-102. doi:10.3103/S106837391902002X

AMAP, (2017). Snow, Water, Ice and Permafrost. Summary for Policy-makers. Arctic Monitoring and Assessment Programme (AMAP), Oslo, Norway. 20 pp. https://www.amap.no/documents/doc/snow-water-ice-and-permafrost.-summary-for-policy-makers/1532

Anquetin, S., Guilbaud, C., and Chollet, J.-P. (1998). The Formation and Destruction of Inversion Layers within a Deep Valley. *Journal of Applied Meteorology (1988-2005)*, ***37***(12), 1547-1560. doi:10.1175/1520-0450(1998)037<1547:TFADOI>2.0.CO;2

Atlas of Canada (1957). Climatic Zones [Map] 3rd edtion. Natural Resources Canada, accessed 10 Novemeber 2020, https://open.canada.ca/data/en/dataset/09ffaeb5-ec8f-5bb5-bdcb-3436ccf26f58

Bader, D. C., and McKee, T. B. (1985). Effects of Shear, Stability and Valley Characteristics on the Destruction of Temperature Inversions. *Journal of Climate and Applied Meteorology*, ***24***(8), 822-832. doi:10.1175/1520-0450(1985)024<0822:EOSSAV>2.0.CO;2

Barszcz, A., Milbrandt, J. A., and Thériault, J. M. (2018). Improving the Explicit Prediction of Freezing Rain in a Kilometer-Scale Numerical Weather Prediction Model. *Weather and Forecasting*, **33**(3), 767-782. doi:10.1175/WAF-D-17-0136.1

Bartleman, A. P., Miyanishi, K., Burn, C. R., and Côté, M. M. (2001). Development of Vegetation Communities in a Retrogressive Thaw Slump near Mayo, Yukon Territory: A 10-Year Assessment. *Arctic*, **54**(2), 149-156. doi:10.14430/arctic774

Barry G. R. (2013). *Mountain Weather and Climate* (2 ed.). Routledge. 261 pp.

Belmecheri, S., Babst, F., Hudson, A. R., Betancourt, J., and Trouet, V. (2017). Northern hemisphere jet stream position indices as diagnostic tools for climate and ecosystem dynamics. *Earth Interactions*, **21**(8), 1-23. doi:10.1175/ei-d-16-0023.1

Bintanja, R., Graversen, R. and Hazeleger, W. (2011). Arctic winter warming amplified by the thermal inversion and consequent low infrared cooling to space. *Nature Geoscience* **4**, 758–761. doi: 10.1038/ngeo1285

Birkeland C. (2016) Elemental Geosystem (8th ed.). Pearson Education. 555 pp.

Blandford, T. R., Humes, K. S., Harshburger, B. J., Moore, B. C., Walden, V. P., and Ye, H. (2008). Seasonal and Synoptic Variations in Near-Surface Air Temperature Lapse Rates in a Mountainous Basin. *J. of Applied Meteorology and Climatology, **47***(1), 249-261. doi:10.1175/2007JAMC1565.1

Bonnaventure, P. P., and Lewkowicz, A. G. (2008). Mountain permafrost probability mapping using the BTS method in two climatically dissimilar locations, northwest Canada. *Canadian Journal of Earth Sciences, **45***(4), 443-455. doi:10.1139/E08-013

Bonnaventure, P. P., Lewkowicz, A. G., Kremer, M., and Sawada, M. C. (2012). A Permafrost Probability Model for the Southern Yukon and Northern British Columbia, Canada. *Permafrost and Periglacial Processes, **23***(1), 52-68. doi:10.1002/ppp.1733

Bonnaventure, P. P., and Lewkowicz, A. G. (2013). Impacts of mean annual air temperature change on a regional permafrost probability model for the southern Yukon and northern British Columbia, Canada. *The Cryosphere, **7***(3), 935-946. doi:10.5194/tc-7-935-2013

Bourne, S. M., Bhatt, U. S., Zhang, J., and Thoman, R. (2010). Surface-based temperature inversions in Alaska from a climate perspective. *Atmospheric Research, **95***(2), 353-366. doi:10.1016/j.atmosres.2009.09.013

Bradley, R. S., Keimig, F. T., and Diaz, H. F. (1992). Climatology of surface-based inversions in the North American Arctic. *Journal of Geophysical Research: Atmospheres, **97***(D14), 15699-15712. doi:10.1029/92JD01451

Bradley, R. S., Keimig, F. T., and Diaz, H. F. (1993). Recent changes in the North American Arctic boundary layer in winter. *Journal of Geophysical Research: Atmospheres*, **98**(D5), 8851-8858. doi:10.1029/93JD00311

Brown, J., O. Ferrians, J. A. Heginbottom, and E. Melnikov (2002). Circum-Arctic Map of Permafrost and Ground-Ice Conditions, Version 2. National Snow and Ice Data Center, accessed Dec 2 2020, doi: 10.7265/skbg-kf16.

Burn, C. R. (1998). The active layer: two contrasting definitions. *Permafrost and Periglacial Processes*, **9**(4), 411-416. doi:10.1002/(SICI)1099-1530(199810/12)9:4<411::AID-PPP292>3.0.CO;2-6

Burn, C. & Moore, J. & O'Neill, Brendan & Hayley, D & Trimble, J & Calmels, Fabrice & Orban, S.N. & Idrees, Mm. (2015). Permafrost characterization of the Dempster Highway, Yukon and Northwest Territories. *7th Canadian Permafrost Conference*. Quebec City, Canada.

https://carleton.ca/geography/2015/7th-canadian-permafrost-conference/

Cannon, A. J., Neilsen, D., and Taylor, B. (2012). Lapse Rate Adjustments of Gridded Surface Temperature Normals in an Area of Complex Terrain: Atmospheric

Reanalysis versus Statistical Up-Sampling. Atmosphere-ocean, **50**(1), 9-16. doi:10.1080/07055900.2011.649035

Cao, B., Gruber, S., and Zhang, T. (2017). REDCAPP (v1.0): parameterizing valley inversions in air temperature data downscaled from reanalyses. *Geoscientific Model Development*, **10**(8), 2905-2923. doi:10.5194/gmd-10-2905-2017

Cao, B., Quan, X., Brown, N., Stewart-Jones, E., and Gruber, S. (2019). GlobSim (v1.0): deriving meteorological time series for point locations from multiple global reanalyses. *Geoscientific Model Development*, **12**(11), 4661-4679. doi:10.5194/gmd-12-4661-2019

Chang, L., Song, S., Feng, G., Zhang, Y., and Gao, G. (2017). Assessment of the Uncertainties in Arctic Low-Level Temperature Inversion Characteristics in Radio Occultation Observations. *IEEE Transactions on Geoscience and Remote Sensing*, **55**(3), 1793-1803. doi:10.1109/TGRS.2016.2633461

Chang, L., Feng, G., Zhang, Y., and He, X. (2018). Effect of Cloud Fraction on Arctic Low-Level Temperature Inversions in AIRS Observations Over Both Land and Ocean. IEEE *Transactions on Geoscience and Remote Sensing*, **56**(4), 2025-2032. doi:10.1109/TGRS.2017.2772297

Changnon, S. A. (2003). Characteristics of Ice Storms in the United States. *Journal of applied meteorology* (1988), **42**(5), 630-639. doi:10.1175/1520-0450(2003)042<0630:COISIT>2.0.CO;2

Chapman, W. L., and Walsh, J. E. (1993). Recent Variations of Sea Ice and Air Temperature in High Latitudes. *Bulletin of the American Meteorological Society*, ***74***(1), 33-47. doi:10.1175/1520-0477(1993)074<0033:RVOSIA>2.0.CO;2

Chasmer, L., and Hopkinson, C. (2017). Threshold loss of discontinuous permafrost and landscape evolution. *Global change biology*, **23**(7), 2672-2686. doi:10.1111/gcb.13537

Chemel, C., and Chollet, J. P. (2006). Observations of the Daytime Boundary Layer in Deep Alpine Valleys. *Boundary-Layer Meteorology*, **119**(2), 239-262. doi:10.1007/s10546-005-9026-4

Chen, W., Zhang, Y., Cihlar, J., Smith, S. L., and Riseborough, D. W. (2003). Changes in soil temperature and active layer thickness during the twentieth century in a region in western Canada. *Journal of Geophysical Research: Atmospheres*, **108**(D22), 4696-n/a. doi:10.1029/2002JD003355

Chen, H., and Yi, C. (2012). Optimal control of katabatic flows within canopies. *Quarterly Journal of the Royal Meteorological Society*, **138**(667), 1676-1680. doi:10.1002/qj.1904

Christensen, J. H., Carter, T. R., Rummukainen, M., and Amanatidis, G. (2007). Evaluating the performance and utility of regional climate models: the PRUDENCE project. *Climatic Change*, **81**(S1), 1-6. doi:10.1007/s10584-006-9211-6

Chutko, K. J., and Lamoureux, S. F. (2009). The influence of low-level thermal inversions on estimated melt-season characteristics in the central Canadian Arctic. *International Journal of Climatology*, **29**(2), 259-268. doi:10.1002/joc.1722

Clements, C. B., Whiteman, C. D., and Horel, J. D. (2003). Cold-Air-Pool Structure and Evolution in a Mountain Basin: Peter Sinks, Utah. *Journal of Applied Meteorology* (1988-2005), **42**(6), 752-768. doi:10.1175/1520-0450(2003)042<0752:CSAEIA>2.0.CO;2

Cohen, J., and Coauthors (2014). Recent Arctic amplification and extreme mid-latitude weather. *Nature Geoscience*, ***7***(9), 627-637. doi:10.1038/NGEO2234

Colette, A., Chow, F. K., and Street, R. L. (2003). A Numerical Study of Inversion-Layer Breakup and the Effects of Topographic Shading in Idealized Valleys. *Journal of Applied Meteorology (1988-2005)*, ***42***(9), 1255-1272. doi:10.1175/1520-0450(2003)042<1255:ANSOIB>2.0.CO;2

Compo, G. P., Whitaker, J. S., and Coauthors (2011). The Twentieth Century Reanalysis Project. *Quarterly Journal of the Royal Meteorological Society*, **137**(654), 1-28. doi:10.1002/qj.776

Connolley, W. M. (1996). The Antarctic temperature inversion. *International Journal of Climatology*, **16**(12), 1333-1342. 10.1002/(SICI)1097-0088(199612)16:12<1333::AID-JOC96>3.0.CO;2-6

Cote, M. M. (2002). The influence of elevation and aspect on permafrost distribution in central Yukon Territory. *M.Sc. thesis, Department of Geography and Environmental Studies*, Carlton University, https://doi.org/10.22215/etd/2002-05303

Daly, C., Conklin, D. R., and Unsworth, M. H. (2010). Local atmospheric decoupling in complex topography alters climate change impacts. International Journal of Climatology, **30**(12), 1857-1864. doi:10.1002/joc.2007

Dawn Reeves, H., Elmore, K. L., Manikin, G. S., and Stensrud, D. J. (2011). Assessment of Forecasts during Persistent Valley Cold Pools in the Bonneville Basin by the North American Mesoscale Model. *Weather and Forecasting*, **26**(4), 447-467. doi:10.1175/WAF-D-10-05014.1

De Wekker, S., Kossmann, M., Knievel, J., Giovannini, L., Gutmann, E., and Zardi, D. (2018). Meteorological Applications Benefiting from an Improved Understanding of Atmospheric Exchange Processes over Mountains. *Atmosphere*, **9**(10), 371. doi:10.3390/atmos9100371

Decker, M., Brunke, M. A., Wang, Z., Sakaguchi, K., Zeng, X., and Bosilovich, M. G. (2012). Evaluation of the Reanalysis Products from GSFC, NCEP, and ECMWF Using Flux Tower Observations. *Journal of Climate*, **25**(6), 1916-1944. doi:10.1175/JCLI-D-11-00004.1

Déry, S. J., Hernández-Henríquez, M. A., Burford, J. E., and Wood, E. F. (2009). Observational evidence of an intensifying hydrological cycle in northern Canada. *Geophysical Research Letters*, **36**(13), L13402-n/a. doi:10.1029/2009GL038852

Deser, C., Tomas, R., Alexander, M., and Lawrence, D. (2010). The Seasonal Atmospheric Response to Projected Arctic Sea Ice Loss in the Late Twenty-First Century. *Journal of Climate*, **23**(2), 333-351. doi:10.1175/2009JCLI3053.1

Desyatkin, R. V. (2018). Climate Change and Dynamics of Permafrost Ecosystems of the Center of the Continental Cryolithozone of the Northern Hemisphere. *Herald of the Russian Academy of Sciences*, **88**(6), 494-501. doi:10.1134/S1019331618060072

Devasthale, A., Tjernström, M., Caian, M., Thomas, M. A., Kahn, B. H., and Fetzer, E. J. (2012). Influence of the Arctic Oscillation on the vertical distribution of clouds as observed by the A-Train constellation of satellites. *Atmospheric Chemistry and Physics*, ***12***(21), 10535-10544. doi:10.5194/acp-12-10535-2012

Dobrowski, S. Z., Abatzoglou, J. T., Greenberg, J. A., and Schladow, S. G. (2009). How much influence does landscape-scale physiography have on air temperature in a mountain environment? *Agricultural and Forest Meteorology*, **149**(10), 1751-1758. doi:10.1016/j.agrformet.2009.06.006

Dockery, D. W. (1994). An association between air pollution and mortality in six US cities. *The Journal of the American Medical Association*, **271**(11). doi:10.1056/NEJM199312093292401

Dong, B., Dai, A (2015). The influence of the Interdecadal Pacific Oscillation on Temperature and Precipitation over the Globe. *Climate Dynamics*, **45**, 2667–2681. doi:10.1007/s00382-015-2500-x

Duk-Rodkin, A., 1999. Glacial limits map of Yukon. *Geological Survey of Canada*, Open File 3694;

Durre, I., Vose, R. S., and Wuertz, D. B. (2006). Overview of the Integrated Global Radiosonde Archive. *Journal of Climate*, **19**(1), 53-68. doi:10.1175/jcli3594.1

El-Sayed, A., and Kamel, M. (2020). Climatic changes and their role in emergence and re-emergence of diseases. *Environmental Science and Pollution Research International*, **27**(18), 22336-22352. doi:10.1007/s11356-020-08896-w

Environment Canada (2020a). Canadian Climate Normals (1981-2010). Canadain Centre for Climate Services, accessed June 10 2020. https://climate.weather.gc.ca/climate_normals/index_e.html

Environment Canada (2020b). Historical Data. Canadian Centre for Climate Services, accessed November 27 2020, https://climate.weather.gc.ca/historical_data/search_historic_data_e.html

Etzelmüller, B. (2013). Recent Advances in Mountain Permafrost Research. *Permafrost and Periglacial Processes*, ***24***(2), 99-107. doi:10.1002/ppp.1772

Feldl, N., Po-Chedley, S., Singh, H. A., Hay, S., and Kushner, P. J. (2020). Sea ice and atmospheric circulation shape the high-latitude lapse rate feedback. *NPJ climate and atmospheric science*, **3**(1), 1-9. doi:10.1038/s41612-020-00146-7

Fetterer, F., K. Knowles, W. N. Meier, M. Savoie, and A. K. Windnagel. 2017, (Updated Daily). Sea Ice Index, Version 3. North Regional Sea Ice Monthly. National Snow and Ice Data Center, accessed June 15 2020. doi: 10.7265/N5K072F8.

Fiddes, J., and Gruber, S. (2014). TopoSCALE v.1.0: downscaling gridded climate data in complex terrain. *Geoscientific Model Development*, **7**(1), 387-405. doi:10.5194/gmd-7-387-2014

Fleming, S. W., and Whitfield, P. H. (2010). Spatiotemporal mapping of ENSO and PDO surface meteorological signals in british columbia, yukon, and southeast alaska. *Atmosphere-Ocean*, **48**(2), 122-131. doi:10.3137/AO1107.2010

Fraser, R. H., Lantz, T. C., Olthof, I., Kokelj, S. V., and Sims, R. A. (2014). Warming-Induced Shrub Expansion and Lichen Decline in the Western Canadian Arctic. *Ecosystems*, **17**(7), 1151-1168. doi:10.1007/s10021-014-9783-3

Frei, C. (2014). Interpolation of temperature in a mountainous region using nonlinear profiles and non-Euclidean distances. *International Journal of Climatology*, ***34***(5), 1585-1605. doi:10.1002/joc.3786

French, H. M., and Williams, P. (2017). *The Periglacial Environment* (4th ed.). Wiley-Blackwell. 544 pp.

Fridley, J. D. (2009). Downscaling Climate over Complex Terrain: High Finescale (<1000 m) Spatial Variation of Near-Ground Temperatures in a Montane Forested Landscape (Great Smoky Mountains). *Journal of Applied Meteorology and Climatology*, **48**(5), 1033-1049. doi:10.1175/2008JAMC2084.1

Gaffen, D. J. (1994), Temporal inhomogeneities in radiosonde temperature records. *Journal of Geophysical Research*., **99**, 3667–3676, doi:10.1029/93JD03179.

Gao, L., Bernhardt, M., and Schulz, K. (2012). Elevation correction of ERA-Interim temperature data in complex terrain. *Hydrology and earth system sciences*, ***16***(12), 4661-4673. doi:10.5194/hess-16-4661-2012

Gao, L., Bernhardt, M., Schulz, K., and Chen, X. (2017). Elevation correction of ERA-Interim temperature data in the Tibetan Plateau. *International Journal of Climatology*, **37**(9), 3540-3552. doi:10.1002/joc.4935

Gardner, A. S., Sharp, M. J., and Coauthors (2009). Near-Surface Temperature Lapse Rates over Arctic Glaciers and Their Implications for Temperature Downscaling. *Journal of Climate*, **22**(16), 4281-4298. doi:10.1175/2009jcli2845.1

Garibaldi, M. C., Bonnaventure, P. P., and Lamoureux, S. F. (2021). Utilizing the TTOP model to understand spatial permafrost temperature variability in a High Arctic landscape, Cape Bounty, Nunavut, Canada. *Permafrost and Periglacial Processes*, ***32***(1), 19-34. doi:10.1002/ppp.2086

Garrett, A. J. (1983). Drainage Flow Prediction with a One-Dimensional Model Including Canopy, Soil and Radiation Parameterizations. *Journal of Climate and Applied Meteorology*, **22**(1), 79-91. doi:10.1175/1520-0450(1983)022<0079:DFPWAO>2.0.CO;2

Gilson, G. F., Jiskoot, H., Cassano, J. J., and Nielsen, T. R. (2018a). Radiosonde-Derived Temperature Inversions and Their Association With Fog Over 37 Melt Seasons in East Greenland. *Journal of Geophysical Research: Atmospheres*, ***123***(17), 9571-9588. doi:10.1029/2018JD028886

Gilson, G. F., Jiskoot, H., Cassano, J. J., Gultepe, I., and James, T. D. (2018b). The Thermodynamic Structure of Arctic Coastal Fog Occurring During the Melt Season over East Greenland. *Boundary-Layer Meteorology*, **168**(3), 443-467. doi:10.1007/s10546-018-0357-3

Gisnås, K., Etzelmüller, B., and Coauthors (2017). Permafrost Map for Norway, Sweden and Finland. *Permafrost and Periglacial Processes*, **28**(2), 359-378. doi:10.1002/ppp.1922

Graham, R. M., Hudson, S. R., and Maturilli, M. (2019). Improved Performance of ERA5 in Arctic Gateway Relative to Four Global Atmospheric Reanalyses. *Geophysical Research Letters*, **46**(11), 6138-6147. doi:10.1029/2019GL082781

Grisogono, B., and Axelsen, S. L. (2012). A Note on the Pure Katabatic Wind Maximum over Gentle Slopes. *Boundary-Layer Meteorology*, **145**(3), 527-538. doi:10.1007/s10546-012-9746-1

Gross, G. (1987). Some effects of deforestation on nocturnal drainage flow and local climate: A numerical study. *Boundary-Layer Meteorology*, ***38***(4), 315-337. doi:10.1007/BF00120851

Gubler, S., Endrizzi, S., Gruber, S., and Purves, R. S. (2013). Sensitivities and uncertainties of modeled ground temperatures in mountain environments. *Geoscientific Model Development*, **6**(4), 1319-1336. doi:10.5194/gmd-6-1319-2013

Guo, J. and Coauthors(2020). The climatology of lower tropospheric temperature inversions in China from radiosonde measurements: roles of black carbon, local meteorology, and large-scale subsidence. *Journal of Climate*, 1-70. doi:10.1175/JCLI-D-19-0278.1

Gustavsson, T., Karlsson, M., Bogren, J., and Lindqvist, S. (1998). Development of Temperature Patterns during Clear Nights. *Journal of Applied Meteorology (1988-2005)*, **37**(6), 559-571. doi:10.1175/1520-0450(1998)037<0559:DOTPDC>2.0.CO;2

Haeberli, W., Noetzli, J., and Coauthors (2010). Mountain permafrost: development and challenges of a young research field. *Journal of glaciology*, **56**(200), 1043-1058. doi:10.3189/002214311796406121

Haiden, T., and Whiteman, C. D. (2005). Katabatic Flow Mechanisms on a Low-Angle Slope. *Journal of applied meteorology* (1988), **44**(1), 113-126. doi:10.1175/JAM-2182.1

Harris, S. A. (1982). Cold Air Drainage West of Fort Nelson, British Columbia. *Arctic*, **35**(4), 537-541. doi:10.14430/arctic2362

Harris, S. A., French, H. M., Heginbottom, J. A., Johnston, G. H., Ladanyi, B., Sego, D. C., and Everdingen, R. O. (1988). Glossary of permafrost and related ground-ice terms. *National Research Council of Canada. Associate Committee on Geotechnical Research. Permafrost Subcommittee.* doi:10.4224/20386561

Hassanzadeh, P., and Kuang, Z. (2015). Blocking variability: Arctic Amplification versus Arctic Oscillation. *Geophysical Research Letters*, **42**(20), 8586-8595. doi:10.1002/2015gl065923

Heginbottom, J., Dubreuil, M., and Haker, P. (1995). Canada Permafrost [Map]. National Atlas of Canada, accessed August 21 2020, doi: https://doi.org/10.4095/294672

Hjort, J., Karjalainen, O., and Coauthors (2018). Degrading permafrost puts Arctic infrastructure at risk by mid-century. *Nature Communications*, ***9***(1), 5147-5147. doi:10.1038/s41467-018-07557-4

Helbig, M., Chasmer, L. E., Kljun, N., Quinton, W. L., Treat, C. C., and Sonnentag, O. (2017). The positive net radiative greenhouse gas forcing of increasing methane emissions from a thawing boreal forest-wetland landscape. *Global change biology*, **23**(6), 2413-2427. doi:10.1111/gcb.13520

Holt, R. D. (1990). The microevolutionary consequences of climate change. *Trends in ecology & evolution*, **5**(9), 311-315. doi: 10.1016/0169-5347(90)90088-U

IPCC (2019). IPCC Special Report on the Ocean and Cryosphere in a Changing Climate [H.-O. Pörtner, D.C. Roberts, V. Masson-Delmotte, P. Zhai, M. Tignor, E. Poloczanska, K. Mintenbeck, A. Alegría, M. Nicolai, A. Okem, J. Petzold, B. Rama, N.M. Weyer. https://www.ipcc.ch/srocc/

Jacques, J.-M. S., and Sauchyn, D. J. (2009). Increasing winter baseflow and mean annual streamflow from possible permafrost thawing in the Northwest Territories, Canada. *Geophysical Research Letters*, **36**(1), L01401-n/a. doi:10.1029/2008GL035822

Johansson, E., Devasthale, A., Tjernström, M., Ekman, A. M. L., and L'Ecuyer, T. (2017). Response of the lower troposphere to moisture intrusions into the Arctic. *Geophysical Research Letters*, **44**(5), 2527-2536. doi:10.1002/2017GL072687

Johannessen, O. M., Kuzmina, S. I., Bobylev, L. P., and Miles, M. W. (2016). Surface air temperature variability and trends in the Arctic: new amplification assessment and regionalisation. *Tellus. Series A, Dynamic meteorology and oceanography*, **68**(1), 28234-28212. doi:10.3402/tellusa.v68.28234

Johnson, M., and Eicken, H. (2016). Estimating Arctic sea-ice freeze-up and break-up from the satellite record: A comparison of different approaches in the Chukchi and

Beaufort Seas. *Elementa (Washington, D.C.)*, **4**, 124. doi:10.12952/journal.elementa.000124

Joly, D., and Richard, Y. (2019). Frequency, intensity, and duration of thermal inversions in the Jura Mountains of France. *Theoretical and Applied Climatology*, **138**(1), 639-655. doi:10.1007/s00704-019-02855-3

Jorgenson, M. T., Romanovsky, V., and Coauthors (2010). Resilience and vulnerability of permafrost to climate change. *Canadian Journal of Forest Research*, **40**(7), 1219-1236. doi:10.1139/X10-060

Jorgenson, M. T., Kanevskiy, M., and Coauthors (2015). Role of ground ice dynamics and ecological feedbacks in recent ice wedge degradation and stabilization. *Journal of geophysical research*, **120**(11), 2280-2297. doi:10.1002/2015JF003602

Kahl, J. D. (1990). Characteristics of the Low-Level Temperature Inversion Along the Alaskan Arctic Coast. *International Journal of Climatology*, ***10***(5), 537-548. https://doi.org/10.1002/joc.3370100509

Kahl, J. D., Serreze, M. C., and Schnell, R. C. (1992). Tropospheric low-level temperature inversions in the Canadian Arctic. *Atmosphere-Ocean.* **30**, 511-529. doi: 10.1080/07055900.1992.9649453

Kahl, J. D. W., Martinez, D. A., and Zaitseva, N. A. (1996). Long-Term Variability in the Low-Level Inversion Layer Over the Arctic Ocean. *International Journal of Climatology*, **16**(11), 1297-1313. doi:10.1002/(SICI)1097-0088(199611)16:11<1297::AID-JOC86>3.0.CO;2-T

Kappos, A. D., Bruckmann, P., and Coauthors (2004). Health effects of particles in ambient air. *International Journal of Hygiene and Environmental Health*, **207**(4), 399-407. doi:10.1078/1438-4639-00306

Kerr, W.S. (1970). The Avocado Industry in Southern California, a Study of Location, Perception, and Prospect. *PhD. Thesis, Department of Geography*, University of Oklahoma. https://www.proquest.com/openview/c3caeafa52f3f545b10a13570f8082ba/1?pq-origsite=gscholar&cbl=18750&diss=y

Klock, R., Hudson, E., Aihosi, D., and Mullock, J. (2002). The Weather of the Yukon, Northwest Territories and Western Nunavut. In: NAV CANADA. https://www.navcanada.ca/EN/media/Publications/Local%20Area%20Weather%20Manuals/LAWM-Yukon-NWT-EN.pdf

Klock, R., and Mullock, j. (2002). The Weather of British Columbia. In: NAV CANADA. https://www.navcanada.ca/EN/media/Publications/Local%20Area%20Weather%20Manuals/LAWM-BC-5-EN.pdf

Kiefer, M. T., and Zhong, S. (2015). The role of forest cover and valley geometry in cold-air pool evolution. Journal of geophysical research. *Atmospheres*, **120**(17), 8693-8711. doi:10.1002/2014JD022998

Kokelj, S. V., and Jorgenson, M. T. (2013). Advances in Thermokarst Research. *Permafrost and Periglacial Processes*, **24**(2), 108-119. doi:10.1002/ppp.1779

Kokelj, S. V., Lantz, T. C., Tunnicliffe, J., Segal, R., and Lacelle, D. (2017). Climate-driven thaw of permafrost preserved glacial landscapes, northwestern Canada. *Geology*, **45**(4), 371-374. doi:10.1130/G38626.1

Kossmann, M., and Sturman, A. P. (2003). Pressure-Driven Channeling Effects in Bent Valleys. *Journal of applied meteorology* (1988), **42**(1), 151-158. doi:10.1175/1520-0450(2003)042<0151:PDCEIB>2.0.CO;2

Kropp, H., Loranty, M. M., and Coauthors (2020). Shallow soils are warmer under trees and tall shrubs across Arctic and Boreal ecosystems. *Environmental research letters*. **16**(1), 1501-1514. doi:10.1088/1748-9326/abc994

LaDochy, S. (2005). The Disappearance of Dense Fog in Los Angeles: Another Urban Impact? *Physical geography*, **26**(3), 177-191. doi:10.2747/0272-3646.26.3.177

Lareau, N. P., Lareau, N. P., Horel, J. D., and Horel, J. D. (2015). Dynamically Induced Displacements of a Persistent Cold-Air Pool. *Boundary-Layer Meteorology*, **154**(2), 291-316. doi:10.1007/s10546-014-9968-5

Lanzante, J. R. (1996). Resistant, Robust and Non-parametric Techniques for the Analysis of Climate Data: Theory and Examples, Including Applications to Historical Radiosonde Station Data. *International Journal of Climatology*, **16**(11), 1197-1226. doi:10.1002/(SICI)1097-0088(199611)16:11<1197::AID-JOC89>3.0.CO;2-L

Lanzante, J. R., Klein, S. A., and Seidel, D. J. (2003). Temporal Homogenization of Monthly Radiosonde Temperature Data. Part I: Methodology. *Journal of Climate*, 16(2), 224-240. doi:10.1175/1520-0442(2003)016<0224:THOMRT>2.0.CO;2

Laprise, R. (2008). Regional climate modelling. *Journal of computational physics*, **227**(7), 3641-3666. doi:10.1016/j.jcp.2006.10.024

Lareau, N. P., Crosman, E., Whiteman, C. D., Horel, J. D., Hoch, S. W., William, O. J. B., and Horst, T. W. (2013). The Persistent Cold-Air Pool Study. *Bulletin of the American Meteorological Society*, **94**(1), 51-63. doi:10.1175/BAMS-D-11-00255.1

Largeron, Y., and Staquet, C. (2016). The Atmospheric Boundary Layer during Wintertime Persistent Inversions in the Grenoble Valleys. *Frontiers in Earth Science*, **4**. doi:10.3389/feart.2016.00070

Launiainen, S., Vesala, T., and Coauthors (2007). Vertical variability and effect of stability on turbulence characteristics down to the floor of a pine forest. *Tellus. Series B, Chemical and physical meteorology*, **59**(5), 919-936. doi:10.1111/j.1600-0889.2007.00313.x

Leitch, D. R., Carrie, J., Lean, D., Macdonald, R. W., Stern, G. A., and Wang, F. (2007). The delivery of mercury to the Beaufort Sea of the Arctic Ocean by the Mackenzie

River. *The Science of the total environment*, **373**(1), 178-195. doi:10.1016/j.scitotenv.2006.10.041

Lesins, G., Duck, T. J., and Drummond, J. R. (2012). Surface energy balance framework for Arctic amplification of climate change. Journal of Climate, **25**(23), 8277-8288. doi: 10.1175/JCLI-D-11-00711.1

Leukauf, D., Gohm, A., Rotach, M. W., and Wagner, J. S. (2015). The Impact of the Temperature Inversion Breakup on the Exchange of Heat and Mass in an Idealized Valley: Sensitivity to the Radiative Forcing. *Journal of Applied Meteorology and Climatology*, **54**(11), 2199-2216. doi:10.1175/JAMC-D-15-0091.1

Lewkowicz, A. G., and Ednie, M. (2004). Probability mapping of mountain permafrost using the BTS method, Wolf Creek, Yukon Territory, Canada. *Permafrost and Periglacial Processes*, ***15***(1), 67-80. doi:10.1002/ppp.480

Lewkowicz, A. G., and Bonnaventure, P. P. (2011). Equivalent Elevation: A New Method to Incorporate Variable Surface Lapse Rates into Mountain Permafrost Modelling. *Permafrost and Periglacial Processes*, **22**(2), 153-162. doi:10.1002/ppp.720

Lewkowicz, A. G., Bonnaventure, P. B., Smith, S. L., and Kuntz, Z. (2012). Spatial and thermal characteristics of mountain permafrost, northwest Canada. *Geografiska Annaler: Series A, Physical Geography*, **94**(2), 195-213. doi:10.1111/j.1468-0459.2012.00462.x

Liu, Y., and Key, J. R. (2003). Detection and Analysis of Clear-Sky, Low-Level Atmospheric Temperature Inversions with MODIS. *Journal of Atmospheric and Oceanic Technology*, ***20***(12), 1727-1737. doi:10.1175/1520-0426(2003)020<1727:DAAOCL>2.0.CO;2

Liu, Y., Key, J. R., Schweiger, A., and Francis, J. (2006). Characteristics of Satellite-Derived Clear-Sky Atmospheric Temperature Inversion Strength in the Arctic, 1980–96. *Journal of Climate*, ***19***(19), 4902-4913. doi:10.1175/JCLI3915.1

Loranty, M. M., Abbott, B. W., and Coauthors (2018). Reviews and syntheses: Changing ecosystem influences on soil thermal regimes in northern high-latitude permafrost regions. *Biogeosciences*, **15**(17), 5287-5313. doi:10.5194/bg-15-5287-2018

Lovatt, A. (2009). Characteristics of low-level temperature inversions, Whitehorse Yukon Territory: 1956–2003. *M.S. thesis, Department of Geography,* University of Ottawa, https://ruor.uottawa.ca/handle/10393/28207

Lu, W., and Zhong, S. (2014). A numerical study of a persistent cold air pool episode in the Salt Lake Valley, Utah. *Journal of Geophysical Research: Atmospheres,* **119**(4), 1733-1752. doi:10.1002/2013JD020410

Lundquist, J. D., and Cayan, D. R. (2007). Surface temperature patterns in complex terrain: Daily variations and long-term change in the central Sierra Nevada, California. *Journal of Geophysical Research - Atmospheres*, **112**(D11), D11124-n/a. doi:10.1029/2006JD007561

Lundquist, J. D., Pepin, N., and Rochford, C. (2008). Automated algorithm for mapping regions of cold-air pooling in complex terrain. *Journal of Geophysical Research - Atmospheres*, ***113***(D22), D22107-n/a. doi:10.1029/2008JD009879

Luo, H., Ge, F., and Coauthors (2019). Assessment of ECMWF reanalysis data in complex terrain: Can the CERA-20C and ERA-Interim data sets replicate the variation in surface air temperatures over Sichuan, China? *International Journal Of Climatology*, **39**(15), 5619-5634. doi:10.1002/joc.6175

Lute, A. C., and Abatzoglou, J. T. (2021). Best practices for estimating near-surface air temperature lapse rates. *International Journal of Climatology*, **41**(S1), E110-E125. doi:10.1002/joc.6668

Martineau, P., Wright, J. S., Zhu, N., and Fujiwara, M. (2018). Zonal-mean data set of global atmospheric reanalyses on pressure levels. *Earth System Science Data*, ***10***(4), 1925-1941. doi:10.5194/essd-10-1925-2018

Mayfield, J. A., and Fochesatto, G. J. (2013). The Layered Structure of the Winter Atmospheric Boundary Layer in the Interior of Alaska. *Journal of Applied Meteorology and Climatology*, **52**(4), 953-973. doi:10.1175/JAMC-D-12-01.1

Maykut, G. A., and Church, P. E. (1973). Radiation Climate of Barrow, Alaska, 1962–66. *Journal of Applied Meteorology* (1962-1982), **12**(4), 620-628. doi:10.1175/1520-0450(1973)012<0620:RCOBA>2.0.CO;2

McCaffrey, K., Wilczak, J. M., and Coauthors (2019). Identification and Characterization of Persistent Cold Pool Events from Temperature and Wind Profilers in the Columbia River Basin. *Journal of Applied Meteorology and Climatology*, ***58***(12), 2533-2551. doi:10.1175/JAMC-D-19-0046.1

McCray, C. D., Atallah, E. H., and Gyakum, J. R. (2019). Long-Duration Freezing Rain Events over North America: Regional Climatology and Thermodynamic Evolution. *Weather and Forecasting*, **34**(3), 665-681. doi:10.1175/WAF-D-18-0154.1

McGuire, A. D., Anderson, L. G., and Coauthors (2009). Sensitivity of the Carbon Cycle in the Arctic to Climate Change. *Ecological monographs*, **79**(4), 523-555. doi:10.1890/08-2025.1

McKnight, P.E. and Najab, J. (2010). Mann-Whitney U Test. In The Corsini Encyclopedia of Psychology (eds I.B. Weiner and W.E. Craighead). doi:10.1002/9780470479216.corpsy0524

Mernild, S. H., and Liston, G. E. (2010). The Influence of air temperature inversions on snowmelt and glacier mass balance simulations, Ammassalik Island, Southeast Greenland. *Journal of Applied Meteorology and Climatology*, **49**(1), 47–67. https://doi.org/10.1175/2009JAMC2065.1

Minder, J. R., Mote, P. W., and Lundquist, J. D. (2010). Surface temperature lapse rates over complex terrain: Lessons from the Cascade Mountains. *Journal of Geophysical Research*, **115**(D14), n/a-n/a. doi:10.1029/2009jd013493

Morison, J., Aagaard, K., and Steele, M. (2000). Recent environmental changes in the arctic: A review. *Arctic*, **53**(4), 359-371. Doi:10.14430/arctic867

Morse, P. D., and Wolfe, S. A. (2015). Geological and meteorological controls on icing (aufeis) dynamics (1985 to 2014) in subarctic Canada. *Journal of geophysical research. Earth surface*, **120**(9), 1670-1686. doi:10.1002/2015JF003534

Müller, H., and Whiteman, C. D. (1988). Breakup of a Nocturnal Temperature Inversion in the Dischma Valley during DISKUS. *Journal of applied meteorology* (1988), **27**(2), 188-194. doi:10.1175/1520-0450(1988)027<0188:BOANTI>2.0.CO;2

NOAA (2020a). Pacific Decadal Oscilation Index (PDO). University of Washinton, accessed May 11 2020, https://psl.noaa.gov/gcos_wgsp/Timeseries/PDO/

NOAA (2020b). Arctic Oscillation Index. National Oceanic and Atmospheric Administration/Climate Prediction Centre, accessed May 11 2020, https://psl.noaa.gov/gcos_wgsp/Timeseries/AO/

NOAA (2021). NOAA Solar Calculator. Earth System Research Laboratories, accessed April 8 2021, https://www.esrl.noaa.gov/gmd/grad/solcalc/

Newman, M., and Coauthors (2016). The pacific decadal oscillation, revisited. *Journal of Climate*, **29**(12), 4399-4427. doi:10.1175/JCLI-D-15-0508.1

Obu, J., Westermann, S., Bartsch, and Coauthors (2019). Northern Hemisphere permafrost map based on TTOP modelling for 2000–2016 at 1 km2 scale. *Earth-Science Reviews*, **193**, 299-316. doi:10.1016/j.earscirev.2019.04.023

Oke T.R. (1987) *Boundary layer climates* (2nd ed.). Taylor and Francis. 464 pp.

Olefeldt, D. and Coauthors (2016). Circumpolar distribution and carbon storage of thermokarst landscapes. *Nature Communications*, ***7***(1), 13043. doi:10.1038/ncomms13043

O'Neill, H. B., Wolfe, S. A., and Duchesne, C. (2019). New ground ice maps for Canada using a paleogeographic modelling approach. *The cryosphere*, **13**(3), 753-773. doi:10.5194/tc-13-753-2019

Ostertagová, E., Ostertag, O., and Kováč, J. (2014). Methodology and Application of the Kruskal-Wallis Test. *Applied Mechanics and Materials*, **611**, 115–120. doi:10.4028.611.115

Overland, J. E., Wang, M., Walsh, J. E., and Stroeve, J. C. (2014). Future Arctic climate changes: Adaptation and mitigation time scales. *Earth's Future*, ***2***(2), 68-74. doi:10.1002/2013EF000162

Palarz, A., Celiński-Mysław, D., and Ustrnul, Z. (2018). Temporal and spatial variability of surface-based inversions over Europe based on ERA-Interim reanalysis. *International Journal of Climatology*, **38**(1), 158-168. doi:10.1002/joc.5167

Palazzi, E., Mortarini, L., and Coauthors (2019). Elevation-dependent warming in global climate model simulations at high spatial resolution. *Climate Dynamics*, **52**(5), 2685-2702. doi:10.1007/s00382-018-4287-z

Palo, T., Vihma, T., Jaagus, J., and Jakobson, E. (2017). Observations of temperature inversions over central Arctic sea ice in summer. *Quarterly Journal of the Royal Meteorological Society*, **143**(708), 2741-2754. doi:10.1002/qj.3123

Pepin, N., Benham, D., and Taylor, K. (1999). Modeling Lapse Rates in the Maritime Uplands of Northern England: Implications for Climate Change. *Arctic, Antarctic, and Alpine Research*, **31**(2), 151. doi:10.2307/1552603

Pepin, N. (2001). Lapse rate changes in northern England. *Theoretical and Applied Climatology*, **68**(1), 1-16. doi:10.1007/s007040170049

Pepin, N., Schaefer, M. K., and Riddy, L. D. (2009). Quantification of the cold-air pool in Kevo Valley, Finnish Lapland. *Weather*, **64**(3), 60-67. doi:10.1002/wea.260

Pepin, N., Bradley, R. S., and Coauthors (2015). Elevation-dependent warming in mountain regions of the world. *Nature Climate Change*, ***5***(5), 424-430. doi:10.1038/NCLIMATE2563

Pielke, R. A. (2002). *Mesoscale meteorological modeling* (2nd ed.). San Diego: Academic Press.696 pp.

Pigeon, K. E., & Jiskoot, H. (2008). Meteorological Controls on Snowpack Formation and Dynamics in the Southern Canadian Rocky Mountains. *Arctic, Antarctic, and Alpine Research*, **40**(4), 716-730. doi:10.1657/1523-0430(07-054)[PIGEON]2.0.CO;2

Pike, G., Pepin, N. C., and Schaefer, M. (2013). High latitude local scale temperature complexity: the example of Kevo Valley, Finnish Lapland. *International Journal of Climatology*, **33**(8), 2050-2067. doi:10.1002/joc.3573

Porter, T. J., Schoenemann, S. W., Davies, L. J., Steig, E. J., Bandara, S., and Froese, D. G. (2019). Recent summer warming in northwestern Canada exceeds the Holocene thermal maximum. *Nature Communications*, **10**(1), 1631-1610. doi:10.1038/s41467-019-09622-y

Praskievicz, S., and Bartlein, P. (2014). Hydrologic modeling using elevationally adjusted NARR and NARCCAP regional climate-model simulations: Tucannon River, Washington. *Journal of hydrology*, **517**, 803-814. doi:10.1016/j.jhydrol.2014.06.017

Prestrud, P (2007) Why are snow and ice important to us? Chapter 2. In: Eamer J (ed) UNEP *Global Outlook for Ice and Snow*. United Nations Environment Program, pp 1928 https://wedocs.unep.org/20.500.11822/13698

Prowse T.D, Furgal C, Chouinard R, Melling H, Milburn D, Smith SL (2009) Implications of climate change for economic development in Northern Canada: energy, resource, and transportation sectors. *Ambio* **38**(5):272281

Przybylak R. (2016) *The Climate of the Arctic* (2nd ed.). Springer International Publishing. 223 pp.

Qin, Y., Wu, T., and Coauthors (2017). Assessment of reanalysis soil moisture products in the permafrost regions of the central of the Qinghai–Tibet Plateau. *Hydrological processes*, **31**(26), 4647-4659. doi:10.1002/hyp.11383

Qin, Y., Zhang, P., Liu, W., Guo, Z., and Xue, S. (2020). The application of elevation corrected MERRA2 reanalysis ground surface temperature in a permafrost model on the Qinghai-Tibet Plateau. *Cold Regions Science and Technology*, **175**, 103067. doi:10.1016/j.coldregions.2020.103067

Quinton, W. L., Hayashi, M., and Chasmer, L. E. (2011). Permafrost-thaw-induced land-cover change in the Canadian subarctic: implications for water resources. *Hydrological processes*, **25**(1), 152-158. doi:10.1002/hyp.7894

Radchuk, V., Reed, T., and Coauthors (2019). Adaptive responses of animals to climate change are most likely insufficient. *Nature Communications*, **10**(1), 3109-3109. doi:10.1038/s41467-019-10924-4

Raza, M. M., Khan, M. A., and Coauthors (2015). Impact of global warming on insects. *Archiv für Phytopathologie und Pflanzenschutz*, **48**(1), 84-94. doi:10.1080/03235408.2014.882132

Revich, B. A., and Podolnaya, M. A. (2011). Thawing of permafrost may disturb historic cattle burial grounds in East Siberia. *Global Health Action*, **4**(1), 8482-8486. doi:10.3402/gha.v4i0.8482

Rigor, I. G., Colony, R. L., and Martin, S. (2000). Variations in surface air temperature observations in the arctic, 1979–97. *Journal of Climate*, **13**(5), 896-914. doi:10.1175/1520-0442(2000)013<0896:VISATO>2.0.CO;2

Rinke, A., Dethloff, K., and Coauthors (2006). Evaluation of an ensemble of Arctic regional climate models: spatiotemporal fields during the SHEBA year. *Climate Dynamics*, **26**(5), 459-472. doi:10.1007/s00382-005-0095-3

Riseborough, D., Shiklomanov, N., Etzelmüller, B., Gruber, S., and Marchenko, S. (2008). Recent advances in permafrost modelling. *Permafrost and Periglacial Processes*, **19**(2), 137-156. doi:10.1002/ppp.615

Rist, A., Roth, L., and Veit, H. (2020). Elevational ground/air thermal gradients in the Swiss inner Alpine Valais. Arctic, *Antarctic, and Alpine Research*, **52**(1), 341-360. doi:10.1080/15230430.2020.1742022

Roberts, D. R., Wood, W. H., and Marshall, S. J. (2019). Assessments of downscaled climate data with a high-resolution weather station network reveal consistent but predictable bias. *International Journal of Climatology*, **39**(6), 3091-3103. doi:10.1002/joc.6005

Röthlisberger, M., Frossard, L., Bosart, L. F., Keyser, D., and Martius, O. (2019). Recurrent Synoptic-Scale Rossby Wave Patterns and Their Effect on the

Persistence of Cold and Hot Spells. *Journal of Climate*, **32**(11), 3207-3226. doi:10.1175/jcli-d-18-0664.1

Rummukainen, M. (2016). Added value in regional climate modeling. *Wiley interdisciplinary reviews. Climate change*, **7**(1), 145-159. doi:10.1002/wcc.378

Ruxton, G. D., and Beauchamp, G. (2008). Time for some a priori thinking about post hoc testing. *Behavioral ecology*, **19**(3), 690-693. doi:10.1093/beheco/arn020

Rydberg, J., Klaminder, J., Rosén, P., Bindler, R., Institutionen för ekologi, m. o. g., Umeå, u., and Teknisk-naturvetenskapliga, f. (2010). Climate driven release of carbon and mercury from permafrost mires increases mercury loading to sub-arctic lakes. *Science of the Total Environment*, **408**(20), 4778-4783. doi:10.1016/j.scitotenv.2010.06.056

Sakiyama, S. K. (1990). Drainage Flow Characteristics and Inversion Breakup in Two Alberta Mountain Valleys. *Journal of Applied Meteorology* (1988-2005), **29**(10), 1015-1030. doi:10.1175/1520-0450(1990)029<1015:DFCAIB>2.0.CO;2

Schaefer, K., Elshorbany, Y., Jafarov, E., Schuster, P. F., Striegl, R. G., Wickland, K. P., and Sunderland, E. M. (2020). Potential impacts of mercury released from thawing permafrost. *Nature Communications*, **11**(1), 4650-4650. doi:10.1038/s41467-020-18398-5

Schielzeth, H., Dingemanse, N. J., and Coauthors (2020). Robustness of linear mixed-effects models to violations of distributional assumptions. *Methods in ecology and evolution*, **11**(9), 1141-1152. doi:10.1111/2041-210X.13434

Schuster, P. F., Schaefer, K. M., and Coauthors (2018). Permafrost Stores a Globally Significant Amount of Mercury. *Geophysical Research Letters*, **45**(3), 1463-1471. doi:10.1002/2017gl075571

Schuur, A. G. E., Bockheim, J., and Coauthors (2008). Vulnerability of Permafrost Carbon to Climate Change: Implications for the Global Carbon Cycle. *Bioscience*, **58**(8), 701-714. doi:10.1641/B580807

Schuur, E. A. G., and Mack, M. C. (2018). Ecological Response to Permafrost Thaw and Consequences for Local and Global Ecosystem Services. *Annual review of ecology, evolution, and systematics*, **49**(1), 279-301. doi:10.1146/annurev-ecolsys-121415-032349

Sedlar, J., Shupe, M. D., and Tjernström, M., (2012). On the Relationship between Thermodynamic Structure and Cloud Top, and Its Climate Significance in the Arctic. *Journal of Climate*, **25**(7), 2374-2393. doi:10.1175/JCLI-D-11-00186.1

Seidel, D. J., Ao, C. O., and Li, K. (2010). Estimating climatological planetary boundary layer heights from radiosonde observations: Comparison of methods and uncertainty analysis. *Journal of Geophysical Research: Atmospheres*, **115**, D16113. doi:10.1029/2009JD013680

Serafin, S., Alder B., and Coauthors (2018). Exchange Processes in the Atmospheric Boundary Layer Over Mountainous Terrain. Atmosphere, **9**(3), 102. doi:10.3390/atmos9030102

Serreze, M. C., Kahl, J. D., and Schnell, R. C. (1992). Low-Level Temperature Inversions of the Eurasian Arctic and Comparisons with Soviet Drifting Station Data. *American Meteorological Society*, **5**, 615-629. doi:0.1175/15200442(1992)005<0615:LLTIOT>2.0.CO;2

Serreze, M. C., and Barry, R. G. (2011). Processes and impacts of Arctic amplification: A research synthesis. *Global and Planetary Change, **77***(1), 85-96. doi:10.1016/j.gloplacha.2011.03.004

Serreze, M. C., and Barrett, A. P. (2011). Characteristics of the beaufort sea high. *Journal of Climate*, **24**(1), 159-182. doi:10.1175/2010JCLI3636.1

Serreze, M. C., Barrett, A. P., and Stroeve, J. (2012). Recent changes in tropospheric water vapor over the arctic as assessed from radiosondes and atmospheric reanalyses. *Journal of Geophysical Research: Atmospheres*, **117**(D10). doi:10.1029/2011JD017421

Serreze, M. C. and R. G. Barry (2014) *The Arctic Climate System* (2nd ed.). Cambridge University Press, 385 pp

Serreze, M. C., and Meier, W. N. (2019). The Arctic's sea ice cover: trends, variability, predictability, and comparisons to the Antarctic. *Annals of the New York Academy of Sciences*, **1436**(1), 36-53.

Shahi, S., Abermann, J., Heinrich, G., Prinz, R., and Schöner, W. (2020). Regional variability and trends of temperature inversions in Greenland. *Journal of Climate*, 1-48. doi:10.1175/JCLI-D-19-0962.1

Shur, Y. L., and Jorgenson, M. T. (2007). Patterns of permafrost formation and degradation in relation to climate and ecosystems. *Permafrost and Periglacial Processes*, **18**(1), 7-19. doi:10.1002/ppp.582

Simnitt, S., Borisova, T., Chavez, D., and Olmstead, M. (2017). Frost Protection for Georgia Peach Varieties: Current Practices and Information Needs. *HortTechnology*, 27(3), 344. doi:10.21273/horttech03590-16

Smith, M. W., and Riseborough, D. W. (2002). Climate and the limits of permafrost: a zonal analysis. *Permafrost and Periglacial Processes, 13*(1), 1-15. doi:10.1002/ppp.410

Smith, C. M., and Skyllingstad, E. D. (2005). Numerical simulation of katabatic flow with changing slope angle. *Monthly Weather Review*, **133**(11), 3065-3080. doi:10.1175/MWR2982.1

Smith, S. A., Brown, A. R., Vosper, S. B., Murkin, P. A., and Veal, A. T. (2010a). Observations and Simulations of Cold Air Pooling in Valleys. *Boundary-Layer Meteorology*, **134**(1), 85-108. doi:10.1007/s10546-009-9436-9

Smith, S. L., Romanovsky, V., and Coauthors (2010b). Thermal state of permafrost in North America: a contribution to the international polar year. *Permafrost and Periglacial Processes*, **21**(2), 117-135. doi:10.1002/ppp.690

Smith, S. L., and Bonnaventure, P. P. (2017). Quantifying Surface Temperature Inversions and Their Impact on the Ground Thermal Regime at a High Arctic Site. *Arctic, Antarctic, and Alpine Research*, ***49***(1), 173-185. doi:10.1657/AAAR0016-039

Smith-Downey, N. V., Sunderland, E. M., and Jacob, D. J. (2010). Anthropogenic impacts on global storage and emissions of mercury from terrestrial soils: Insights from a new global model. *Journal of Geophysical Research: Biogeosciences*, **115**, G03008. doi:10.1029/2009JG001124

Sterk, H. A. M., Steeneveld, G. J., Vihma, T., Anderson, P. S., Bosveld, F. C., and Holtslag, A. A. M. (2015). Clear-sky stable boundary layers with low winds over snow-covered surfaces. Part 1: WRF model evaluation. *Quarterly Journal of the Royal Meteorological Society*, **141**(691), 2165-2184. doi:10.1002/qj.2513

Stern, G. A., Macdonald, R. W., and Coauthors (2012). How does climate change influence arctic mercury? The Science of the total environment, **414**, 22-42. doi:10.1016/j.scitotenv.2011.10.039

Sun, X., and Holmes, H. A. (2019). Surface Turbulent Fluxes during Persistent Cold-Air Pool Events in the Salt Lake Valley, Utah. Part I: Observations. *Journal of Applied Meteorology and Climatology*, **58**(12), 2553-2568. doi:10.1175/JAMC-D-19-0053.1

Tao, J., Koster, R. D., Reichle, R. H., Forman, B. A., Xue, Y., Chen, R. H., and Moghaddam, M. (2019). Permafrost variability over the Northern Hemisphere based on the MERRA-2 reanalysis. *The Cryosphere*, **13**(8), 2087-2110. doi:10.5194/tc-13-2087-2019

Tape, K. E. N., Sturm, M., and Racine, C. (2006). The evidence for shrub expansion in Northern Alaska and the Pan-Arctic. *Global change biology*, **12**(4), 686-702. doi:10.1111/j.1365-2486.2006.01128.x

Taylor A.E., Nixon M., Eley J., Burgess M., and Egginton P. (1998). Effects of atmospheric inversions on ground surface temperatures and discontinuous permafrost, Norman Wells, Mackenzie valley, Canada. *In Proceedings of the 7th International Conference on Permafrost*, Yellowknife, Canada, International Permafrost Association. Collection Nordicana, 55: 1043-1047. https://www.arlis.org/docs/vol1/ICOP/40770716/CD-ROM/Proceedings/PDF001189/157254.pdf

Trenberth, K. E., and Hurrell, J. W. (1994). Decadal atmosphere-ocean variations in the Pacific. *Climate Dynamics*, **9**(6), 303-319. doi:10.1007/BF00204745

Turner, M. G., O'Neill, R. V., Gardner, R. H., and Milne, B. T. (1989). Effects of changing spatial scale on the analysis of landscape pattern. *Landscape ecology*, **3**(3-4), 153-162. doi:10.1007/BF00131534

Urban, M., Eberle, J., Hüttich, C., Schmullius, C., and Herold, M. (2013). Comparison of satellite-derived land surface temperature and air temperature from meteorological stations on the Pan-Arctic scale. *Remote Sensing*, ***5***(5), 2348-2367. doi:10.3390/rs5052348

Vergeiner, I., and Dreiseitl, E. (1987). Valley Winds and Slope Winds - Observations and Elementary Thoughts. *Meteorology and Atmospheric Physics*, **36**(1-4), 264-286. doi:10.1007/BF01045154

Vitasse, Y., Klein, G., and Coauthors (2017). Intensity, frequency and spatial configuration of winter temperature inversions in the closed La Brevine valley, Switzerland. *Theoretical and Applied Climatology*, **130**(3), 1073-1083. doi:10.1007/s00704-016-1944-1

Volney, W. J. A., and Fleming, R. A. (2000). Climate change and impacts of boreal forest insects. *Agriculture, Ecosystems & Environment*, **82**(1-3), 283-294. doi:10.1016/s0167-8809(00)00232-2

Vonk, J. E., Tank, S. E., and Coauthors (2015). Reviews and syntheses: Effects of permafrost thaw on Arctic aquatic ecosystems. *Biogeosciences*, 12(23), 7129-7167. doi:10.5194/bg-12-7129-2015

Vosper, S. B., and Brown, A. R. (2008). Numerical Simulations of Sheltering in Valleys: The Formation of Nighttime Cold-Air Pools. *Boundary-Layer Meteorology*, **127**(3), 429-448. doi:10.1007/s10546-008-9272-3

Wagner, J. S., Gohm, A., and Rotach, M. W. (2015). The impact of valley geometry on daytime thermally driven flows and vertical transport processes. *Quarterly Journal of the Royal Meteorological Society*, **141**(690), 1780-1794. doi:10.1002/qj.2481

Wahl, H., (2004). Yukon overview: climate. In: Smith, C.A.S., Meikle, J.C. and Roots, C.F., Ecoregions of the Yukon Territory – Biophysical Properties of Yukon Landscapes. *Agriculture and Agri-Food Canada, PARC Technical Bulletin 04-01*, Part I: 19–23 pp. https://yukon.ca/sites/yukon.ca/files/env/env-ecoregions-yukon-territory.pdf

Walden, V. P., Mahesh, A., and Warren, S. G. (1996). Comment on "Recent changes in the North American Arctic boundary layer in winter" by R. S. Bradley et al. *Journal of Geophysical Research: Atmospheres*, **101**(D3), 7127-7134. doi:10.1029/95JD03233

Wang, B., Paudel, B., and Li, H. (2009). Retrogression characteristics of landslides in fine-grained permafrost soils, Mackenzie Valley, Canada. *Landslides*, **6**, 121–127. doi:10.1007/s10346-009-0150-y

Wang, T., Hamann, A., Spittlehouse, D. L., and Murdock, T. Q. (2012). ClimateWNA—High-Resolution Spatial Climate Data for Western North America. *Journal of Applied Meteorology and Climatology*, **51**(1), 16-29. doi:10.1175/JAMC-D-11-043.1

Wang, Q., Fan, X., and Wang, M. (2013). Recent warming amplification over high elevation regions across the globe. *Climate Dynamics*, **43**(1-2), 87-101. doi:10.1007/s00382-013-1889-3

Wang, T., Hamann, A., Spittlehouse, D., and Carroll, C. (2016). Locally Downscaled and Spatially Customizable Climate Data for Historical and Future Periods for North America. *PloS One*, **11**(6), e0156720-e0156720. doi:10.1371/journal.pone.0156720

Ward Jones, M. K., Pollard, W. H., and Jones, B. M. (2019). Rapid initialization of retrogressive thaw slumps in the Canadian high Arctic and their response to climate and terrain factors. *Environmental Research Letters*, **14**(5), 055006. doi:10.1088/1748-9326/ab12f

Way, R. G., and Lewkowicz, A. G. (2018). Environmental controls on ground temperature and permafrost in Labrador, northeast Canada. *Permafrost and Periglacial Processes*, **29**(2), 73-85. doi:10.1002/ppp.1972

Way, R. G., and Lapalme, C. M. (2021). Does tall vegetation warm or cool the ground surface? Constraining the ground thermal impacts of upright vegetation in northern environments. *Environmental Research Letters*, **16**(5), 54077. doi:10.1088/1748-9326/abef31

Wei, L., Pu, Z., and Wang, S. (2013). Numerical Simulation of the Life Cycle of a Persistent Wintertime Inversion over Salt Lake City. *Boundary-Layer Meteorology*, **148**(2), 399-418. doi:10.1007/s10546-013-9821-2

Weigel, A. P., Chow, F. K., Rotach, M. W., Street, R. L., and Xue, M. (2006). High-Resolution Large-Eddy Simulations of Flow in a Steep Alpine Valley. Part II: Flow Structure and Heat Budgets. *Journal of Applied Meteorology and Climatology*, **45**(1), 87-107. doi:10.1175/JAM2323.1

Whiteman, C. D. (1982). Breakup of Temperature Inversions in Deep Mountain Valleys: Part I. Observations. *Journal of Applied Meteorology* (1962-1982), **21**(3), 270-289. doi:10.1175/1520-0450(1982)021<0270:BOTIID>2.0.CO;2

Whiteman, C. D., and Doran, J. C. (1993). The Relationship between Overlying Synoptic-Scale Flows and Winds within a Valley. *Journal of Applied Meteorology* (1988), **32**(11), 1669-1682. doi:10.1175/1520-0450(1993)032<1669:TRBOSS>2.0.CO;2

Whiteman, C. (2000). *Mountain Meteorology: Fundamentals and Applications*. United States: Oxford University Press. 376 pp.

Whiteman, C. D., Zhong, S., Shaw, W. J., Hubbe, J. M., Bian, X., and Mittelstadt, J. (2001). Cold Pools in the Columbia Basin. *Weather and Forecasting*, **16**(4), 432-447. doi:10.1175/1520-0434(2001)016<0432:CPITCB>2.0.CO;2

Whiteman, C. D., Pospichal, B., and Coauthors (2004). Inversion Breakup in Small Rocky Mountain and Alpine Basins. *Journal of Applied Meteorology*, **43**(8), 1069-1082. doi:10.1175/1520-0450(2004)043<1069:IBISRM>2.0.CO;2

Williams, R., and Thorp, T. (2015). Characteristics of springtime nocturnal temperature inversions in a high latitude environment. *Weather*, **70**(S1), S37-S43. doi:10.1002/wea.2554

Williamson, S. N., Zdanowicz, C., and Coauthors (2020). Evidence for Elevation-Dependent Warming in the St. Elias Mountains, Yukon, Canada. *Journal of Climate*, 33(8), 3253-3269. doi:10.1175/JCLI-D-19-0405.1

Yukon Government (2020a). Tombstone Weather Station # 1 Interpretive Centre. Yukon Departement of Environment, accessed November 2 2020, https://datagarrison.com/users/300034012127970/300234011202310/plots.php?plot=3

Yukon Government (2020b). Tombstone Weather Station # 2 North Fork Mtn. Yukon Departement of Environment Accessed November 2, 2020, https://datagarrison.com/users/300034012127970/300234010496280/plots.php?plot=1

Zeng, W., Zeng, W., Yu, Z., Yu, Z., Li, X., and Li, X. (2018). The influence of elevation, latitude and Arctic Oscillation on trends in temperature extremes over northeastern China, 1961–2011. *Meteorology and Atmospheric Physics*, **130**(2), 191-209. doi:10.1007/s00703-017-0509-x

Zhang, Y., Chen, W., and Cihlar, J. (2003). A process-based model for quantifying the impact of climate change on permafrost thermal regimes. *Journal of Geophysical Research: Atmospheres*, **108**(D22), 4695-n/a. doi:10.1029/2002JD003354

Zhang, Y., Seidel, D. J., Golaz, J.-C., Deser, C., and Tomas, R. A. (2011). Climatological Characteristics of Arctic and Antarctic Surface-Based Inversions. *Journal of Climate*, ***24***(19), 5167-5186. doi:10.1175/2011JCLI4004.1

Zhang, Y., and Seidel, D. J. (2011). Challenges in estimating trends in Arctic surface-based inversions from radiosonde data. *Geophysical Research Letters*, **38**(17), doi:10.1029/2011GL048728

Zhang, X., Flato, G., Kirchmeier-Young, M., Vincent, L., Wan, H., Wang, X., Rong, R., Fyfe, J., Li, G., and Kharin, V.V. (2019). Changes in Temperature and Precipitation Across Canada; Chapter 4 in Bush, E. and Lemmen, D.S. (Eds.*) Canada's Changing Climate Report. Government of Canada.* pp 112-193. https://changingclimate.ca/CCCR2019/chapter/4-0/

Zhou, C., Wang, J., Dai, A., and Thorne, P. W. (2021). A New Approach to Homogenize Global Subdaily Radiosonde Temperature Data from 1958 to 2018, *Journal of Climate*, **34**(3), 1163-1183. doi: 10.1175/JCLI-D-20-0352.1